EQUATIONS OF STATE OF OXIDES AND SILICATES AND NEW DATA ON THE ELASTIC PROPERTIES OF SPINEL, MAGNETITE, AND CADMIUM OXIDE

by

Anthony Wayne England

S.B., Massachusetts Institute of Technology
(1965)

S.M., Massachusetts Institute of Technology
(1965)

SUBMITTED IN PARTIAL FULFILLMENT
OF THE REQUIREMENTS FOR THE
DEGREE OF DOCTOR OF
PHILOSOPHY
at the
MASSACHUSETTS INSTITUTE OF
TECHNOLOGY

May 1970

Signature of Author.....
Department of Geology and Geophysics, May 1970

Certified by.....
Thesis Supervisor

Accepted by.....
Chairman, Departmental Committee
on Graduate Students

Lindgren
WITHDRAWN
JUN 4 1970
FROM
MIT LIBRARIES

EQUATIONS OF STATE OF OXIDES AND SILICATES AND NEW DATA ON THE ELASTIC PROPERTIES OF SPINEL, MAGNETITE, AND CADMIUM OXIDE

by Anthony Wayne England

Submitted to the Department of Geology and Geophysics in May, 1970, in partial fulfillment of the requirement for the degree of Doctor of Philosophy.

ABSTRACT

The elastic constants and their pressure and temperature derivatives are presented for single-crystal $MgO \cdot 3.0Al_2O_3$ spinel and for polycrystalline cadmium oxide. The elastic constants and their pressure derivatives are reported for a natural magnetite and for a polycrystalline $MgO \cdot 1.1Al_2O_3$ spinel. The measured volume thermal expansion of cadmium oxide is $(32 \pm 1) \times 10^{-6}$. Some of the more important results are:

Parameter	Spinel $MgO \cdot 1.1Al_2O_3$	Spinel* $MgO \cdot 3.0Al_2O_3$	Magnetite *	Cadmium oxide
Density	3.58**	3.6245	5.163	7.8438
K_s (kb)	2060**	2026	1596	1280**
$\left(\frac{\partial K_s}{\partial P}\right)_T^o$	5.40	4.58	20.3	5.31
$\left(\frac{\partial K_s}{\partial T}\right)_P^o \left(\frac{kb}{^oC}\right)$	--	-0.257	--	-0.215

*Voigt-Reuss-Hill average.
**Corrected to zero porosity.

Parameter	Spinel $MgO \cdot 1.Al_2O_3$	Spinel* $MgO \cdot 3.0Al_2O_3$	Magnetite *	Cadmium oxide
G (kb)	1020**	1155	893	520**
$\left(\frac{\partial G}{\partial P}\right)_T^o$	0.82	0.753	-11.7	1.23
$\left(\frac{\partial G}{\partial T}\right)_P^o \left(\frac{kb}{°C}\right)$	--	-0.106	--	-0.125
v_p (km/sec)	9.8**	9.918	7.35	4.92**
v_s (km/sec)	5.4**	5.644	4.16	2.53**
Gruneisen's ratio	0.87	0.69	--	1.49

*Voigt-Reuss-Hill average.
**Corrected to zero porosity.

A comparison of four spinels shows their elastic properties to be independent of the magnesia-alumina ratio. This is consistent with the universal equations of state.

A new technique for measuring ultrasonic velocity in coarse grained samples was used to study the effect of spherical pores on dynamic elastic properties. Various forms of Mackenzie's equations adequately predict the change in elastic parameters with porosities to approximately 10%. No adequate theory exists for the effect of porosity on the pressure derivatives of the elastic parameters.

A critical review in the light of most of the applicable data indicates that the universal equations of state are of marginal value. A modified quasi-harmonic equation of state tailored to a specific composition is required for reliable extrapolations to mantle temperatures and pressures.

Key parameters in the quasi-harmonic theory are the mode Gruneisen's ratios. Theoretically, it is shown that the mode Gruneisen's ratios of covalently bonded crystals are independent of wave vector. This new argument implies that the ultrasonic mode Gruneisen's ratios apply to all wave vectors in that mode. The result is a modified quasi-harmonic equation of state that is more rigorous than the Mie-Gruneisen equation.

A new theoretical expression is derived for the volume derivative of Gruneisen's ratio, and the results are listed for 10 compounds. The volume dependence of neither the Slater nor the Dugdale-MacDonald formulation of γ is correct. The implication to the reduction of shock data is discussed.

ACKNOWLEDGMENTS

The assistance of unnumerable talented people has made this work possible. I am indebted particularly to Dr. D. H. Chung for his time, counsel, experimental equipment, and expertise, especially in the art of hot-pressing. Dr. W. F. Brace provided valuable counsel in pressure techniques. Dr. D. Readey and D. Camilli of Raytheon generously assisted with hot-pressing. Professor C. Frondel of Harvard University generously provided the magnetite sample. I sincerely thank Dr. Dave McKay of the Manned Spacecraft Center for his microprobe analysis of the samples.

Appreciation is extended to Professor Gene Simmons for guidance throughout this work. Greatest debt is to my wife, Kathi, for monumental patience.

Financial support was provided by a National Science Foundation Graduate Fellowship, by the National Science Foundation grant GA 579, and by the National Aeronautics and Space Administration contract NGR 22-009-176. The support by the Manned Spacecraft Center of the National Aeronautics and Space Administration of manuscript preparation, electron microprobe analysis, and digital computation is acknowledged.

TABLE OF CONTENTS

	Page
ABSTRACT	2
ACKNOWLEDGMENTS	5
TABLE OF CONTENTS	6
LIST OF TABLES	7
LIST OF FIGURES	9
I. INTRODUCTION	15
II. EFFECT OF SPHERICAL PORES ON THE ELASTIC CONSTANTS AND THEIR PRESSURE DERIVATIVES	17
III. THE ELASTIC PROPERTIES OF SPINEL, MAGNETITE, AND CADMIUM OXIDE	33
IV. UNIVERSAL EQUATIONS OF STATE FOR OXIDES AND SILICATES	59
V. A MODIFIED QUASI-HARMONIC EQUATION OF STATE AND GRUNEISEN'S RATIO	80
VI. CONCLUSIONS	100
APPENDIX A: DERIVATION OF THE BIRCH-MURNAGHAN RELATION	102
APPENDIX B: ULTRASONIC WAVE REFLECTION AND REFRACTION AT A SEAL	108
APPENDIX C: WAVE PROPAGATION IN A CRYSTALLINE MEDIA, THE ELASTIC CONSTANTS, THE ISOTHERMAL CORRECTION, AND THE ULTRASONIC ESTIMATE OF GRUNEISEN'S RATIO	114
APPENDIX D: CRYSTAL CUTTING AND POLISHING TECHNIQUES	124
APPENDIX E: THE PHASE COMPARISON TECHNIQUE AND ERROR ANALYSIS	127
APPENDIX F: COMPUTER PROGRAMS	142
APPENDIX G: ELASTICITY DATA OF THE POROUS GLASS SAMPLES	147
REFERENCES CITED	151
BIOGRAPHICAL NOTE	159

LIST OF TABLES

Table		Page
II - 1.	ELASTIC PROPERTIES OF POROUS GLASS	24
- 2.	COMPARISON OF THE PRESSURE DERIVATIVES FOR POROUS AND NONPOROUS MATERIALS	25
III - 1.	CHEMICAL COMPOSITIONS OF THE SAMPLE	41
- 2.	DENSITIES AND LENGTHS OF THE SAMPLES	42
- 3.	EQUATIONS USED TO REDUCE DATA	43
- 4.	NEW DATA	45
- 5.	ELASTIC CONSTANTS OF THE SINGLE CRYSTALS	46
- 6.	ELASTIC CONSTANTS OF THE POLYCRYSTALS	47
- 7.	A COMPARISON OF DATA OBTAINED FOR SEVERAL COMPOSITIONS OF SPINEL	48
- 8.	A COMPARISON OF THE POINTON AND TAYLOR DATA (1968) FOR SPINEL AT 4.2° K WITH AN EXTRAPOLATION OF THE NEW DATA	49
IV - 1.	MEASUREMENT TECHNIQUES FOR THE ELASTIC PROPERTIES OF MATERIALS	67
- 2.	ULTRASONIC DATA	68
- 3.	DATA ON OXIDES WITH NaCl STRUCTURE	72
- 4.	COMPARISON AND MEAN ATOMIC WEIGHT OF THE END MEMBERS OF COMMON HORNBLENDE	73
- 5.	MATERIALS THAT DO NOT CONFORM TO THE DENSITY-MEAN ATOMIC WEIGHT RELATIONSHIP OF BIRCH	74
- 6.	STATISTICAL PARAMETERS DERIVED FROM DATA OF TABLES IV-2 AND IV-3	75
V - 1.	DATA USED IN CHAPTER IV	94
- 2.	A COMPARISON OF THE DENSITY DERIVATIVES OF THE ELASTIC PARAMETERS AT CONSTANT TEMPERATURE WITH THOSE AT CONSTANT PRESSURE	95

Table Page

V - 3. $\left(\frac{\partial \ \ell n \ \gamma}{\partial \ \ell n \ V}\right)$ FOR SLATER'S DEPENDENCE OF γ ON VOLUME 96

- 4. THE VOLUME DERIVATIVE OF GRUNEISEN'S PARAMETER FOR SEVERAL MATERIALS 97

LIST OF FIGURES

Figure		Page
II - 1.	Arrangement of specimen in pressure vessel. The glass sample was bonded to the plug with Eastman 910 quick-setting cement. The transducer is outside the pressure envelope	26
- 2.	Idealized signals at transducer. The vertical hash marks represent the beginning of each sweep on the CRT. Because of Z-axis modulation, only the two sweeps containing reflections B and C are seen . . .	27
- 3.	Oscilloscope traces of typical shear wave signals. The lower two traces show reflections B and C in a matched condition. The upper traces are mismatched by 1 part in 10^3	28
- 4.	Block diagram. The discriminator is a simple resistor-bucking diode divider that provides high-voltage protection for the amplifier. Also included is a passive filter designed to reduce 60-cycle ac pickup	29
- 5.	Effect of porosity on bulk and shear moduli. The lines are the trace of the theoretical expression equation II-1	30
- 6.	Effect of porosity on sound velocities. The lines are the traces of the theoretical expression equation II-1	31
- 7.	Effect of porosity on $\partial(F/F_o)/\partial P$	32
III - 1.	The Pulse-Echo Overlap System of Chung, et al. (1969). System is functionally similar to that described in Chapter II	50
- 2.	F/F_o versus pressure for spinel single crystal . . .	51
- 3.	F/F_o versus temperature for spinel single crystal	52
- 4.	F/F_o versus pressure for polycrystalline spinel	53
- 5.	F/F_o versus pressure for polycrystalline CdO	54
- 6.	F/F_o versus temperature for polycrystalline CdO	55

Figure		Page
III - 7.	F/F_o versus pressure magnetite single crystal . . .	56
- 8.	F/F_o versus pressure magnetite single crystal . . .	57
- 9.	Lattice spacing versus temperature of cadmium oxide	58
IV - 1.	Test of O. Anderson-Nafe relationship, $\ell nK = A\ell n(2\bar{m}/\rho) + C$. Data from table IV-2	76
- 2.	Test of D. Anderson relationship $\rho = A\bar{m}\Phi^n$. Data from table IV-2	77
- 3.	Test of relationship $\rho = A\bar{m}\Phi^n$ with data on oxides with the NaCl structure. Data from table IV-3 . . .	78
- 4.	Test of relationship $\ell nK = A\ell n(2\bar{m}/\rho) + C$ with data on oxides with the NaCl structure. Data from table IV-3	79
V - 1.	The effect of the choice of $\gamma(v)$ on the isotherm for silver	98
- 2.	The dependence of the volume derivative of Gruneisen's parameter on specific volume	99
B - 1.	A schematic of the transmission u_5 and reflection u_2 of ultrasonic wave u_1 as it interacts with a seal. The K_i and Z_i are the wave vector and mechanical impedance, respectively	113
D - 1.	Frame for holding sample during polishing. The stainless steel piston floats freely in the cylinder. The polishing force can be varied by changing the length of the piston since the piston's weight is on the surface being polished	126
E - 1.	Circuit for the measurement ultrasonic velocity. Adapted from McSkimin (1964)	136
E - 2.	Diagram of the buffer rod and sample assembly and a schematic of the traveling elastic waves. Multiple reflections are ignored in the drawing for conceptual simplicity. Note that everything shown in the assembly is inside the pressure vessel	137
E - 3.	Block diagram of the electronics used	138

Figure		Page
E - 4.	Idealizations of the two electrical networks in figure III-3; v and i are the voltage and current between points A and B; V_B and V_C are voltages with respect to ground at points B and C	139
E - 5.	Schematic of equipment used to measure the mechanical impedance to shear waves of General Electric's Clear Seal	140
E - 6.	Mechanical impedance to shear waves of the silicone rubber, Clear Seal	141

SYMBOLS

A	Helmholtz free energy
A_k	amplitude of wave k
A_{ni}	transformation matrix
a	constant
a_i	components of a position vector
b	constant
C	constant
C_{ijkl}	components of the elastic stiffness tensor
C_V	specific heat at constant volume
D	determinant of coefficient matrix
D_{ij}	components of the dynamical matrix
E_n	energy in mode n
E_{vib}	lattice vibrational energy
F_i	reciprocal of travel time in the ith mode
f	frequency
G	shear modulus
K_s	adiabatic bulk modulus
K_T	isothermal bulk modulus
$\bar{k}$	wave vector
L	length of sample

m_s	mass of atom s
$\bar{m}$	mean atomic weight
$\bar{P}$	average pressure in the solid
P	hydrostatic pressure
q_i	an elastic parameter
S_{ijkl}	components of elastic compliance
T	temperature
t	time
U	internal energy
u_i	components of displacement vector
V	total volume
v_p	velocity of compressional waves
v_s	velocity of shear waves
$\bar{x}(\ell)$	position vector of 1st cell
z	mechanical impedance
α	volume thermal expansion
β	compressibility
γ	Gruneisen's parameter
γ_{DM}	Dugdale-MacDonald Gruneisen's ratio
γ_{SL}	Slater Gruneisen's ratio
Δ	seal thickness
$\bar{\Delta}$	vector to atomic nearest neighbor
δ_{jk}	kronecker delta

ε_{jk} Eulerian finite strain tensor

η porosity

λ_{ik} Christoffel constants

ξ third order term in the Birch-Murnaghan equation

ρ density

σ_{ij} components of stress tensor

$\phi(^{i}_{j})$ phase lag between elastic waves i and j

$\phi(V)$ configurational energy at volume V

$\phi_o(V)$ rest potential at volume V

$\psi(V)$ = $\phi(V)$ plus zero point vibrational energy

ω angular frequency or eigenfrequency

Subscripts:

p compressional wave

R Reuss averaging scheme

s shear wave

V Voigt averaging scheme

VRH Hill averaging scheme

Conventions:

$y,_x$ partial derivatives of y with respect to x

$\dot{y}$ time derivative of y

I. INTRODUCTION

Theoretically based equations of state relate properties of materials to pressure, temperature, and composition. With such equations of state, it is possible to extend laboratory measurements made at low pressures and moderate temperatures to the pressures and temperatures that exist in planetary interiors. Certain forms of these equations are used to reduce shock-wave data. Some of these equations of state are reviewed by Knopoff (1963) and Brush (1967). Examples of geophysical applications of these and of empirical equations of state are found in Birch (1961a, 1963), Clark and Ringwood (1964), and D. Anderson (1967a,b).

Of the empirical relations, a Birch-type equation (Simmons, 1964a) most satisfactorily relates an elastic property to density and composition. (The effect of crystal structure can be ignored to the level of approximation in these empirical equations.) A weakness of the empirical equations is that they cannot be extrapolated to high pressures and/or temperatures without corroborating measurements (such as the Hugoniot). Complete theoretical equations of state exist for pressures in the millions of bars and/or temperatures greater than 50,000° K. For pressures and temperatures corresponding to the interior of the earth, a basis for an equation of state is found in the quasi-harmonic theory of lattice vibrations, but the parameters in the resulting equation have to be determined experimentally. A difficulty is that these parameters vary with density. This dependence on density is a prime concern of this study.

For the purely empirical laws, it is assumed that data for a few key rocks and minerals can be cast into a law applicable to all geophysically interesting materials. For example, if the equations of state for important

end-member oxides were known, the equations of state of more complex minerals might be inferred through some mixing law. Detailed studies of several end members as a function of pressure or temperature are underway in several laboratories. Results are available for quartz (Thurston, et al., 1965), periclase (Chung, et al., 1964; Bogardus, 1965), alumina (Schreiber and O. Anderson, 1966), forsterite (Schreiber and O. Anderson, 1967), polycrystalline calcia (Soga, 1968), and rutile (Chung and Simmons, 1969).

In this report, several new materials are added to the list of those studied. The elastic properties, along with their pressure and temperature derivatives, were measured on single crystals of $MgO \cdot 3.0Al_2O_3$ spinel and magnetite and on polycrystals of $MgO \cdot 1.1Al_2O_3$ spinel and cadmium oxide (CdO). The temperature derivatives were omitted in the case of magnetite because several kilobars of confining pressure were required to obtain consistent data.

Often, only very small crystals of a substance are available. Cadmium oxide and high-pressure polymorphs such as stishovite are examples. In such cases, hot-pressing provides samples large enough to measure the elastic constants. Hot-pressed products are seldom free from pores. After repeated attempts to hot-press cadmium oxide, the best specimen still had a 3.8% porosity. This report includes an experimental study of the effect of porosity on the elastic constants and their pressure derivatives.

II. EFFECT OF SPHERICAL PORES ON THE ELASTIC CONSTANTS AND THEIR PRESSURE DERIVATIVES

For precise measurements of the elastic constants of a crystal, the specimen must have dimensions of several millimeters. Such relatively large crystals are not available for all materials. In addition, for less symmetrical crystal structures, elastic constants are more complex, and hence, more difficult to obtain. For these reasons, often it is simpler to study an isotropic hot-pressed product rather than a single crystal.

A hot-pressed specimen free from pores is difficult to manufacture. The porosity of most products is several percent. As in sintering (Mackenzie and Shuttleworth, 1949), the dynamics of hot-pressing favor formation of spherically shaped pores. An exception is the porosity caused by differential thermal contraction (Coble and Kingery, 1956). In this chapter, only spherically shaped pores are discussed. The goal is to relate the effective elastic properties to intrinsic elastic properties and porosity.

The seven largest porous glass samples were selected from a set of thirteen samples fabricated for an earlier study. The details of the manufacture of the samples can be found in Walsh, Brace, and England (1965) and England (1965). Each sample was cut into a right circular cylinder approximately 1.5 centimeters in diameter by 2 centimeters long. The ends were cut parallel to 6 minutes of arc and polished on a 1μ wheel. The pores within the samples are generally smaller than 0.1 millimeter, are almost spherical, and are not contiguous.

A variation on the Papadakis (1967) pulse-echo overlap method was used to measure compressional and shear-wave velocities in the specimen. The geometry of the sample and the pressure system is shown in figure II-1. A

plug made of 4340 steel hardened to R_c 55 was used as a sound transmission line and as the upper end of the pressure vessel. Peselnick, et al. (1967) originally showed the advantages of such an arrangement: elimination of electrical leads into the vessel and of the need to bond a transducer to each sample. The transducers can be bonded permanently to the plug. An X-cut quartz transducer was epoxied to one steel plug, and an ac-cut quartz transducer was epoxied to another. Both transducers were 1/2 inch in diameter and cut to a 5-MHz fundamental.

The sample-to-plug bonding was Eastman 910 quick-setting cement. This cement is ideal because it is not a filler and requires close juxtaposition of the surfaces before it will harden. To remove the sample, the bond was softened by baking the plug-sample assembly at 150° C for half an hour. This baking did not damage the epoxy seals.

The pressure system was a standard piston and cylinder apparatus capable of 10 kilobars. Because the porous glass samples were relatively fragile, pressures were kept at less than 3 kilobars. The pressure medium was petroleum ether, and the pressure was measured on a recently calibrated Heise gauge. Accuracies of the pressure measurement are discussed in chapter III.

The ultrasonic round-trip travel time in the sample can be obtained by pulsing the transducer once, by watching the multiple reflections inside the specimen, and by triggering the oscilloscope sweep so that these reflections appear superimposed on the cathode ray tubes (CRT). The reciprocal of the triggering frequency becomes the travel time. A schematic of the signal seen at the transducer is shown in figure II-2. If the oscilloscope is triggered at the times indicated by vertical hash marks and the times are chosen properly, the reflections become superimposed. The sweep

rate must be such that a complete sweep is shorter than the time between hash marks. Phase stability of event A with respect to sweep triggering was obtained by use of the same source frequency divided by 64. The result is an event A for every 64 sweeps across the scope. The reflected signals decay completely between events A.

Oscilloscope clutter is reduced by trace-intensity modulation which highlights a chosen time period. Event A, with a variable delay line, triggers a variable length pulse that then is applied to the Z-axis of the oscilloscope. For best signal-to-noise ratio, a time that included only reflections B and C was selected.

By use of the alternate trace feature of a dual-trace scope, with inputs connected in parallel, reflections B and C are obtained on separate traces. This allows selective amplifications of the reflections and choice of their vertical separation; both features aid identification of the exact overlap. Typical reflections of a shear-wave signal are shown in figure II-3. The bottom traces match exactly, whereas the triggering frequency for the top two traces is mismatched by one part in 10^3. This sensitivity in the identification of the overlap in this new method is improvement of an order of magnitude in precision over the pulse-mercury delay-line technique frequently used to measure velocities of rocks. More than one order of magnitude improvement in accuracy exists because the signal in the delay-line method passes through media with different filter characteristics before the comparison. Points between dissimilar waveforms then must be matched. Systematic errors are likely. A schematic of the electronic components is shown in figure II-4.

Velocity data, lengths, porosities, and densities of the samples are given in table II-1. Raw data are listed in Appendix G. Because pores

were not interconnected, porosity could be measured by a comparison of the dry weight and the weight submerged in carbon tetrachloride, i.e., by measurement of the density. The uncertainty in porosity reported in table II-1 is ±0.01. Velocities are valid to 0.1%. The uncertainty in P-wave pressure derivatives is $\pm 1.8 \times 10^{-3}$ km/sec kb and that of S-wave pressure derivatives is $\pm 1.0 \times 10^{-3}$ km/sec kb. These uncertainties in the derivatives are caused by scatter in measured velocities rather than by uncertainties in pressure.

The results (table II-1) are plotted in figures II-5, II-6, and II-7. Mackenzie (1950) suggested a thick spherical shell embedded in a matrix as a model of material containing spherically shaped pores that were distributed homogeneously. The properties of the thick shell are taken equal to the intrinsic elastic constants; the elastic properties of the matrix are equal to the elastic properties of the overall porous medium. The theory can be recast as

II-1)

$$K' = K\left(\frac{1 - \eta}{1 + \frac{3}{4}\frac{K}{G}\eta}\right)$$

$$G' = G\left[1 - 5\eta\left(\frac{3K + 4G}{9K + 8G}\right)\right]$$

$$v_p' = v_p\left[\frac{K' + \frac{4}{3}G'}{\left(K + \frac{4}{3}G\right)(1 - \eta)}\right]^{1/2}$$

$$v_s' = v_s\left[\frac{G'}{G(1 - \eta)}\right]^{1/2}$$

where K', G', v_p' and v_s' refer to the bulk modulus, the shear modulus, the compressional velocity, and the shear velocity of the porous medium, respectively; η is porosity. The trace of equations II-1 are included in figures II-5, II-6, and II-7. The agreement is good at porosities less

than 10% of values commonly found in hot-pressed samples. A similar agreement was observed for the static bulk modulus (Walsh, Brace, and England, 1965).

For sufficiently low porosities, approximations for K' and G' are

II-2)
$$K' = K\left\{1 - \eta\left[1 + \frac{3}{4}\left(\frac{K}{G}\right)\right]\right\}$$
$$G' = G\left[1 - \frac{5}{3}\eta\left(1 + \frac{1}{\frac{9}{4}\frac{K}{G} + 2}\right)\right].$$

The pressure derivatives of equations II-2 are

II-3
$$\frac{\partial K'}{\partial P} = \frac{\partial K}{\partial P}\left\{1 - \eta\left[1 + \frac{3}{2}\left(\frac{K}{G}\right)\right]\right\}$$
$$+ \frac{\partial G}{\partial P}\left[\eta\left(\frac{3}{4}\right)\left(\frac{K}{G}\right)^2\right] - \left(\frac{\partial \eta}{\partial P}\right)K\left[1 + \frac{3}{4}\left(\frac{K}{G}\right)\right]$$
$$\frac{\partial G'}{\partial P} = \frac{\partial G}{\partial P}\left\{1 - \frac{5}{3}\eta\left[1 + \frac{2}{\left(\frac{9}{4}\frac{K}{G} + 2\right)^2}\right]\right\}$$
$$- \frac{5}{3}G\frac{\partial \eta}{\partial P}\left(1 + \frac{1}{\frac{9}{4}\frac{K}{G} + 2}\right) - \frac{\partial K}{\partial P}\frac{\frac{15}{4}\eta}{\left(\frac{9}{4}\frac{K}{G} + 2\right)^2}$$

From the equation for K' in equations II-1, it is easily shown that $\left(\frac{\partial \eta}{\partial P}\right) = -\left(\frac{3}{4}\right)\left(\frac{\eta}{G}\right)$. Assume linear K and G, i.e.,

II-4)
$$K = K_o + \left(\frac{\partial K}{\partial \bar{P}}\right)_o \bar{P}$$
$$G = G_o + \left(\frac{\partial G}{\partial \bar{P}}\right)_o \bar{P}$$

where $\bar{P}$ is the average pressure in the solid. Note that $\bar{P} = \dfrac{P}{(1-\eta)^{2/3}}$, and that $\left(\dfrac{\partial K,G}{\partial P}\right)_o = \left(\dfrac{\partial K,G}{\partial \bar{P}}\right)(1-\eta)^{-2/3}$.

Equations II-3 become

$$\text{II-5)} \qquad \left(\frac{\partial K'}{\partial P}\right)_o = \left(\frac{\partial K}{\partial \bar{P}}\right)\left\{1 - \eta\left[\frac{1}{3} + \frac{3}{2}\frac{K}{G}\right]\right\}$$

$$+ \left(\frac{\partial G}{\partial \bar{P}}\right)\left[\eta\left(\frac{3}{4}\right)\left(\frac{K}{G}\right)^2\right] + \frac{3}{4}\left(\frac{K}{G}\right)\eta\left[1 + \frac{3}{4}\left(\frac{K}{G}\right)\right]$$

$$\left.\frac{\partial G'}{\partial P}\right)_o = \frac{\partial G}{\partial \bar{P}}\left\{1 - \left[\eta\ 1 + \frac{\frac{10}{3}}{\left(\frac{9}{4}\frac{K}{G} + 2\right)^2}\right]\right\}$$

$$+ \frac{5}{4}\eta\left(1 + \frac{1}{\frac{9}{4}\frac{K}{G} + 2}\right) - \frac{\partial K}{\partial \bar{P}}\frac{\frac{15}{4}\eta}{\left(\frac{9}{4}\frac{K}{G} + 2\right)^2}.$$

For $\eta = 0$, $\left.\partial K/\partial \bar{P}\right)_o = \left.\partial K/\partial P\right)_o$. Therefore, for small η,

$$\text{II-6)} \qquad \left.\frac{\partial K}{\partial P}\right)_o = \frac{\partial K'}{\partial P}\left\{1 + \eta\left[\frac{1}{3} + \frac{3}{2}\left(\frac{K}{G}\right)\right]\right\}$$

$$- \eta\left(\frac{3}{4}\right)\left(\frac{K}{G}\right)\left[1 + \left(\frac{K}{G}\right)\left(\frac{3}{4} + \frac{\partial G'}{\partial P}\right)\right]$$

$$\left.\frac{\partial G}{\partial P}\right)_o = \frac{\partial G'}{\partial P}\left\{1 + \eta\left[1 + \frac{\frac{10}{3}}{\left(\frac{9}{4}\frac{K}{G} + 2\right)^2}\right]\right\} - \frac{5}{4}\eta\left(1 + \frac{1}{\frac{9}{4}\frac{K}{G} + 2}\right) + \frac{\partial K'}{\partial P}\frac{\frac{15}{4}\eta}{\left(\frac{9}{4}\frac{K}{G} + 2\right)^2}.$$

Except for the inclusion of the average pressure $\bar{P}$ the derivation is equivalent to that of O. Anderson, et al. (1968). Equations II-6 provide poor fits to the pressure derivatives obtained for the porous glass. The assumption of a linear dependence of K and G on pressure (eq. II-4) is particularly poor for glass, and this may have caused the discrepancy. As

presented in chapter III, the elastic properties and their pressure derivatives were obtained for both a single-crystal spinel and for a porous polycrystalline spinel. Although the (MgO/Al_2O_3) ratios differed, the comparison should be valid. As will be shown in chapter III, the elastic properties are weak functions of stoichiometry. Schreiber and O. Anderson (1967) obtained the pressure derivatives of a 6% porous forsterite. Kumazawa and O. Anderson (1969) did the same for single-crystal forsterite. These data and values corrected according to equations II-6 are listed in table II-2. The corrections were generally inadequate.

Although equations II-1 provide adequate corrections to v_p, v_s, K, and G, the values of $\frac{\partial K}{\partial P}$ and $\frac{\partial G}{\partial P}$ given by equations II-6 are unreliable, perhaps because of the combined effect of the assumptions of spherical pores, noninteraction of stress fields, and linearity of the elastic parameters with pressure.

TABLE II-1.- ELASTIC PROPERTIES OF POROUS GLASS. (THE UNITS OF DENSITY AND LENGTH ARE cgs, OF PRESSURE AND ELASTIC MODULI ARE kb, AND OF VELOCITY km/sec.)

Sample identification							
Property	F	680	750	30	29	27	720
Porosity	0	0.05	0.11	0.33	0.39	0.46	0.50
Density	2.511	2.390	2.232	1.672	1.534	1.356	1.245
Length	1.3160	2.4300	2.3012	1.5878	1.7496	2.2298	2.7437
K_T*	458	413	362	210	179	135	120
K_S	460	401	383	211	199	148	
G	302	276	235	145	120	100	86
v_p	5.862	5.673	5.584	4.920	4.845	4.555	
v_s	3.469	3.400	3.245	2.945	2.800	2.719	2.620
$\frac{\partial(F/F_o)_p}{\partial P} \times 10^3$	.32	.00	-.45	-1.42	-2.37	-3.92	
$\frac{\partial(F/F_o)_s}{\partial P} \times 10^3$	1.17	-.36	-1.28	-4.01	-4.50	-6.10	-6.49
$\left(\frac{\partial v_p}{\partial P}\right) \times 10^3$	-2.41	-4.6	-7.7	-14.8	-20.5	-29.1	
$\left(\frac{\partial v_s}{\partial P}\right) \times 10^3$	1.5	-4.0	-7.1	-16.5	-17.8	-23.3	-24.3
$\left(\frac{\partial K}{\partial P}\right)$	-.05	.59	.53	.74	.05	-.21	
$\left(\frac{\partial G}{\partial P}\right)$	.93	.03	-.39	-.93	-.86	-.98	-.87

*From Walsh, Brace, and England, 1965.

TABLE II-2.- COMPARISON OF THE PRESSURE DERIVATIVES

FOR POROUS AND NONPOROUS MATERIALS

	Spinel			Forsterite		
Porosity	0.02	0*	0**	0.06	0*	0**
$\frac{\partial K}{\partial P}$	5.40	5.60	4.58	4.87	5.38	5.37
$\frac{\partial G}{\partial P}$	.82	.82	.75	1.3	1.34	1.80

*Reduced to zero porosity through application of equations II-6.

**Voigt-Reuss-Hill averages of single crystal data.

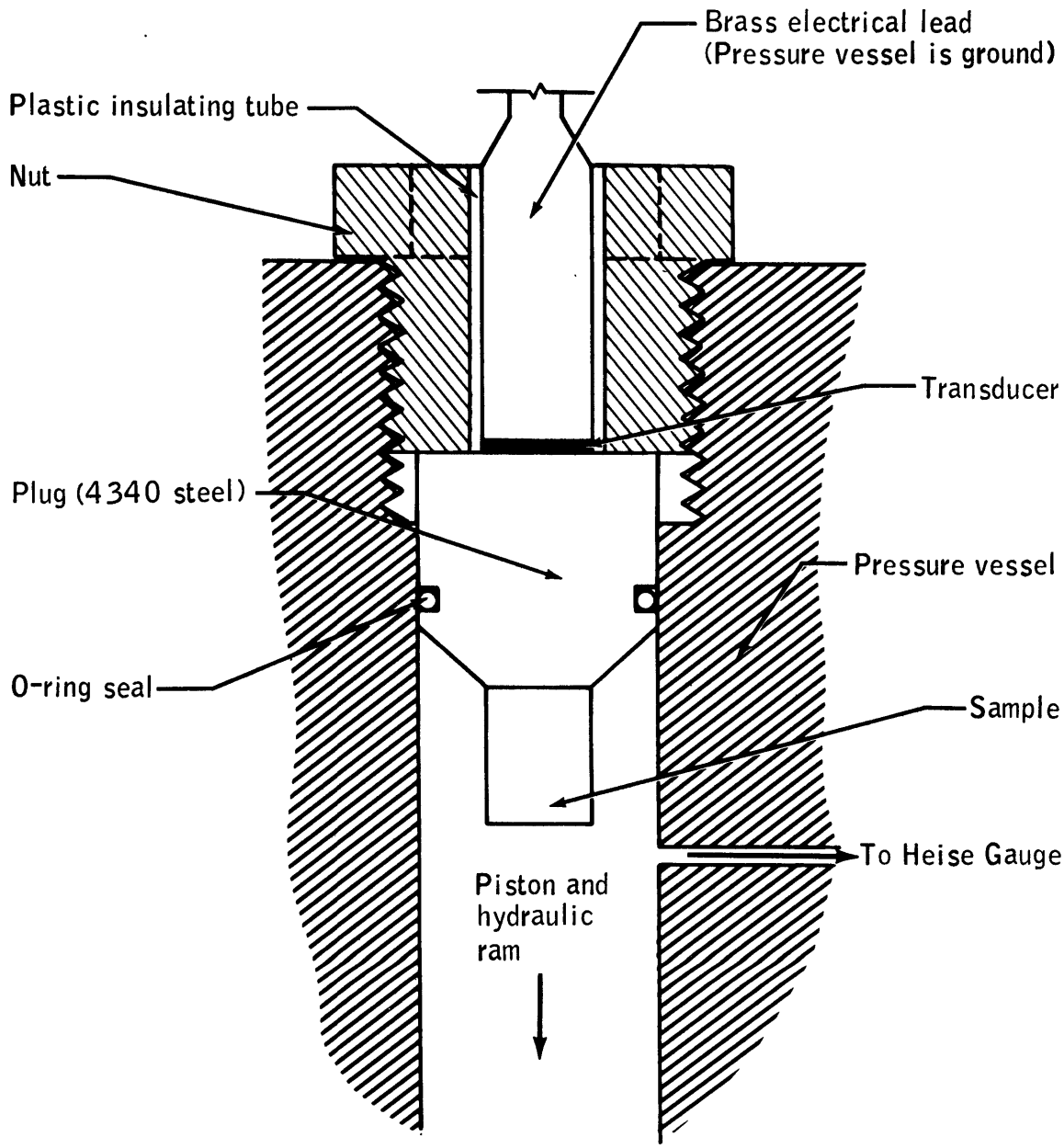

Figure II-1.- Arrangement of specimen in pressure vessel. The glass sample was bonded to the plug with Eastman 910 quick-setting cement. The transducer is outside the pressure envelope.

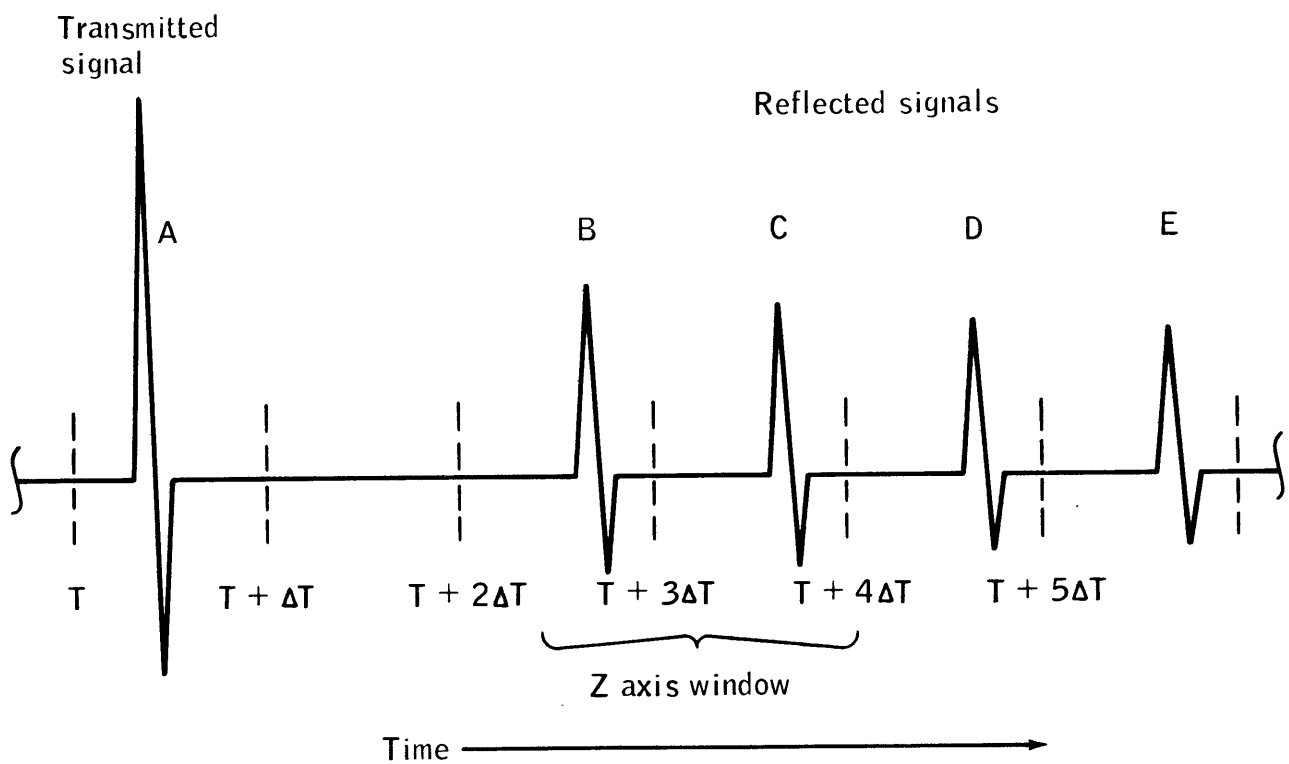

Figure II-2.- Idealized signals at transducer. The vertical hash marks represent the beginning of each sweep on the CRT. Because of Z-axis modulation, only the two sweeps containing reflections B and C are seen.

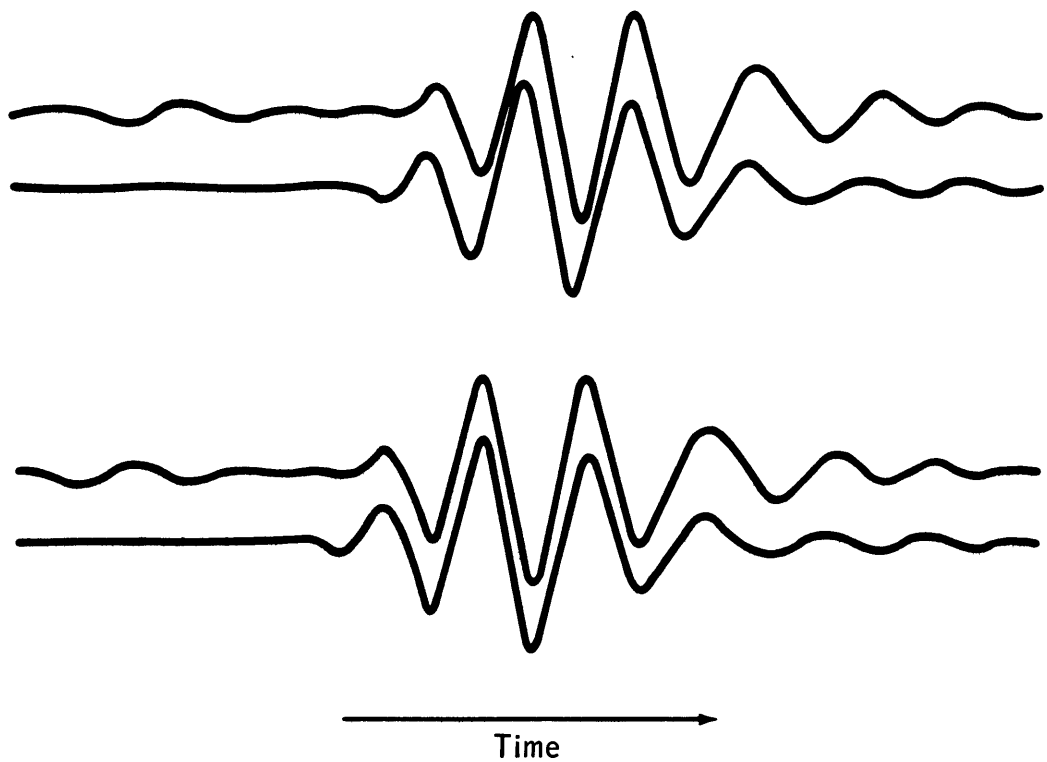

Figure II-3.- Oscilloscope traces of typical shear wave signals. The lower two traces show reflections B and C in a matched condition. The upper traces are mismatched by 1 part in 10^3.

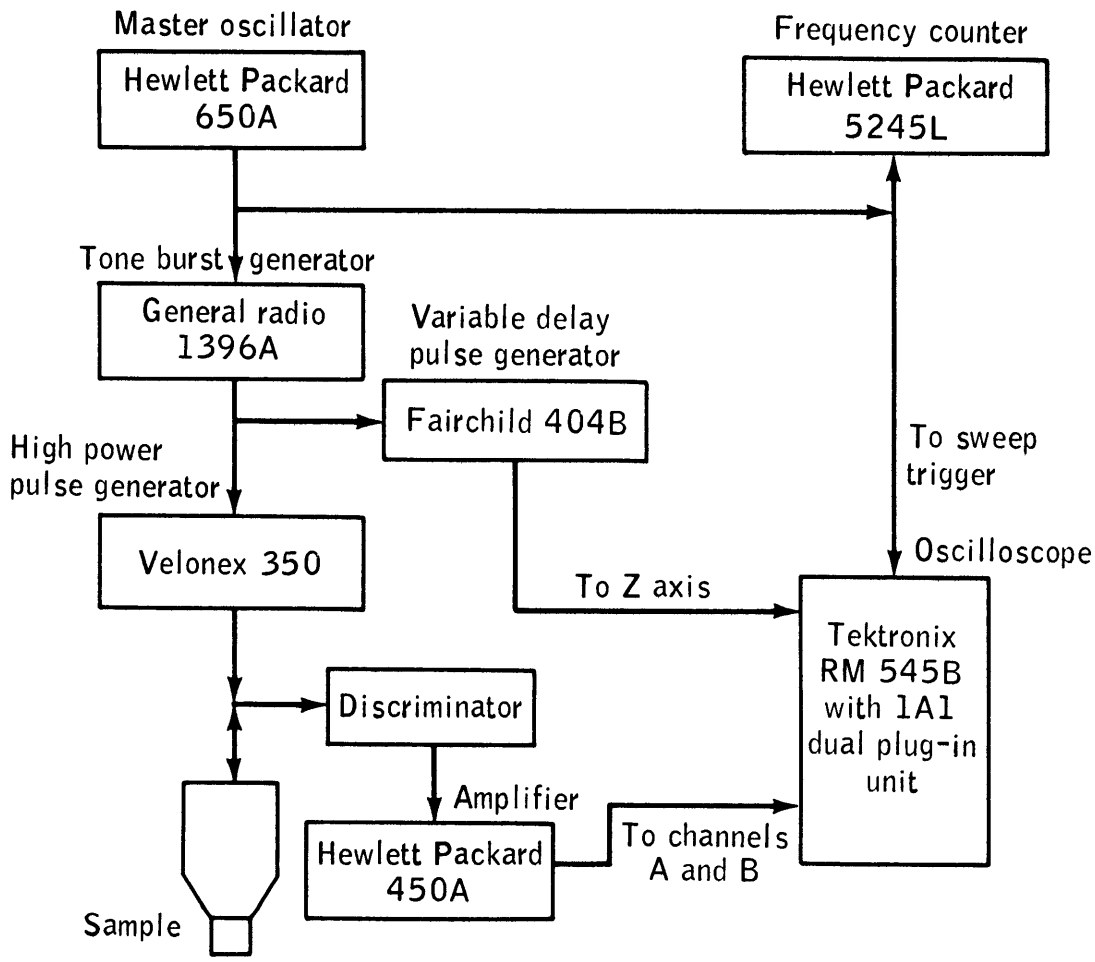

Figure II-4.- Block diagram. The discriminator is a simple resistor-bucking diode divider that provides high-voltage protection for the amplifier. Also included is a passive filter designed to reduce 60-cycle ac pickup.

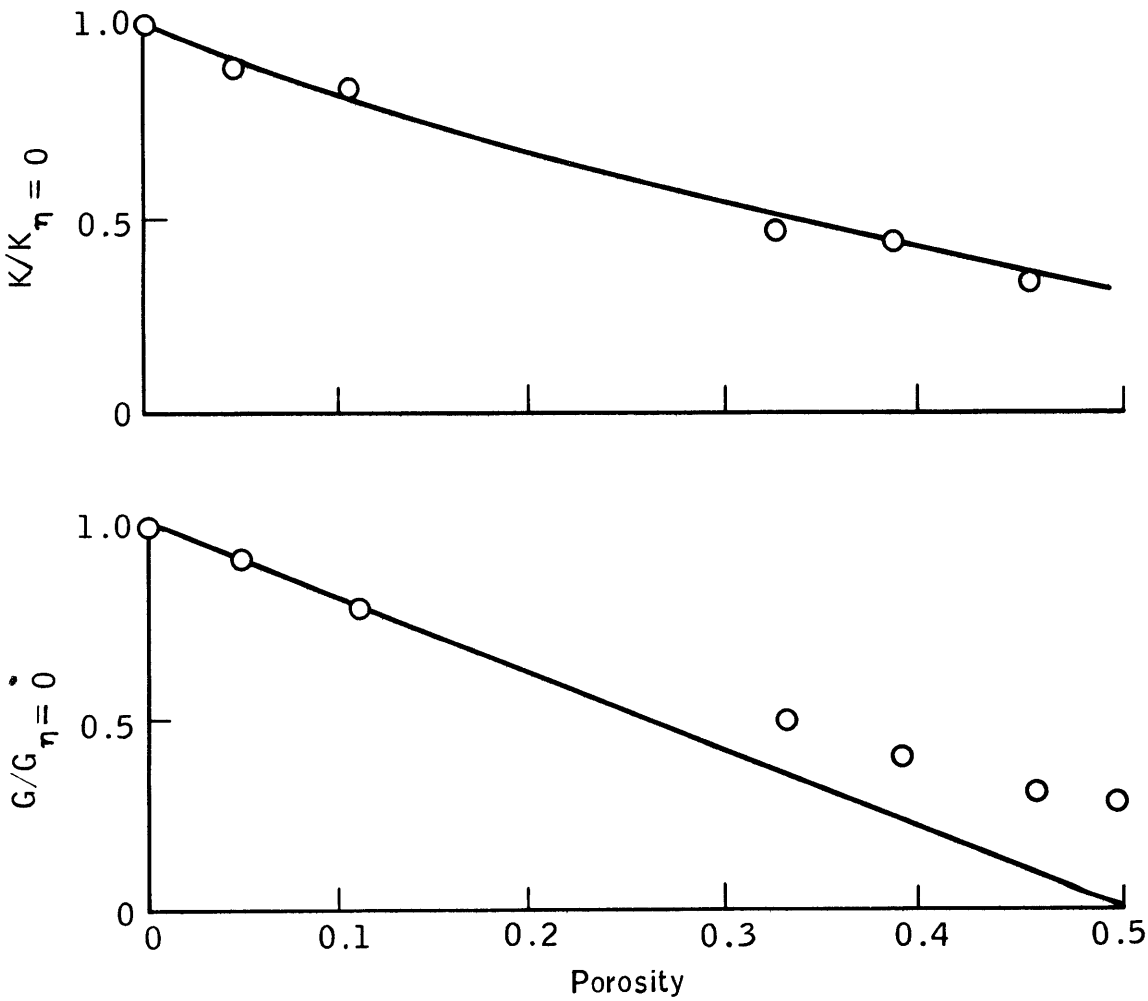

Figure II-5.- Effect of porosity on bulk and shear moduli. The lines are the trace of the theoretical expression equation II-1.

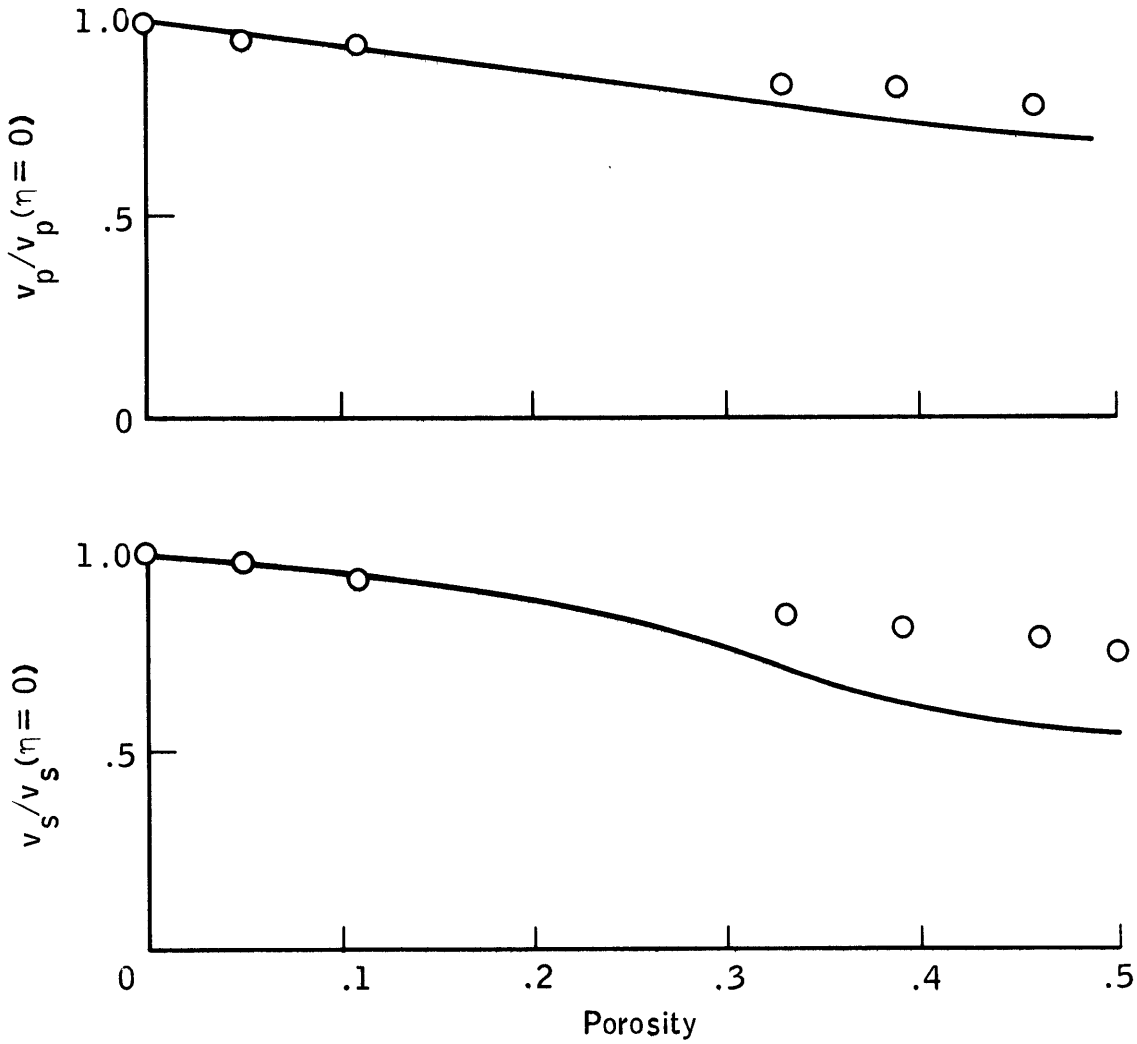

Figure II-6.- Effect of porosity on sound velocities. The lines are the traces of the theoretical expression equation II-1.

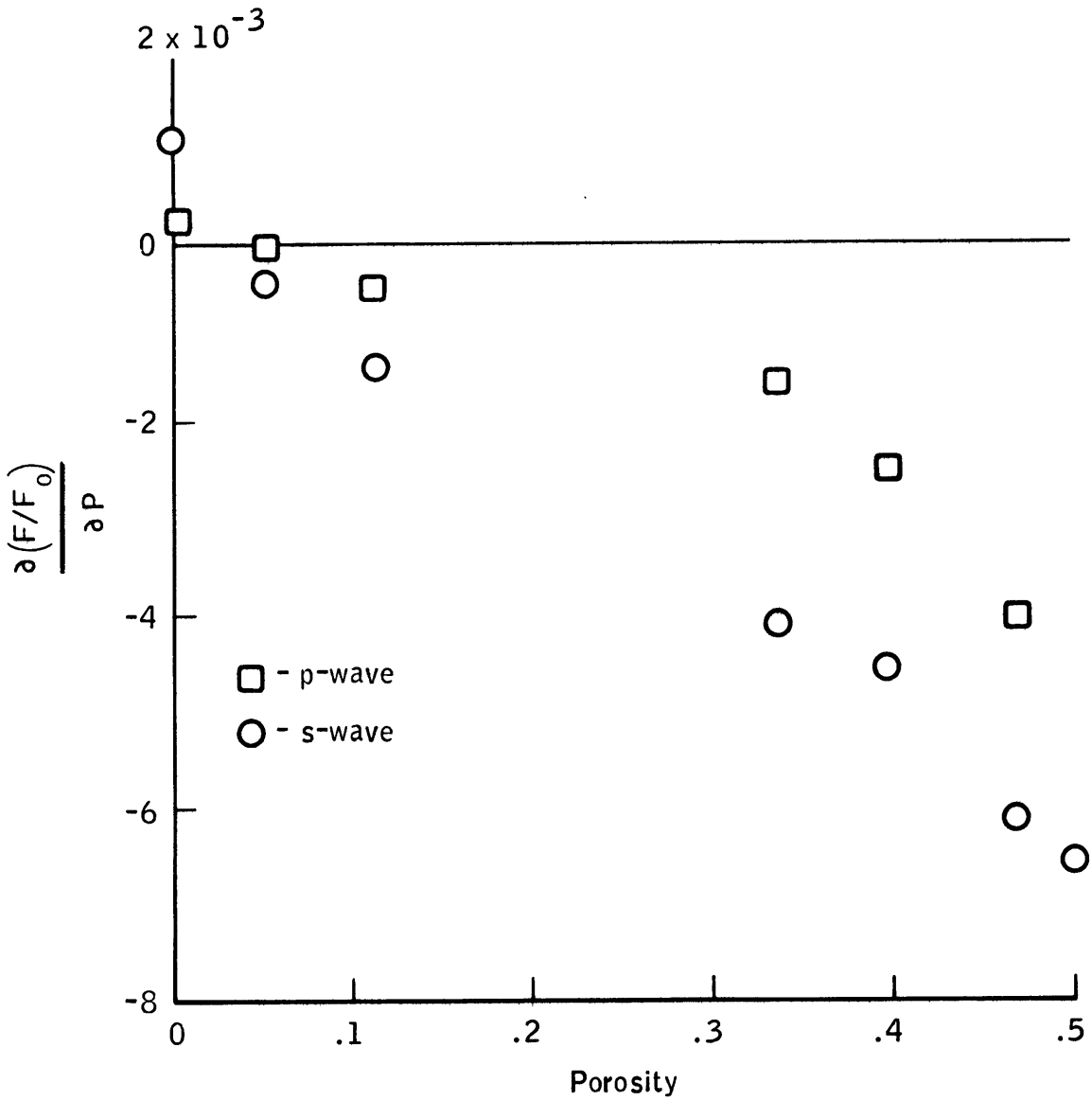

Figure II-7.- Effect of porosity on $\partial(F/F_o)/\partial P$.

III. THE ELASTIC PROPERTIES OF SPINEL, MAGNETITE, AND CADMIUM OXIDE

The Samples

Ultrasonic velocities and their pressure and temperature derivatives were measured on a single-crystal spinel. Velocities and their pressure derivatives were measured on a polycrystalline, hot-pressed spinel. At ambient pressure, cracks in the polycrystalline spinel badly attenuated the signals so that the temperature derivatives, which were obtained at ambient pressure, could not be measured. A few kilobars of confining pressure closed these cracks.

A microprobe analysis of the gem-quality single-crystal spinel yielded $MgO \cdot 3.0Al_2O_3$. (Compositions of the samples are listed in table III-1.) The matrix of the polycrystalline spinel had a composition of $MgO \cdot 1.1Al_2O_3$. The polycrystalline specimen was degraded by inclusion of nearly pure alumina (Al_2O_3). These inclusions occupied less than 5% volume and were not distributed homogeneously. Because velocity measurements taken at several points across the specimen were not noticeably different, the effect of the inclusions is considered small.

Velocities in a natural magnetite crystal were measured as a function of pressure. Although the specimen was superior to most natural magnetite, it contained many flaws. Like the polycrystalline spinel, a confining pressure was required for acceptable signal-to-noise ratios. Internally consistent data were taken between 5 and 10 kilobars. These results were extrapolated to obtain the zero pressure parameters.

The microprobe analysis showed the magnetite to be essentially pure iron oxide (table III-1). Such analyses are insensitive to the oxidation

state. A chemical analysis of Newhouse and Glass (1936) of magnetite collected from the same area (Mineville, New York) showed an FeO to Fe_2O_3 ratio of 0.45. All their listed concentrations (table III-1) were close to the microprobe results.

Several cadmium oxide polycrystalline samples were hot-pressed. The best of these had a density that was 96.2% of X-ray density. Velocities and their pressure and temperature derivatives were measured on this specimen. The successful manufacture of the specimen involved sieving reagent-grade cadmium oxide to obtain a 1μ powder. The powder was packed into a 1-inch-diameter graphite die with an ultrasonic tamper. The die, mounted in a press, was heated in an oxidizing atmosphere to 950° C and was maintained at that temperature for several hours to calcine off absorbed carbon dioxide. A pressure of 3000 psi was applied for 3 hours while the assembly cooled. Although the microprobe analysis was relatively insensitive to carbon, an upper limit of 2% could be assigned to the cadmium carbonate concentration. The other contaminants are listed in table III-1.

The weight of each sample when dry and the weight of the sample after being immersed in carbon tetrachloride were used to obtain the density. The balance was a Sartorius precision instrument.

The single-crystal specimens were oriented by use of the Laue X-ray technique (Binnie and Geib, 1959) to ±1/2 degree, and the faces were cut parallel to the (100) and (110) crystallographic planes. The cutting and polishing techniques are described in appendix D. The polished faces were flat to a few wavelengths of sodium light and were parallel to 3 minutes of arc. The dimensions, measured with a Starrett T221L high-precision micrometer, and the densities are listed in table III-2.

The Velocity Measurements

Ultrasonic velocities in magnetite were measured at 5 MHz. The phase-comparison technique was used on the magnetite rather than the more convenient pulse-echo overlap (PEO) method described in chapter II. The techniques, equipment, and analysis developed for phase comparison and an error study applicable to all measurements are presented in appendix E. The phase-comparison method is less restrictive because the transducer is isolated from the sample by a buffer rod. This arrangement allows velocity to be measured over extended temperature ranges. The phase-comparison technique could be used at temperatures greater than 500° C, at which most transducers are ineffective. The phase-comparison technique should be more accurate because the simple bond geometry facilitates a calculation of the phase lag at interfaces. In practice, the result of the calculation is inaccurate, and reducing the phase-lag effect to near zero by the use of very thin bonds, as in the PEO technique, is undoubtedly the better approach. The phase-comparison technique is slightly more sensitive than the PEO method. In the phase-comparison technique, the signals are added electrically, and the maximum is determined unambiguously; for PEO, two traces are compared visually. The principal advantages of the PEO method are a much better signal-to-noise ratio, steady-state operation of all components, and less opportunity for operator error.

The PEO equipment assembly used to obtain velocities in all samples but the magnetite is shown in figure III-1. The function of the assembly (Chung, et al., 1969) is similar to that described for the apparatus used to measure velocity in porous glass (chapter II). In this case, rather than a simple pulse, a pulse envelope of 20 MHz continuous wave (cw) is

transmitted. Exact overlap could be determined to less than one part in 10^4. The transducers were quartz, either X- or AC-cut, were polished for third overtone operation at a fundamental of 20 MHzs; they were coated coaxially. The transducer was bonded to the sample with a 50/50 phthalic anhydride and glycerine mixture that was chosen for its resistance to dissolution in petroleum ether.

Pressures of 7 kilobars (10 kilobars in the case of magnetite) were achieved in a piston-in-cylinder pressure vessel. The useful volume inside the vessel was 1-1/4 inches in diameter by 8 inches long. The pressure medium, petroleum ether, was chosen for its low viscosity. For instance, kerosene becomes so viscous at 10 kilobars that the manganin pressure sensor is damaged.

A recently calibrated Heise bourdon tube gauge was used to measure pressure in the 7-kilobar runs. Above 7 kilobars, a manganin coil was used. In all cases, accuracies of the pressure meassurements were better than 0.5%. Because these 0.5% errors were systematic, they are not additive, and pressure differences are good to approximately 0.5%. The temperature in the pressure vessel was held at 25.0° C by a water jacket and a temperature-controlled bath.

All measurements as a function of temperature were made at 1 bar in a refrigerated, circulating, ethanol bath. Temperatures between 25° C and minus 35° C were obtained. Temperature could be held to ±0.1° C.

Results

As in chapter II, the oscilloscope sweep frequency F is the reciprocal of travel time in the sample. F/F_o as a function of pressure or temperature (F_o refers to ambient pressure or temperature) can be related

to changes in the elastic constants (table III-3). Figures III-2 to III-8 are the plots of F/F_o for the several samples. Tables III-4, III-5, and III-6 are lists of elastic properties derived from the previously mentioned figures, from the equations in table III-3, and from equations in the review of the elasticity of crystalline solids presented in appendix C.

Accuracy was limited by the uncertain effect of the bonds between the transducer and the sample. Great care was taken to reduce the thickness of the bonds, but it is still probable that the thickness contributed a few degrees of phase lag. Measuring the thickness of the sample and transducer separately and then when bonded yielded an upper limit to the bond thickness of 1μ. For an estimated velocity of 1 km/sec in the bond, the uncertainty in the round-trip travel time would be 2×10^{-9} seconds. Because travel times were generally greater than 6×10^{-6} seconds, the error in velocity would be less than three parts in 10^4. A precise treatment of bond effect may be found in appendix B.

Accuracies of pressure and temperature derivatives are determined by the scatter in the data, by the uncertainty in the pressure of 0.5%, and by the uncertainty in the temperature of ±0.1° C. These errors are discussed in appendix E.

Only three independent elastic constants exist for crystals that have cubic symmetry. One of the four velocities obtained on each of the single crystals is redundant and serves as a check. It is easily shown that (appendix C)

$$\text{III-1)} \qquad v_s^2(110)[110] = v_s^2(110)[100] - \left[v_p^2(110) - v_p^2(100)\right]$$

where $v_s(ijk)[lmn]$ is the shear-wave velocity normal to the (ijk) crystallographic plane, $[lmn]$ is its displacement vector, and $v_p(ijk)$ is the compressional wave velocity normal to the (ijk) plane. In addition, it is easily shown that

$$\frac{\partial}{\partial\chi}\left(\frac{F}{F_o}\right)(100)[110] = \frac{1}{v_s^{\,2}(110)[110]}\left\{v_s^{\,2}(110)[100]\frac{\partial}{\partial\chi}\left(\frac{F}{F_o}\right)(110)[100]\right.$$

$$\text{III-2)}\qquad \left.-\left[v_p^{\,2}(110)\frac{\partial}{\partial\chi}\left(\frac{F}{F_o}\right)(110) - v_p^{\,2}(100)\frac{\partial}{\partial\chi}\left(\frac{F}{F_o}\right)(100)\right]\right\}$$

where χ is pressure or temperature. The parameters computed from equations III-1 and III-2 are included in table III-4. These derived parameters in the case of spinel are in excellent agreement with the measured parameters. The difference between the derived and the measured velocities for the magnetite was less than 0.5%. The check involves small differences of large numbers. For magnetite, the inaccuracy of the check of velocity was 1%, and the inaccuracy of the check of pressure derivative was approximately 6%. Although agreement in velocity was excellent, agreement of pressure derivatives for magnetite was relatively poor. It is likely that pressure derivatives were influenced to an unknown extent by the flaws in the natural magnetite crystal. Intrinsic derivatives in the magnetite should not differ by more than 10% or 20% from the measured derivative, because most cracks were closed in the 5- to 10-kilobar range in which the measurements were made.

Dorasiwami (1947) measured the elastic constants of magnetite and obtained $C_{11} = 2.70$, $C_{12} = 1.08$, $C_{44} = 0.987$, and $K = 1.62$ megabars. The new zero pressure constants, $C_{11} = 2.676$, $C_{12} = 1.056$, $C_{44} = 0.953$,

and $K = 1.596$ megabars are in fair agreement. Dorasiwami did not report the composition of his magnetite.

O. Anderson (1968a) discussed the significance of the negative pressure derivatives of v_s found in some oxides. His examples, zinc oxide and α-quartz, were not nearly as extreme as is magnetite ($\frac{\partial v_s}{\partial P}$ (zinc oxide) $= -0.0032$, $\frac{\partial v_s}{\partial P}$ (α-quartz) $= -0.0034$, and $\partial v_s/\partial P$ (magnetite) $= -0.025$). Anderson's theory applies to oxides with relatively low shear moduli and low atomic coordination. Although neither is true of magnetite, an alternative explanation is not apparent.

The polycrystalline spinel was 2% porous. If the corrections for porosity discussed in chapter II are applied, the corrected values for the polycrystalline sample are close to those of the single crystal (table III-4). Verma (1960) and Schreiber (1967, 1968) list data for spinel. Their compositions were $MgO \cdot 3.5Al_2O_3$ (Verma) and $MgO \cdot 2.61Al_2O_3$ (Schreiber). A comparison with the new data for $MgO \cdot 1.1Al_2O_3$ and for $MgO \cdot 3.0Al_2O_3$ is shown in table III-7. No strong systematic variation of the elastic properties exists with stoichiometry. The factor of 2 difference in Schreiber's value of $(\frac{\partial K_s}{\partial T})_P$ compared with the new data (table III-7) has its origin in the difference between Schreiber's value of $(\frac{\partial v_p}{\partial T})_P$, -0.00031 (unpublished data), and the new $(\frac{\partial v_p}{\partial T})_P$, -0.000441. Pointon and Taylor (1968) measured $v_p(100)$ and $v_p(110)$ in a spinel at 4.2° K. From these velocities and the Cauchy relation, the three elastic constants listed in table III-8 were inferred. The use of the Cauchy relation for this purpose appears to be satisfactory because the new data reported here for spinel obey the Cauchy relation. An extrapolation of the new temperature data falls reasonably close. The small difference between the C_{11} may be caused by the smaller thermal contribution to the dynamic

elastic constants at temperatures near absolute zero. Because the new temperature derivatives are consistent with the data of Pointon and Taylor and are internally consistent, the derivatives are probably correct.

The thermal expansion of cadmium oxide was needed to find $(\partial q/\partial T)_P$ where q is any elastic constant. The thermal expansion of cadmium oxide had not been measured. A platinum-rhodium ribbon furnace (Smith, 1963) in a Norelco X-ray diffractometer was used to obtain lattice spacing as a function of temperature to 847° C. Magnesium oxide mixed with cadmium oxide powder provided a standard. Data on magnesium oxide (Skinner, 1957) were used to calibrate the 2θ angles. The calibrated data are shown in figure III-9. The National Bureau of Standards value for the 27° C (111) lattice dimension of cadmium oxide is 2.712 Å. This compares favorably with the measured dimension of 2.709 Å. The measured volume thermal expansion of cadmium oxide is $(32 \pm 1) \times 10^{-6}$.

TABLE III-1.- CHEMICAL COMPOSITIONS OF THE SAMPLE. (WEIGHT PERCENT OF THE OXIDE).

	Spinel single crystal	Spinel polycrystal	CdO polycrystal	Magnetite single crystal	Magnetite (Mineville)*
MgO	11.40	25.82	0.11	0.08	Trace
Al_2O_3	86.99	73.23	.00	.01	.21
Fe_2O_3	.11	.08	.08	>99.00	68.85
FeO					30.78
CdO			>98.00		
SiO_2			.00	.00	.27
MnO_2				<.10	
TiO_2				<.10	
CaO			.13	.01	Trace

*From Newhouse and Glass (1936).

TABLE III-2.- DENSITIES AND LENGTHS OF THE SAMPLES

Sample	Origin	Density	L[100]	L[110]	Porosity
Spinel	Synthetic	3.6245	1.2767	1.1032	--
Polyxtal spinel	Synthetic	3.510	.5632**	--	0.02
Magnetite	Lyon Mountain, N.Y.	5.163	1.2923	1.3658	--
Cadmium oxide	Synthetic	7.8438	1.2416*	--	.038

*Units are cgs.

**In the case of polycrystalline samples, only one length is listed and it does not refer to a crystallographic direction.

TABLE III-3.- EQUATIONS USED TO REDUCE DATA*

$$v_i = 2LF_i$$

$$\left(\frac{\partial v_i}{\partial P}\right)_T = v_i^{\,o}\left(-\frac{1}{3K_T} + \frac{\partial\left(\frac{F}{F_o}\right)_i}{\partial P}\right)$$

$$\left(\frac{\partial v_i}{\partial T}\right)_P = v_i^{\,o}\left(\frac{\alpha_v}{3} + \frac{\partial\left(\frac{F}{F_o}\right)_i}{\partial T}\right)$$

$$q_i = \rho v_i^{\,2}$$

$$\left(\frac{\partial q_i}{\partial P}\right)_T = q_i^{\,o}\left(\frac{1}{3K_T} + 2\,\frac{\partial\left(\frac{F}{F_o}\right)_i}{\partial P}\right)$$

$$\left(\frac{\partial q_i}{\partial T}\right)_P = q_i^{\,o}\left(-\frac{\alpha_v}{3} + 2\,\frac{\partial\left(\frac{F}{F_o}\right)_i}{\partial T}\right)$$

*F is the reciprocal of travel time, L is sample length, q_i is an appropriate constant or combination of constants, and naught refers to ambient.

TABLE III-3.- EQUATIONS USED TO REDUCE DATA* - Concluded

For isotropic materials

$$K_s = \rho\left(v_p^{\,2} - \frac{4}{3} v_s^{\,2}\right)$$

$$G = \rho\, v_s^{\,2}$$

$$\left(\frac{\partial K_s}{\partial P}\right)_T \cong \frac{1}{3} + 2\rho v_p^{\,2} \frac{\partial\left(\frac{F}{F_o}\right)_p}{\partial P} - \frac{8}{3} G \frac{\partial\left(\frac{F}{F_o}\right)_s}{\partial P}$$

$$\left(\frac{\partial K_s}{\partial T}\right)_P = -\frac{1}{3} K_T \alpha_v + 2\rho v_p^{\,2} \frac{\partial\left(\frac{F}{F_o}\right)_p}{\partial T} - \frac{8}{3} G \frac{\partial\left(\frac{F}{F_o}\right)_s}{\partial T}$$

$$\left(\frac{\partial G}{\partial P}\right)_T = G\left(\frac{1}{3K_T} + 2 \frac{\partial\left(\frac{F}{F_o}\right)_s}{\partial P}\right)$$

$$\left(\frac{\partial G}{\partial T}\right)_P = G\left(-\frac{\alpha_v}{3} + 2 \frac{\partial\left(\frac{F}{F_o}\right)_s}{\partial T}\right)$$

*F is the reciprocal of travel time, L is sample length, q_i is an appropriate constant or combination of constants, and naught refers to ambient.

TABLE III-4.- NEW DATA

	v km/sec	$\left(\frac{\partial F/F_o}{\partial P}\right)_T$ kb^{-1}	$\left(\frac{\partial F/F_o}{\partial T}\right)_P$ °C^{-1}
Spinel			
P wave (100)	9.0827	0.000814	-.0000592
P wave (110)	10.3020	.000651	-.0000478
S wave (110)[100]	6.6023	.000200	-.0000367
S wave (110)[110)	4.4667	.000311	-.0000578
*S wave (110)[110]	4.4670	.0003	-.00006
Spinel polycrystal			
P wave	9.695	.00090	--
S wave	5.309	.00033	--
Magnetite			
P wave (100)	7.200	.00142	--
P wave (110)	7.380	.00164	--
S wave (110)[100]	4.296	-.0072	--
S wave (110)[110]	3.960	-.0058	--
*S wave (110)[110]	3.98	-.009	--
CdO polycrystal			
P wave	4.8256	.00176	-.000099
S wave	2.4961	.00112	-.000123

*Parameters derived from the cross-check equations.

TABLE III-5.- ELASTIC CONSTANTS OF THE SINGLE CRYSTALS. THE SUBSCRIPTS V, R, AND H REFER TO THE VOIGT, REUSS, AND HILL AVERAGING SCHEMES. P IS kb AND $\Delta T = T - 25^\circ$ C.

kb	Spinel	Magnetite
C_{11}	2990 + 5.35 P - 0.376 ΔT	2676 + 8.03 P
C_{12}	1544 + 4.21 P - 0.198 ΔT	1056 - 16.0 P
C_{44}	1580 + 0.89 P - 0.128 ΔT	953 - 13.5 P
K_{VRH}	2026 + 4.59 P - 0.257 ΔT	1596 + 20.3 P
G_v	1237 + 0.760 P - 0.122 ΔT	896 - 11.8 P
G_R	1072 + 0.746 P - 0.100 ΔT	890 - 11.5 P
G_{VRH}	1155 + 0.753 P - 0.106 ΔT	893 - 11.7 P

TABLE III-6.- ELASTIC CONSTANTS OF THE POLYCRYSTALS

[The various Gruneisen's parameters, λ, are explained in chapter IV]

	Spinel*	Polycrystal spinel	Polycrystal spinel**	Magnetite*	Polycrystal CdO	Polycrystal CdO**
K_s(kb)	2026	1980	2060	1596	1157.0	1280
$\left(\frac{\partial K_s}{\partial P}\right)_T$	4.58	5.40		20.3	5.31	
$\left(\frac{\partial K_s}{\partial T}\right)_P \left(\frac{kb}{°C}\right)$	-.257	--		--	-.215	
G (mb)	1155	989	1020	893	488.7	520
$\left(\frac{\partial G}{\partial P}\right)_T$	.753	.821		-11.7	1.23	
$\left(\frac{\partial G}{\partial T}\right)_P$	-.106	--		--	-.125	
v_p(km/sec)	9.918	9.695	9.8	7.35	4.826	4.92
$\left(\frac{\partial v_p}{\partial P}\right)_T$	.00530	.0071		.0040	.00714	
$\left(\frac{\partial v_p}{\partial T}\right)_P$	-.000441	--		--	-.000425	
v_s(km/sec)	5.644	5.309	5.4	4.16	2.4961	2.53
$\left(\frac{\partial v_s}{\partial P}\right)_T$	.00043	.00080		-.025	.00210	
$\left(\frac{\partial v_s}{\partial T}\right)_P$	-.00020	--		--	-.000280	
λ_p	1.41	1.78		1.2	2.07	
λ_s	.49	.63		-9.6	1.32	
λ_{low}	.57	.73			1.41	
λ_{high}	.80	1.01			1.57	
$\bar{\lambda}$	.69	.87			1.49	
$T\alpha_v\bar{\lambda}$	.005	.006			.014	

*Voigt-Reuss-Hill averages of single-crystal properties.

**Data, exclusive of derivatives, corrected to zero porosity.

TABLE III-7.- A COMPARISON OF DATA OBTAINED FOR SEVERAL COMPOSITIONS OF SPINEL.

	New* $MgO \cdot 1.1Al_2O_3$	Schreiber (1967, 1968) $MgO \cdot 2.61Al_2O_3$	New $MgO \cdot 3.0Al_2O_3$	Verma (1960) $MgO \cdot 3.5Al_2O_3$
ρ_o	3.58	3.6193	3.6245	3.63
$V_p(100)$		9.0833	9.0827	9.10
$V_p(110)$		10.296	10.3020	10.30
$V_s(110)[100]$		6.5978	6.6023	6.61
$V_s(110)[110]$		4.4733	4.4667	4.52**
$\bar{v}_p$	9.8	9.914	9.918	9.93
$\bar{v}_s$	5.4	5.645	5.644	5.66
K_s	2060	2020	2026	2026
G	1020	1153	1155	1164
$\left(\frac{\partial K_s}{\partial p}\right)_T$		4.2	4.58	
$\left(\frac{\partial K_s}{\partial T}\right)_P$		-.13	-.257	
$\left(\frac{\partial G}{\partial P}\right)_T$		.75	.753	
$\left(\frac{\partial G}{\partial T}\right)_P$		-.11	-.106	

*Corrected to zero porosity (chapter II).

**Calculated from $v_s^2(110)[110] = V_p^2(100) - V_p^2(110) + v_s^2(100)[100]$.

TABLE III-8.- A COMPARISON OF THE POINTON AND TAYLOR DATA (1968) FOR SPINEL AT 4.2° K WITH AN EXTRAPOLATION OF THE NEW DATA. (Units of 10^{11} dynes/cm^2.)

	Pointon and Taylor	New data
C_{11}	29.9 ± 0.6	31.00
C_{12}	16.5 ± 1.2	16.03
C_{44}	16.5 ± 1.2	16.18

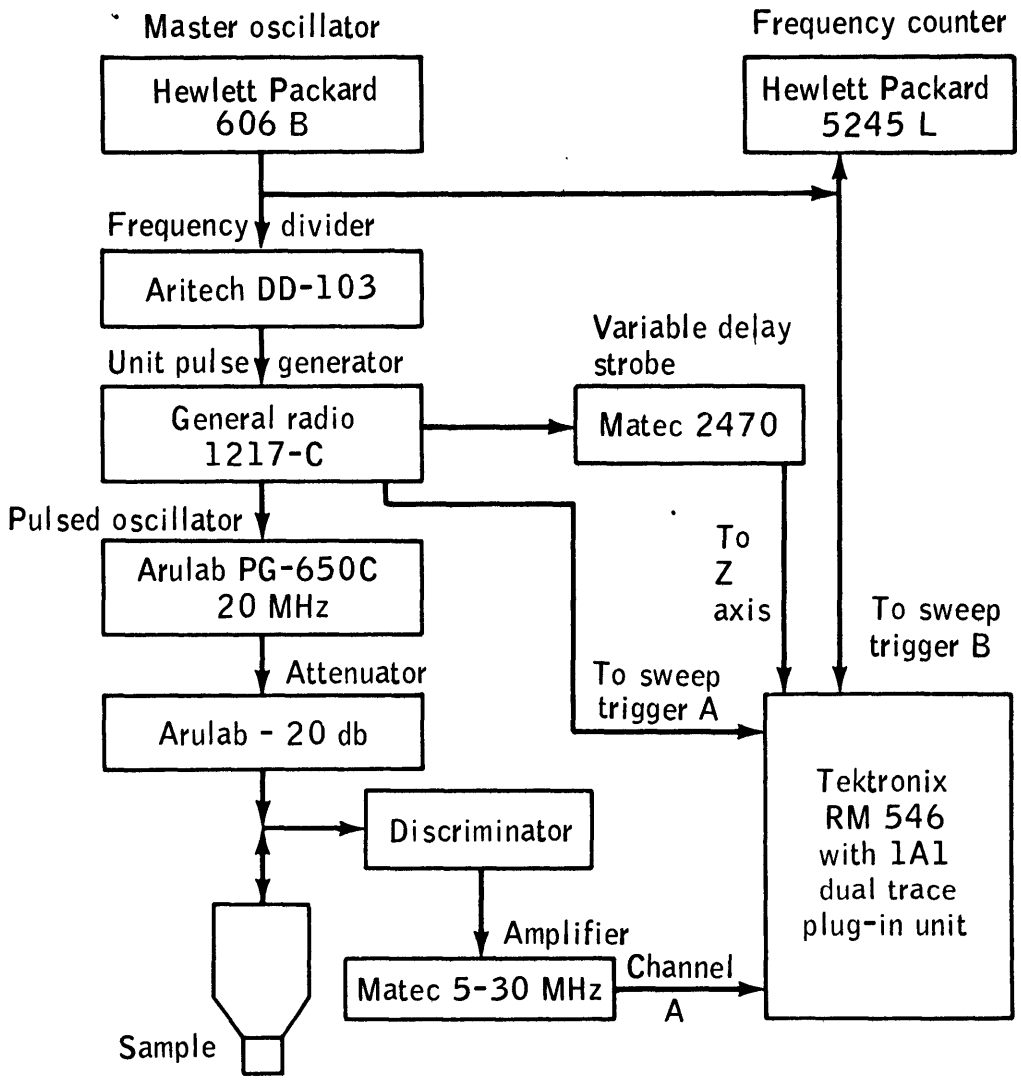

Figure III-1.- The Pulse-Echo Overlap System of Chung, et al. (1969). System is functionally similar to that described in Chapter II.

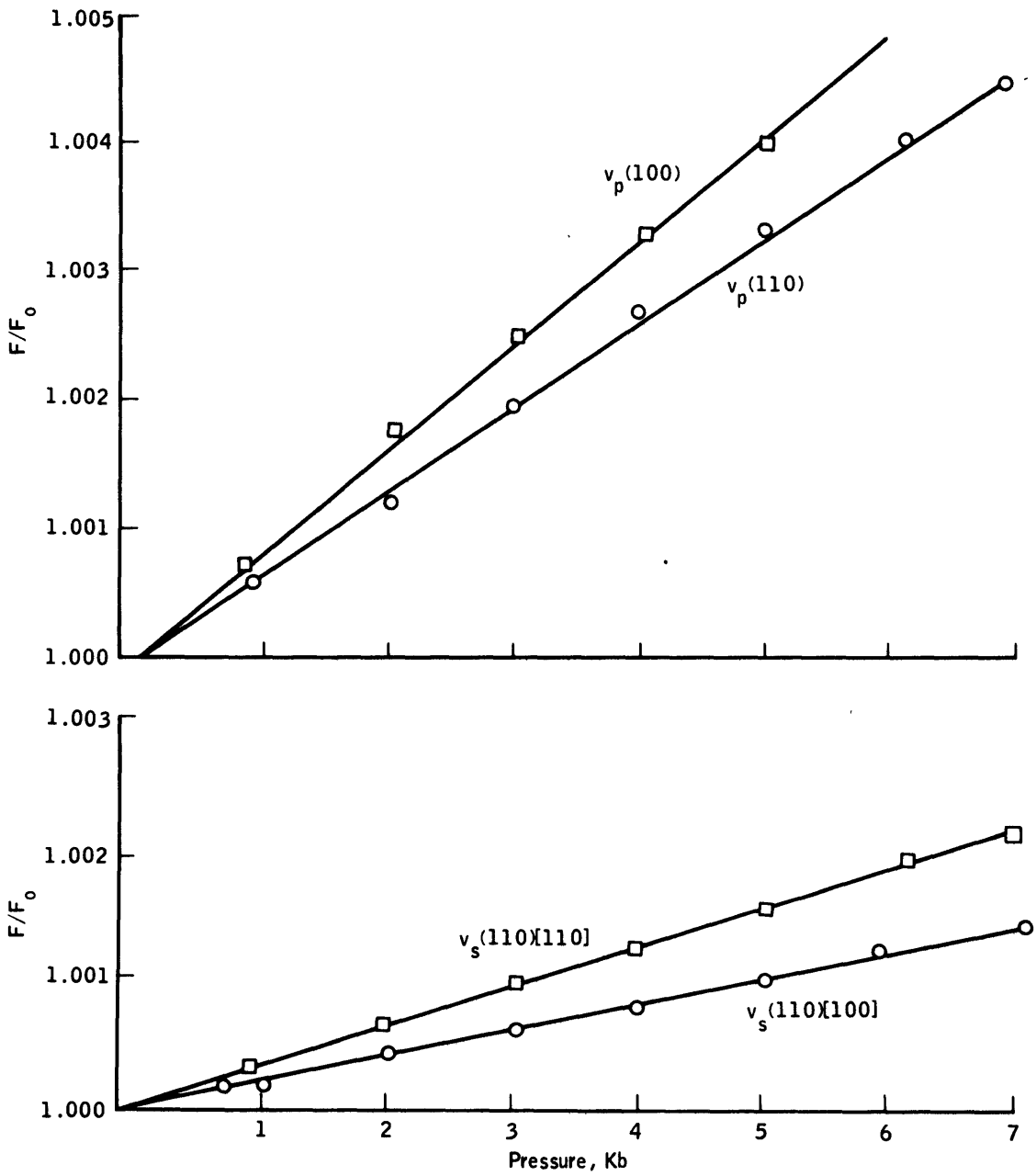

Figure III-2.- F/F_o versus pressure for spinel single crystal.

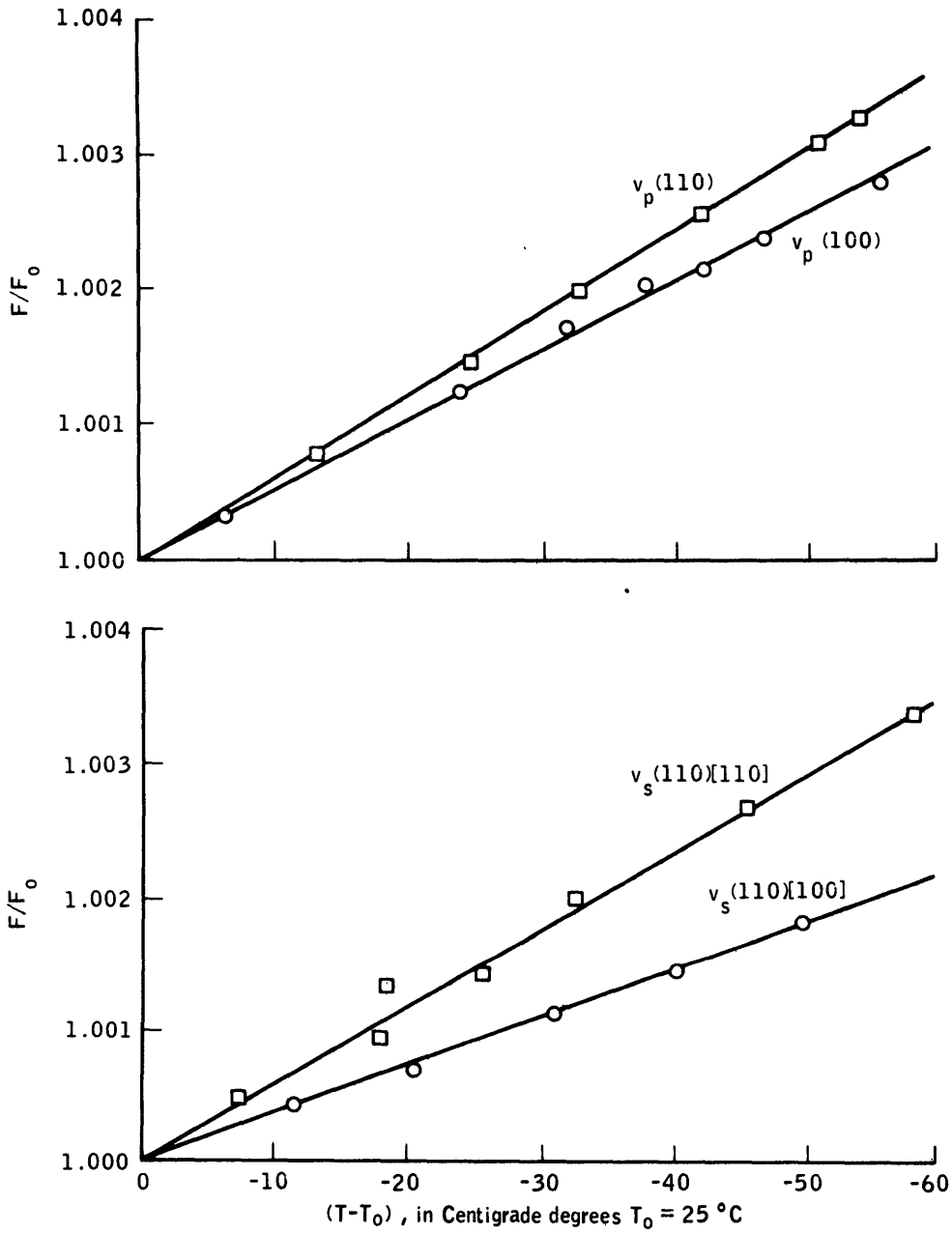

Figure III-3.- F/F_o versus temperature for spinel single crystal.

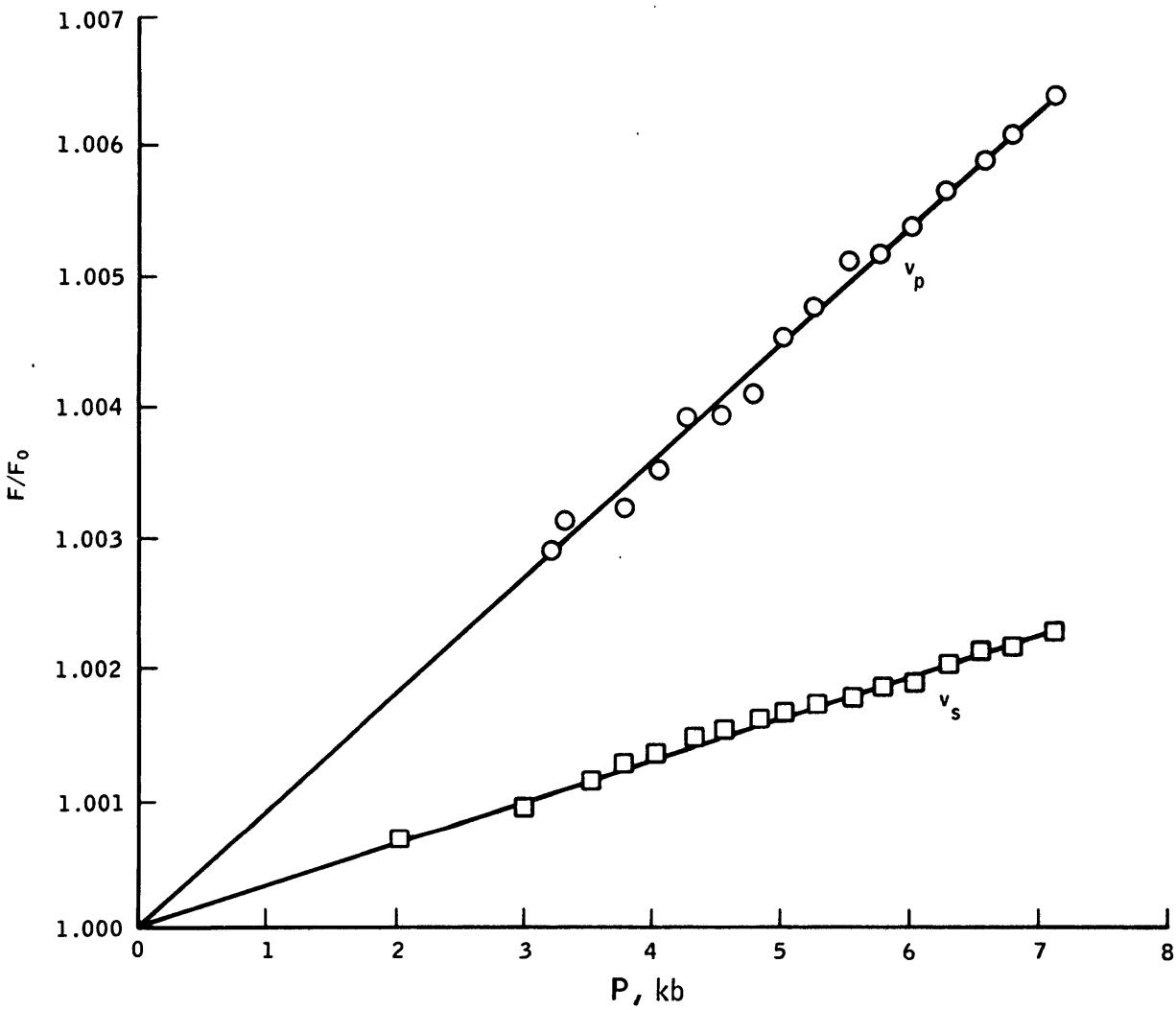

Figure III-4.- F/F_o versus pressure for polycrystalline spinel.

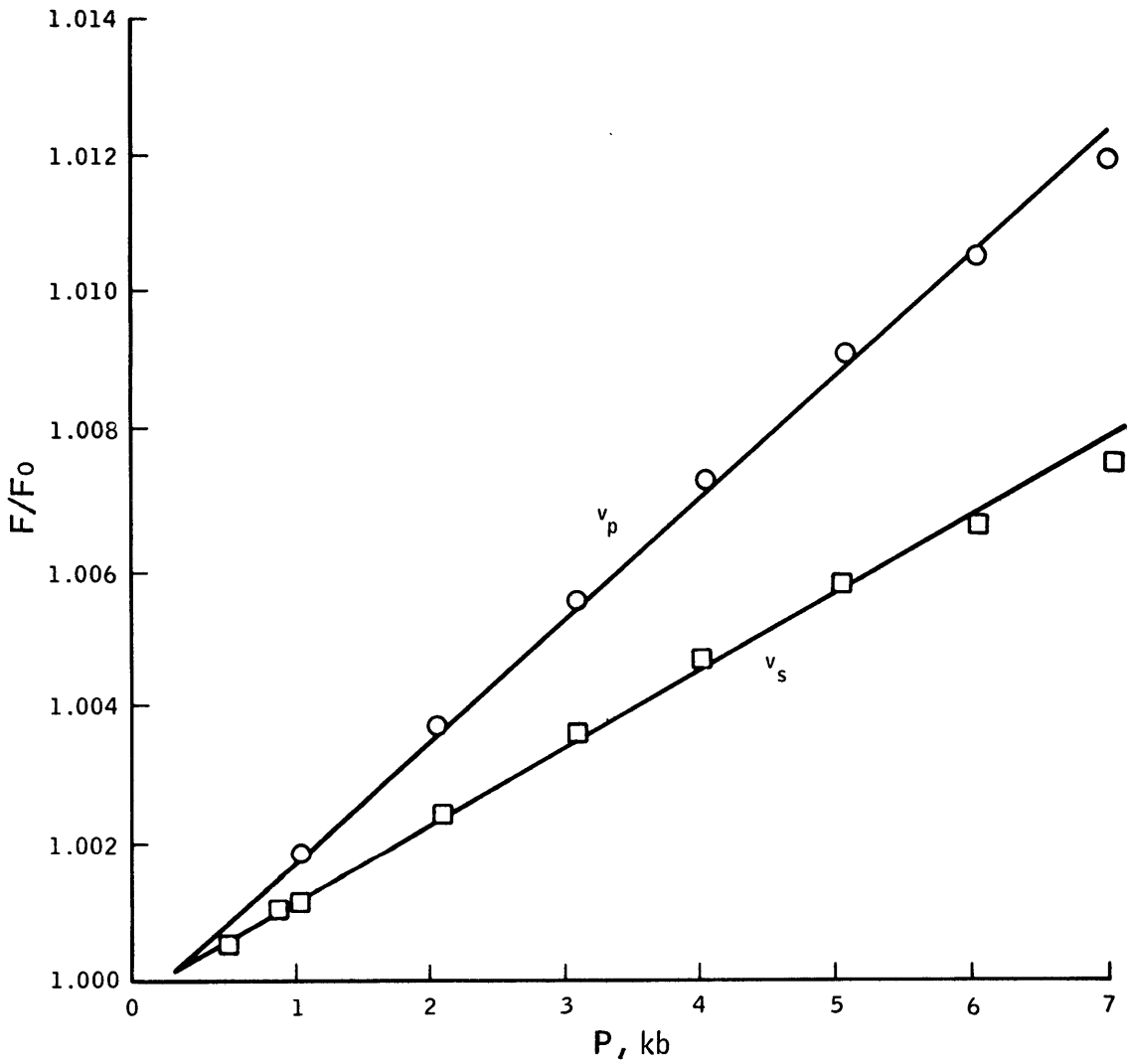

Figure III-5.- F/F_o versus pressure for polycrystalline CdO.

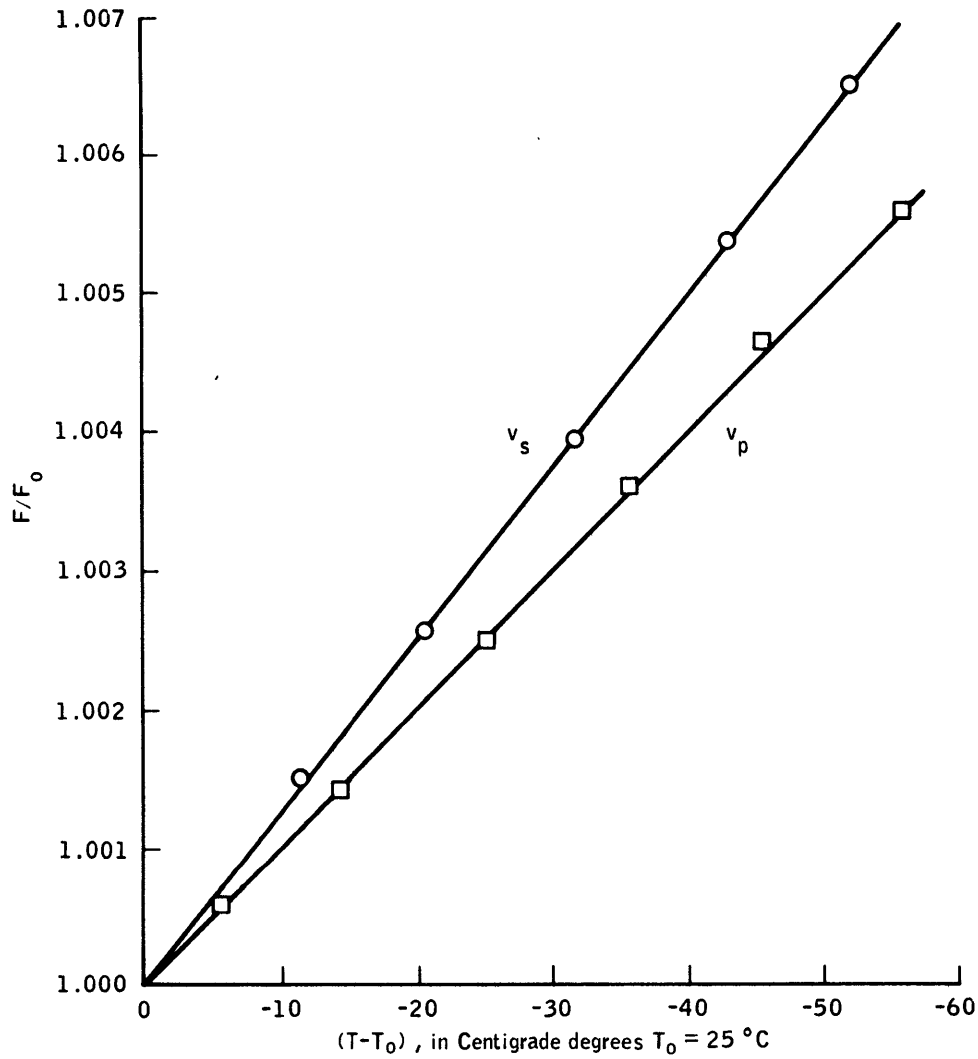

Figure III-6.- F/F_o versus temperature for polycrystalline CdO.

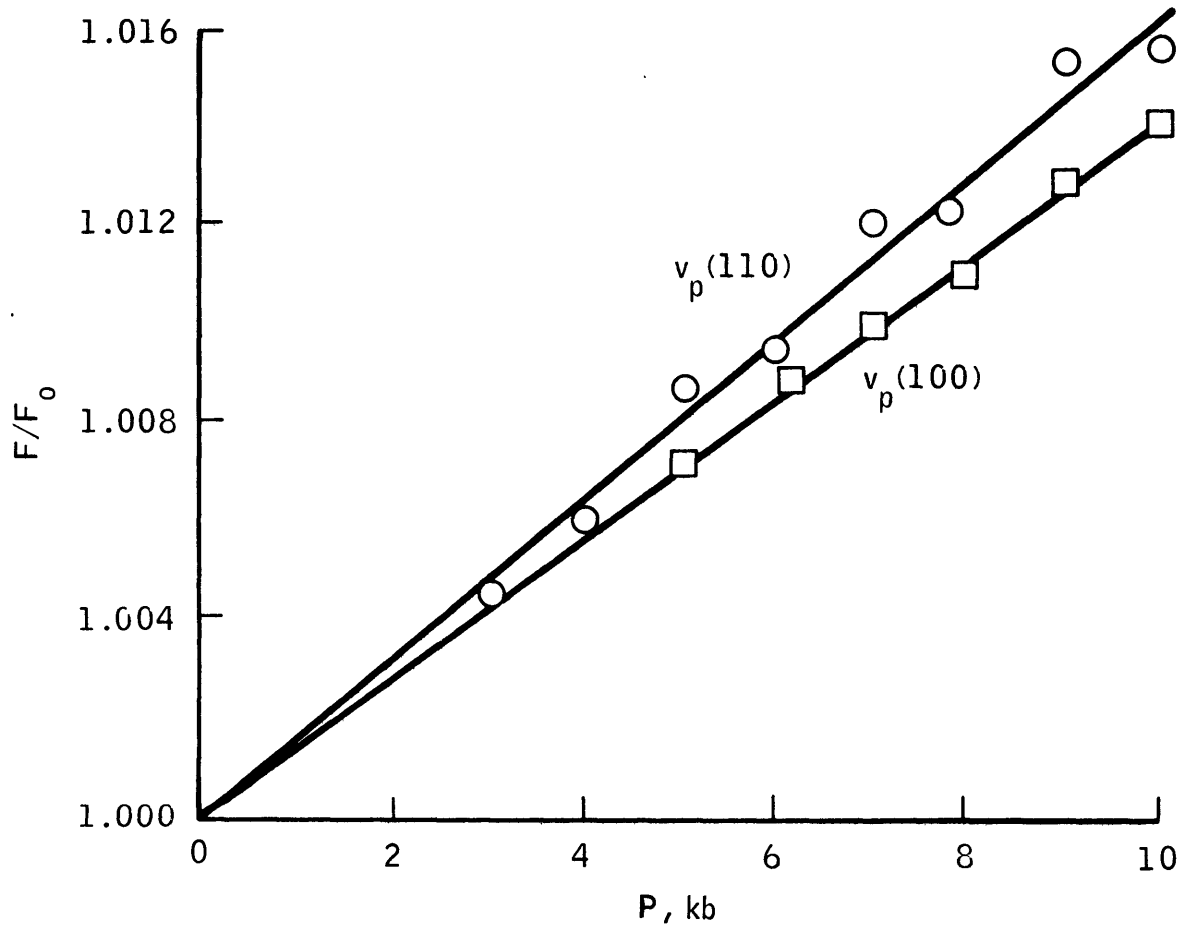

Figure III-7.- F/F_o versus pressure magnitite single crystal.

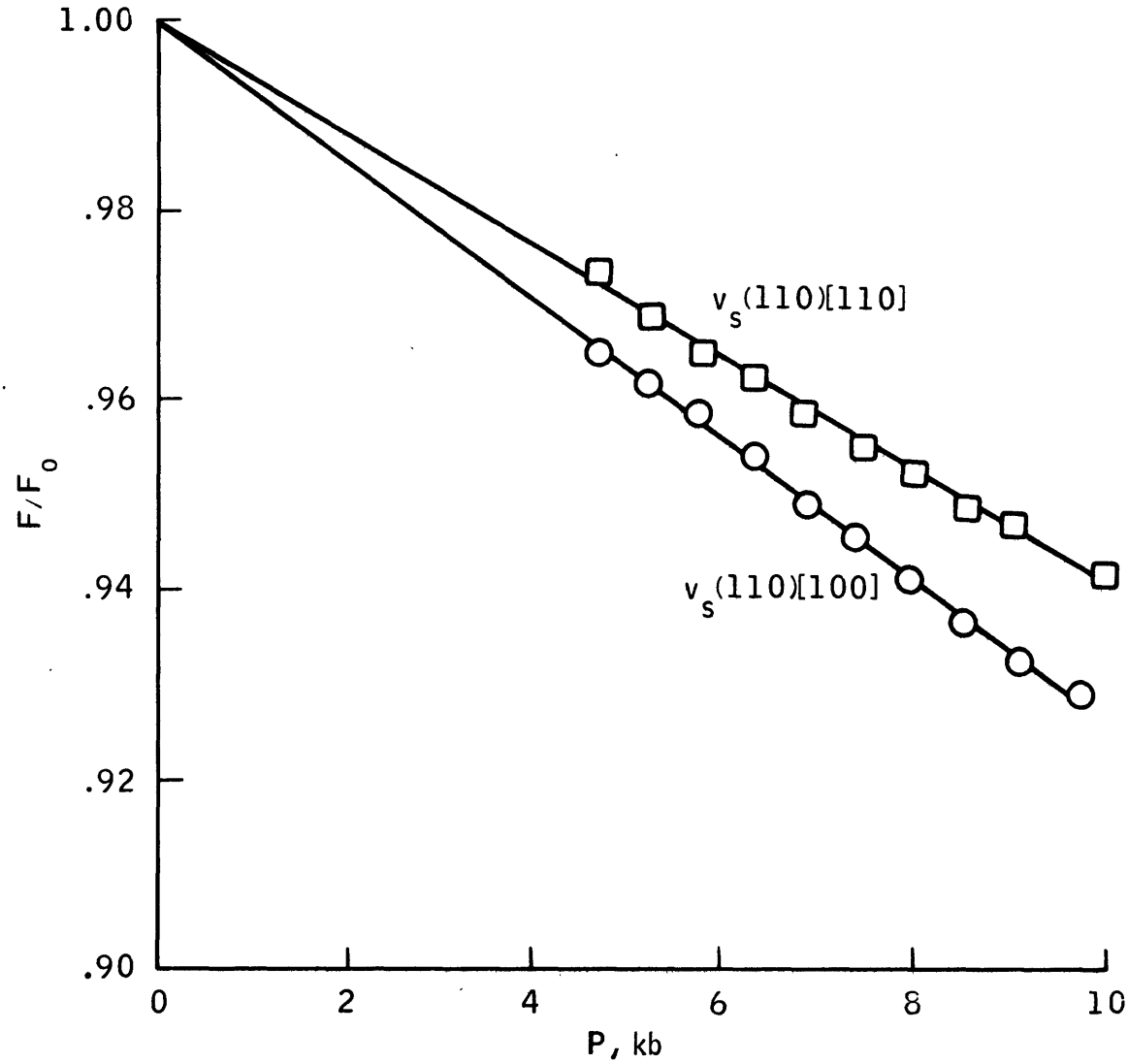

Figure III-8.- F/F$_o$ versus pressure magnetite single crystal.

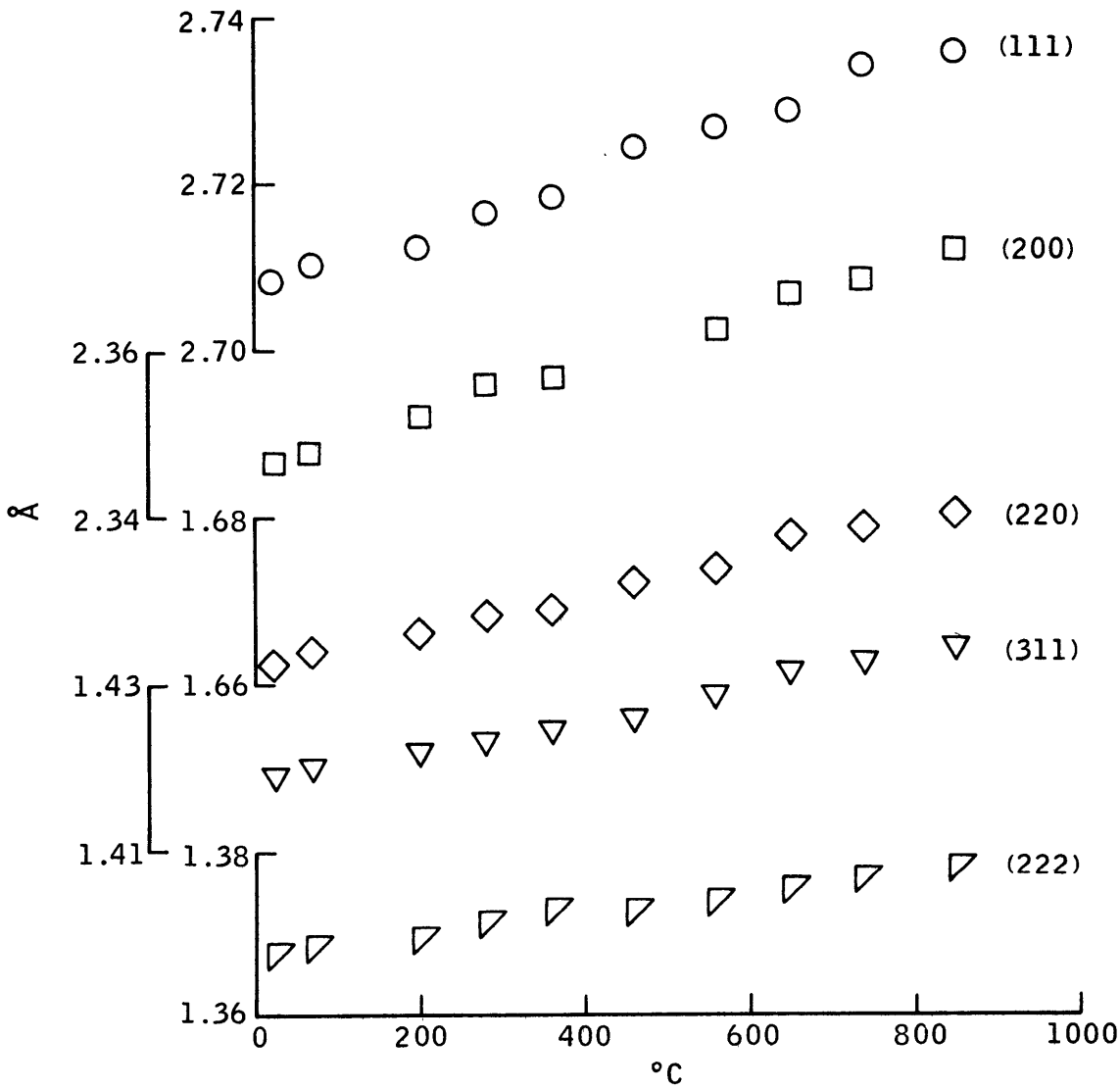

Figure III-9.- Lattice spacing versus temperature of cadmium oxide.

IV. UNIVERSAL EQUATIONS OF STATE FOR OXIDES AND SILICATES

Equations of state relate such material parameters as elastic constants and density to pressure and temperature. Although equations of state are used to interpolate laboratory measurements, the main use is the extrapolation of such measurements to conditions outside the range of measurements. The success of various forms of equations of state (reviewed by Knopoff, 1963, for example) is well known. In general, the constants of the equations differ for each material. Recently, several relations that are believed to be independent of the details of composition and crystallographic structure have been proposed in the geophysical literature (Birch, 1961b; O. Anderson-Nafe, 1965; and D. Anderson, 1967). These relations, which may be called universal equations of state, express uniquely the elastic parameters as explicit functions of density only and are believed to apply to all, or at least most, of the oxides and silicates. In these equations, composition and pressure do not appear explicitly, but enter implicitly through such variables as density and mean atomic weight or volume per ion pair. These relations have been used to interpret the velocities of elastic waves and densities of the interior of the earth (Birch, 1964; D. Anderson, 1965; and Press, 1968). However, all three relations are empirical, and many data show significant departures from each. The purpose here is to examine these universal equations of state on the basis of available data.

The elastic properties of materials of significance to the interpretation of observations on the interior of the earth have been measured by several techniques. For the purpose of examining the proposed relations among the elastic properties and such parameters as pressure and

composition, data obtained with field techniques are excluded because of uncertainties in the composition and state of the rocks through which the seismic waves propagate. Attention is focused on data obtained in the controlled conditions of the laboratory where, in principle at least, all the parameters can be measured precisely. (In practice, data of very high precision are often so incomplete as to be almost useless.) Various classes of techniques for measuring elastic properties are summarized in table IV-1, together with sufficient references to allow examination of the techniques in detail. Because the universal equations of state are designed to apply to the bulk properties of elastically isotropic aggregates, only those techniques which lead to this information are listed in table IV-1. Both precision and accuracy of the bulk properties computed from single-crystal data are reduced to approximately 10^{-4} because of uncertainties in the schemes, such as those of Voigt and Reuss (Hearmon, 1961) and Hashin and Strikman (1962), that must be used to estimate the properties of elastically isotropic, monomineralic aggregates from the single-crystal measurements.

The ultrasonic data obtained on both single crystals and rocks are shown in table IV-2 with mean atomic weight, density, and other parameters. Similar data obtained with either high-pressure X-ray techniques or simple compression measurements on the compressibility of oxides with sodium chloride structure are given in table IV-3.

The difficulties in obtaining from the literature all the requisite data for a given material for such studies may be illustrated by the work on hornblende. Alexandrov and Ryzhova (1961), as part of their extensive work on the elastic properties of rock-forming minerals, determined a complete set of single-crystal second-order elastic constants for two samples

of hornblende. The only information they presented that can be used to estimate the composition consisted of optical properties (2V, dispersion, and qualitative statement of pleochroism) and density; they concluded from these data that both samples were "ordinary hornblendes." However, the composition of common hornblende ranges between the various end members shown in table IV-4 (Winchell and Winchell, 1951). In an attempt to salvage something from Alexandrov and Ryzhova's data but without placing too much reliance upon it, take the composition of both samples to be 40% $H_2Ca_2Fe_5Si_8O_{24}$ and 60% $H_2Ca_2Mg_5Si_8O_{24}$, a composition that is consistent with the scanty data. For this (possible) composition, $\bar{m} = 22.4$. Hornblende is no exception to the fact that most rock-forming minerals show such large variation in composition that the designation (even if correct) of spinel, magnetite, pyroxene, garnet, etc., is insufficient to express the composition of a particular specimen.

Birch (1961b) noted that the velocity of compressional waves is a function of the density and mean atomic weight. For those oxides and silicates with $\bar{m} \approx 21$ and $v_p = a + b\rho$, several values of the two constants were obtained by Birch from the linear regression analysis of various subsets of his data. Additional data that have been obtained later continue to show the general relationship, but with a number of exceptions. Simmons (1964a) called attention to the failure of materials with high contents of calcium oxide to conform to the Birch relationship. Materials for which the experimental data differ from the predicted compressional velocities by 0.5 km/sec are listed in table IV-5. Several of these materials contain high contents of calcium oxide. Particularly disturbing are the discrepancies of sillimanite, aegirite, apatite, and α-quartz.

In a study of ultrabasic rocks in which there was little variation in content of either iron or calcium, Christensen (1966) showed that the velocities of both compressional and shear waves, at 10 kilobars, are related linearly to density with correlation coefficients greater than 0.999. The rocks that he studied were chiefly mixtures of olivine (approximately fo_{92}), enstatite, and chrysotile. The range of mean atomic weights of these minerals is approximately 19.8 to 20.8. The chief variation of chemical composition in the rocks, although not explicitly examined by Christensen, is probably in water content. The implication of Christensen's data is that Birch's relation describes adequately the properties of materials of restricted composition.

O. Anderson and Nafe (1965) observed that the bulk modulus of many "oxide compounds" followed the relationship

IV-1) $$\ell nK = -x\ell n\left(\frac{2\bar{m}}{\rho}\right) + C$$

where $(2\bar{m}/\rho)$ is twice the average volume per atom and C is a constant. In the context of their work, the phrase "oxide compounds" is used not only for such oxides as magnesium oxide and titanium oxide, but also for silicates, nitrates, and pyrex. This usage is neither common in mineralogy nor to be recommended in geophysics. More data are now available then were used in the initial compilation. Figure IV-1 is a plot of bulk modulus K compared to $(2\bar{m}/\rho)$ and includes most available data. Linear scales are used to show the large scatter; log-log plots tend to emphasize the gross relationships at the expense of showing clearly any large variation that may exist. O. Anderson and Nafe showed that many silicates and oxides for

which data are available fall within a region bounded by

IV-2)
$$\ell nK = 4\ell n\left(\frac{2\bar{m}}{\rho}\right) + 17.3$$

$$\ell nK = -3\ell n\left(\frac{2\bar{m}}{\rho}\right) + 15.1$$

where the same values of K and $2\bar{m}/\rho$ used by Anderson and Nafe for stishovite have been used to evaluate the constant C. Even neglecting the fact that hematite, rutile, chromite, sillimanite, beryl, topaz, barium titanate, aegirite, montecellite, calcium oxide, cadmium oxide, and zircon do not satisfy the relationship, the limits are so large that the relationship is of little value in predicting the bulk modulus of a material from its density and mean atomic weight. Only in the most qualitative sense is it true that bulk modulus is related (by the Anderson-Nafe law) to composition through the parameter $(2\bar{m}/\rho)$.

D. Anderson (1967a) extended and modified Birch's relation to the form $\rho = A\bar{m}\Phi^n$, where $\Phi \equiv K/\rho$. A least square fit to the data for 31 selected minerals and rocks gave $\rho = 0.048\bar{m}\Phi^{0.323} \pm 0.12$. (This standard deviation, given by Anderson in his equation 37 is that of ρ, rather than $\rho/\bar{m}$ [D. Anderson, personal communication].) An equivalent statement of the Φ-law is that the bulk modulus is a linear function of pressure. This relation is shown in figure IV-2 with the data used by Anderson to evaluate the constants and many other data from table IV-2. There seems to be little reason to select some of these data and discard all the others. From inspection of figure IV-2, it can be seen that the data for many materials — and including the precise single-crystal values of α-quartz, magnetite,

garnet, periclase, alumina, rutile, and calcia — depart more than one standard deviation (as determined by Anderson for his smaller set of selected data).

Implicit in the use of the D. Anderson Φ-law to interpret the properties of the earth is the assumption that the only important parameters for the determination of Φ for earth materials are ρ and $\bar{m}$ and that details of crystallographic structure and composition are (relatively) unimportant. Specifically, it is hoped that the properties of high-pressure phases can be predicted from ρ and $\bar{m}$. Data for such phases obtained with static pressures are not yet available. Inasmuch as the plausible suggestion has been made that the material in the deep interior may be present as oxides, it seems desirable that any relation used to predict the properties of these hypothetical oxides should at least fit the available data on oxides that have the sodium chloride structure at atmospheric conditions. These data are shown in figure IV-3. Although neither cadmium oxide, europium oxide, strontium oxide, nor several of the other oxides is likely present in sufficient quantities in the interior of the earth to affect the physical properties of the earth, it would seem fair to use these data to test relationships expected to be useful in predicting the properties of simple oxides with close-packed structures. No data are closer than two standard deviations (taking $\bar{m} \geq 20$) determined for the original set of data. It is concluded that the relation lacks general validity and suggested that application of the relation to the prediction of the elastic properties of high-pressure phases is at least doubtful.

It is instructive to test also the O. Anderson-Nafe law with the data for oxides with the sodium chloride structure. These test results are

shown in figure IV-4. Very large discrepancies exist between the values predicted from the O. Anderson-Nafe law and the values determined experimentally. Clearly, the Anderson-Nafe relationship does not fit the observed data well enough to justify its use as a tool for predicting K.

An alternate test of the several relations is afforded by the correlation coefficients (C.C.) and the standard errors (S.E.) that can be obtained by analysis of the data of tables IV-2 and IV-3 which constitute a larger set of data than was used initially by the various authors. For this purpose, take D. Anderson's relation in the form $\ln(\rho/\bar{m}) = a + b\ln\Phi$ for ease of computation and Birch's relation in the form $v_p = a + b\rho + c\bar{m}$. The results are shown in table IV-6. From a geophysical viewpoint, the correlation coefficients are uncomfortably small, and the standard errors are large. (Although the S.E. for the D. Anderson relation (~15%) may appear small, it is a larger fraction of the total range of the variable.) The standard error (or similar statistical parameter) is a measure of the dispersion of a given sample set (e.g., S_1) of data. Its use as a statistical estimator of the S.E. for the population (e.g., S) consisting of the appropriate data on all oxides and silicates at pressures from 4 to 2000 kilobars depends on the sample set S_1 having been obtained in such a way that the following two requirements are satisfied: (1) each element of S_1 is independent of the other elements, and (2) the distribution function for set S_1 is the same as it is for the population S. Because neither of these requirements is satisfied by the present set of data, it is incorrect (statistically) to use the standard errors of table IV-6 to estimate the S.E. of such parameters as $\bar{m}$ for the earth derived from seismic and other data by means of the various relations. It is the hope of those who use the relations to interpret the data on the earth that the

S.E. given for the relations do apply to the data for the earth. At best, these standard errors should be considered minimum values. The S.E. for any relation can be made as small as desired by selecting the subset of data used to evaluate it. For example, by restricting the set of data to those materials for which $20 \leq \bar{m} \leq 25$, quite high correlation coefficients for the Birch relation (>0.95) may be obtained.

TABLE IV-1.- MEASUREMENT TECHNIQUES FOR THE ELASTIC PROPERTIES OF MATERIALS

Class	Precision	Accuracy	References
A. Single crystal elastic constants[a]	10^{-7}	10^{-4}	Hearmon (1961), Huntington (1958) McSkimin (1964, 1967), Alers and Neighbours (1958), Daniels and Smith (1963)
B. P and S velocities (rocks)	10^{-4}	10^{-3}	Simmons (1965), O. Anderson and Liebermann (1966)
C. Compressibilities			
Strain gage	10^{-3}	10^{-2}	Brace (1965)
Volume compression	10^{-3}	10^{-2}	Bridgman (1964)
X-ray	10^{-4}	10^{-3}	Drickamer et al. (1966), McWhan (1967)
D. Shock wave	5×10^{-3}	10^{-2}	McQueen et al. (1967), Doran and Linde (1966)

[a]Also used for high Q polycrystalline aggregates (O. Anderson, 1966c; Chung and Simmons, 1968).

TABLE IV-2.- ULTRASONIC DATA*

Material	$\bar{m}$	ρ	$\rho/\bar{m}$	V_P	Ref.	[FeO] + [Fe_2O_3]	[CaO]	V_s	ϕ	K	β
Granite, G-1	20.9	2.619	0.125	6.23	1,2	1.9	1.4	3.58	21.7	0.57	1.75
Quincy	20.9	2.621	.125	6.45	1	3.6	.4				
Rockport	20.6	2.624	.125	6.51	1,2	1.5	.3	3.77	23.4	.61	1.62
Stone Mt.	20.7	2.625	.125	6.40	1,2	.8	1.1	3.80	21.7	.57	1.75
Barre	20.8	2.655	.125	6.39	1,2	2.7 +	1.8	3.70	22.6	.60	1.67
Gneiss, Pelham	20.8	2.643	.127	6.31	1	2.5	1.8				
Qtz monz, Butte	21.2	2.705	.128	6.56	1	5.0	4.3				
Augite syenite	22.1	2.780	.126	6.79	1	11.6	4.6				
Anorthosite, New Glasgow	21.1	2.708	.128	6.85	1	4.4	11.3				
Bushveld	21.3	2.807	.132	7.21	1	1.1	16.0				
Gabbro, Mellen	21.8	2.931	.134	7.21	1	8.7 +	9.7				
Diabase, Centerville	22.0	2.976	.135	6.93	1,2	10.5	11.0	3.80	28.8	.86	1.16
Holyoke	22.0	2.977	.135	6.63	1	11.8	9.4				
Frederick, Md.	22.0	3.012	.137	6.92	1,2	10.4	11.4	3.85	28.1	.85	1.18
Cobalt, Ont.	21.8	2.964	.136	6.82	1	11.5	6.9				
Sudbury	22.2	3.003	.135	6.91	1	13.5 +	6.6				
Gabbro, F. Creek	21.8	3.054	.140	7.23	1	9.0	11.9				
Jadeite, Japan	20.4	3.180	.156	8.28	1,2	.5 +	1.3	4.82	37.6	1.20	.83
Burma	20.4	3.331	.163	8.78	1	.5	.8				
Bronzitite, Stillwater	21.2	3.279	.155	7.83	1,2	9.7	2.2	4.66	32.4	1.06	.94
Bushveld	21.0	3.288	.157	8.02	1	9.4 +	.5				
Harzburgite	21.7	2.978	.137	7.28	1	12.2	1.4				
Dunite, Webster, N.C.	21.0	3.244	.154	7.78	1,2	8.3 +		4.40	34.7	1.13	.88
Mt. Dun	21.1	3.258	.154	8.00	1,2	8.3		4.54	36.5	1.19	.84
Balsam Gap	20.9	3.267	.156	8.28	1	8.2	.1				
T. S.	20.9	3.312	.158	8.42	1,2	8.0	.1	4.83	39.8	1.32	.75
Burma	20.9	3.324	.159	8.56	1	8.0	.1				
Bushveld	24.3	3.744	.154	7.36	1,2	38.0	.5	3.90	33.9	1.27	.78
Chromite		4.45		8.78	3			4.85	45.73	2.03	.49
1090 $FeCr_2O_4$	31.98	5.058[x]	.158[x]								
Diamond 1005 C	12.01	3.511	.292	17.22	3			11.55	118.66	4.17	.24

*See note z at end of table for explanation of symbols and units.

TABLE IV-2.- ULTRASONIC DATA* - Continued

Material	$\bar{m}$	ρ	$\rho/\bar{m}$	V_P	Ref.	[FeO] + [F_2O_3]	[CaO]	V_s	ϕ	K	β
Galena 1158 PbS	119.64	7.597	0.063	3.75	3			2.08	8.29	.62	1.61
Magnetite 1252 Fe_3O_4	33.08	5.18	.157	7.40	3	100.0		4.30	31.24	1.62	.62
Pyrite 1354 FeS_2	40.03	4.929	.123	8.09	3			5.17	29.81	1.47	.68
Barium titanate 2009 $BaTiO_3$	46.65	5.5	.118	6.69	3			3.12	31.78	1.75	.57
Barium titanate 2010	46.65	5.5	.118	6.97	3			3.51	32.15	1.77	.56
Zircon 2046 $ZrSiO_4$	30.55	4.56	.149	3.20	3			2.09	4.42	.20	4.96
Staurolite 3023 $HFe_2Al_9Si_4O_{24}$	21.82	3.369	.154	7.58	3	16.9		4.66	28.50	.96	1.04
Sulphur 3025 S	32.07	2.07	.065	3.68	3			1.80	9.22	.19	5.23
Topaz 3039 $(AlF)_2SiO_4$	26.29	3.52	.134	9.55	3			5.71	47.73	1.68	.59
Aegirite 4019 $NaFeSi_2O_6$	25.67	3.50	.136	7.32	3			4.10	31.28	1.09	.91
Augite 4027 $Ca(Mg,Fe)Si_2O_6$	22.29	3.32	.149	7.22	3			4.18	28.78	.96	1.04
Diopside 4026 $CaMgSi_2O_6$	21.66	3.31	.153	7.70	3			4.38	33.63	1.12	.89
Hornblende 4020 $.4(H_2Ca_2Fe_5Si_8O_{24})$ $.6(H_2Ca_2Mg_5Si_8O_{24})$	22.4	3.12	.139	6.81	3			3.72	27.92	.87	1.14
Hornblende 4021	22.4	3.15	.141	7.04	3			3.81	30.22	.95	1.05
Labradorite 4024 $An_{58.5}$	20.89	2.68	.128	6.69	3			3.55	28.07	.75	1.33
Microcline 4022 $Or_{78.5}Ab_{19.4}An_{2.1}$	21.17	2.56	.121	6.01	3			3.34	21.31	.54	1.83
Oligoclase 4023 $An_{15.5}$	20.36	2.64	.130	6.22	3			3.23	24.81	.65	1.52
Apatite 5001 $Ca_5FP_3O_{12}$	24.02	3.218	.134	7.16	3			4.34	26.18	.84	1.18
Beryl 5008 $Be_3Al_2Si_6O_{18}$	18.54	2.72	.147	9.70	3			5.56	52.99	1.44	.69
Cancrinite 5021 A	19.92	2.46	.123	4.92	3			3.23	10.37	.25	3.94
Cancrinite 5022 A	19.92	2.44	.122	4.99	3			3.29	10.45	.26	3.91

*See note z at end of table for explanation of symbols and units.

TABLE IV-2.- ULTRASONIC DATA* - Continued

Material	$\bar{m}$	ρ	$\rho/\bar{m}$	V_P	Ref.	[FeO] + [Fe_2O_3]	[CaO]	V_s	ϕ	K	β
Ice 5025 H_2O	16	1.064	0.067	3.57	3			1.82	8.36	.089	11.3
Nepheline 5099 $NaAlSiO_4$	20.98	2.62	.125	5.91	3			3.49	19.02	.49	2.04
Nepheline 5100	20.98	2.62	.125	5.63	3			3.28	17.39	.45	2.19
Tourmaline 6035 $(NaAl,CaMg)Mg_3Al_5B_3Si_6O_{27}(OH)_4$		3.10		8.32	3			5.25	32.40	1.01	.99
Rutile 2020 TiO_2	26.63	4.26	.160	8.78	3			4.57	49.29	2.10	.47
Cadmium oxide CdO	64.21	8.238	.128	4.92	9			2.53	15.5	1.28	.78
Magnetite Fe_3O_4	33.08										
Eclogite, Sunnmore	21.7	3.376	.156	7.69	1	8.2	13.9				
Healdsburg	22.2	3.441	.155	8.01	1,2	12.9	11.9	4.58	36.2	1.25	.80
Garnet (gross)	22.8	3.561	.156	8.99	1	5.4	34.9				
(al-py)	24.1	3.950	.164	8.07	1	32.1	2.0				
Anorthosite, Stillwater	21.25	2.770	.130	7.10	1,2		17.8	3.81	31.1	.86	1.16
Gabbro, San Marcos		2.874			2			3.84			
Quartz diorite, Dedham, Mass.		2.906		6.71	1,2			3.84	25.4	.74	1.35
Monticellite, Crestmore	22.7	2.995	.132	7.50	2	3 +	37.0	4.06	34.27	1.03	.97
Norite, Pretoria		2.978		7.28	1,2			3.94	32.3	.96	1.03
Idocrase, Crestmore	22.8	3.14	.138		2	3.6	33.8	4.28			
Amphibolite, Mont.		3.120		7.35	1,2			4.30	29.4	.92	1.09
Eclogite 1552, Norway		3.577			2			4.60			
Eclogite 1553, Norway	22.1	3.578	.162	8.35[B]	2			4.66	40.77	1.46	.86
Albitite, Sylmar, Pa.	20.3	2.687	.132	6.76	1,2			3.73	27.1	.73	1.37
Serpentinite, Thetford, Que.		2.601		6.00	1,2			2.90	24.8	.65	1.55
Wollastonite	23.2	2.873	.124	7.71	2		48.3				

*See note z at end of table for explanation of symbols and units.

TABLE IV-2.- ULTRASONIC DATA* - Concluded

Material	$\bar{m}$	ρ	$\rho/\bar{m}$	V_P	Ref.	[FeO] + [Fe_2O_3]	[CaO]	V_s	ϕ	K	β
Microcline	21.4	2.571	0.120	7.15	2		48.3				
Garnet #1 (23.8% MnO)	24.9	4.247	.171	8.47	1	19.1	.4	4.77	41.4	1.76	0.56
Garnet #2	24.3	4.183	.172	8.52	1	37.1	1.5	4.77	42.3	1.77	.56
"Spinel" $MgO \cdot 3.5Al_2O_3$	20.37	3.63	.178	9.93	1			5.66	55.9	2.03	.49
α-Quartz SiO_2	20.03	2.649	.132	6.05	4	0	0	4.09	14.3	.38	2.64
Spinel $MgAl_2O_4$	20.32	3.619	.178	9.91	5	0	0	5.65	55.8	2.02	.49
Sillimanite Al_2SiO_5	20.25	3.187	.157	9.73	2	0	0	5.15	59.3	1.89	.52
Calcia CaO	28.04	3.285	.117	7.945	6	0	100.0	4.85	33.1	1.09	.90
Garnet	23.79	4.1602	.175	8.531	7	33.5	1.1	4.762	42.5	1.77	.56
Magnetite Fe_3O_4	33.08	5.1633	.156	7.35	9	99 +		4.16	31.0	1.60	.62
Hematite Fe_2O_3	31.94	5.254	.164	7.90	8	100		4.16	39.3	2.066	.48

*Notes for Table IV-2:

A. Composition is an average given by Dana (1949), p. 587.

B. Previously unpublished value. Composition calculated from Schmitt (1963).

x. Determined by x-ray measurements.

z. Explanation of symbols and units.

$\bar{m}$ = mean atomic weight
ρ = density, gm/cm^3
V_P = velocity of compressional waves, km/sec
Ref. = references
[FeO] + [Fe_2O_3] = weight percent of oxide
V_s = velocity of shear waves, km/sec
$\phi = V_p^2 - \frac{4}{3} V^2$, km^2/sec^2
K = bulk modulus = $\rho\phi/100$, mb
β = compressibility = $1/K$, mb^{-1}

+. Minimum value because either FeO or Fe_2O_3 not reported in original reference.

References for Table IV-2:

1. Birch (1960, 1961)
2. Simmons (1964 a,b)
3. Simmons (1965b)
4. McSkimin, Andreatch, and Thurston (1965)
5. Schreiber (1967)
6. Soga (1968)
7. Soga (1967)
8. Lieberman and Schreiber (1968)
9. Chapter III

TABLE IV-3.- DATA ON OXIDES WITH NaCl STRUCTURE. ALL VALUES OF β FROM REFERENCES 1 AND 3 WERE OBTAINED WITH X-RAYS; THOSE FROM REF. 2, WITH COMPRESSION MEASUREMENTS. SEE FOOTNOTE TO TABLE IV-2 FOR MEANINGS OF SYMBOLS AND FOR UNITS.

Material	$\bar{m}^b$	ρ^b	$\rho/\bar{m}$	K	β	ϕ	Ref.
MgO	20.16	3.584	0.178	1.780	0.562	49.67	1
CaO	28.04	3.345	.119	1.120	.893	33.48	1
CoO	37.47	6.438	.172	1.905	.525	29.59	1
NiO	37.36	6.808	.182	1.990	.503	29.23	1
FeO[a]	35.45	5.745	.162	1.540	.649	26.81	1
MnO	35.47	5.365	.151	1.440	.694	26.84	1
SrO	51.82	5.008	.097	1.18	.85	23.49	2
CdO	64.20	8.238	.128	1.280	.780	15.54	4
EuO	84.0	8.191	.098	1.070	.935	13.06	3
BaO	76.68	6.045	.079	.568	1.76	9.40	2

[a]Wustite, $Fe_{.935}O$.

[b]Values determined from unit cell dimensions of Robie et al. (1966) or Wyckoff (1963).

References for table IV-3:

1. Drickamer et al. (1966)

2. Weir (1956)

3. McWhan et al. (1966)

4. Chapter III

TABLE IV-4.- COMPOSITION AND MEAN ATOMIC WEIGHT OF THE END MEMBERS OF COMMON HORNBLENDE.

Composition	$\bar{m}$
$H_2Ca_2Mg_5Si_8O_{24}$	20.78
$H_2Ca_2Fe_5Si_8O_{24}$	24.82
$H_2Ca_2Mg_3Al_4Si_6O_{24}$	20.86
$H_2Ca_2Fe_3Al_4Si_6O_{24}$	23.28
$H_2NaCa_2Mg_5AlSi_7O_{24}$	20.75
$H_2NaCa_2Fe_5AlSi_7O_{24}$	24.80
$H_2NaCa_2Mg_4Al_3Si_6O_{24}$	20.85
$H_2NaCa_2Fe_4Al_3Si_6O_{24}$	24.00

TABLE IV-5.- MATERIALS THAT DO NOT CONFORM TO THE DENSITY-MEAN ATOMIC WEIGHT RELATIONSHIP OF BIRCH. $\Delta V_p = V_p$ (OBSERVED) — V_p (CALCULATED).

Material	ΔV_p (km/s)
Sillimanite	1.2
Topaz	>3-1/2
Beryl	.8
Grossularite	1.3
Chromite	1.3
Calcium oxide	4
Aegerite	1.6
Wollastonite	2.4
Monticellite	1.4
Harzburgite	.5
Apatite	1.3
Bushveld anorthosite	.6
Stillwater anorthosite	.6
Microcline	1.3
Mellon gabbro	.6
α-quartz	-1.2
Cancrinite	-1.8

TABLE IV-6.- STATISTICAL PARAMETERS DERIVED FROM DATA OF TABLES IV-2 AND IV-3.

Relation	Correlation coefficient	Standard error
$V_P = a + b\rho + c\bar{m}$	0.716	1.22
$\ell nK = a + b\ell n\ (2\bar{m}/\rho)$	.429	.60[a]
$\ell n\rho/\bar{m} = a + b\ell n\Phi$	.752	.017[b]

[a]S.E. for K is about 80%.

[b]S.E. for $\rho/\bar{m}$ is about 15%.

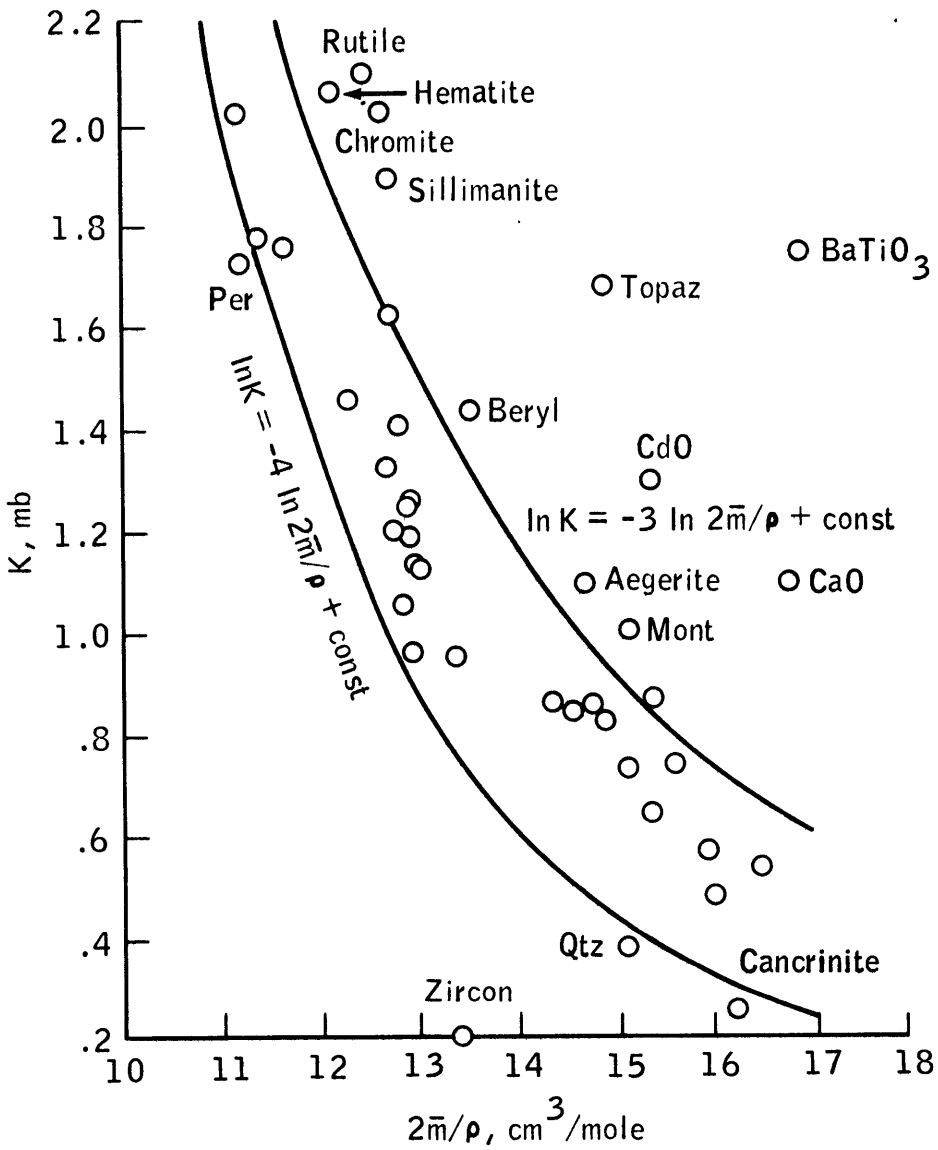

Figure IV-1.- Test of O. Anderson-Nafe relationship, $\ell nK = A\ell n(2\bar{m}/\rho) + C$. Data from table IV-2.

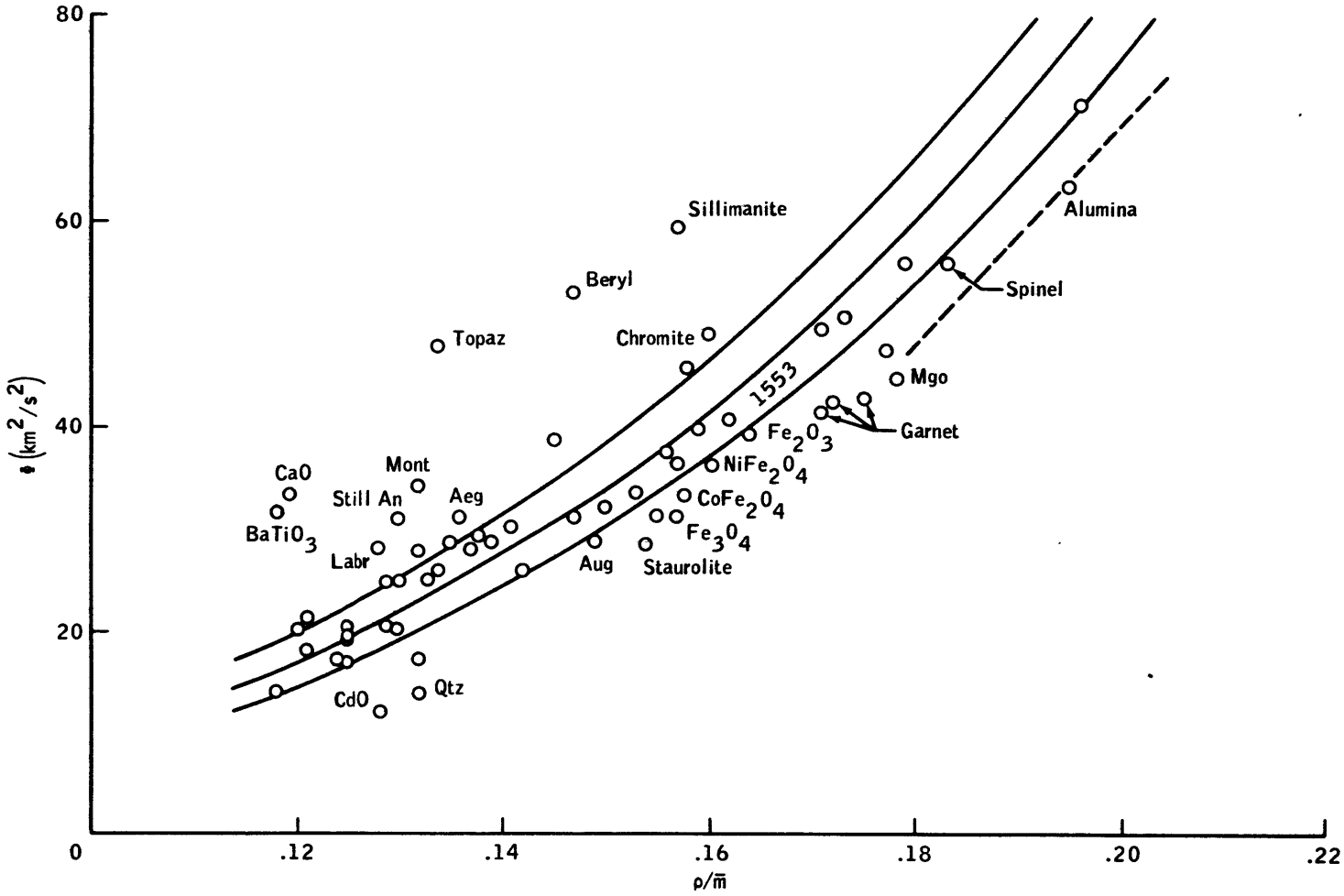

Figure IV-2.- Test of D. Anderson relationship $\rho = A\bar{m}\Phi^{n}$. Data from table IV-2.

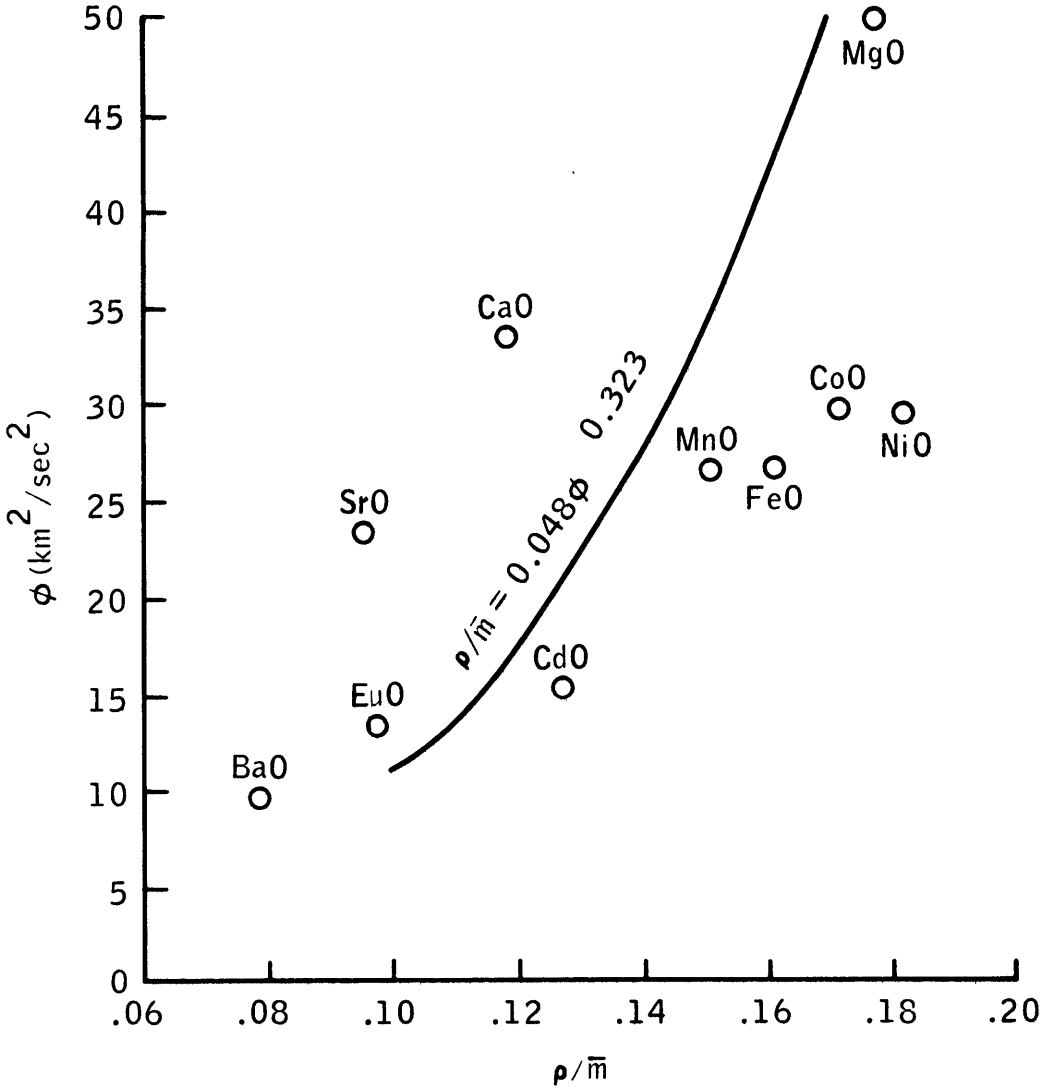

Figure IV-3.- Test of relationship $\rho = A\bar{m}\phi^n$ with data on oxides with the NaCl structure. Data from table IV-3.

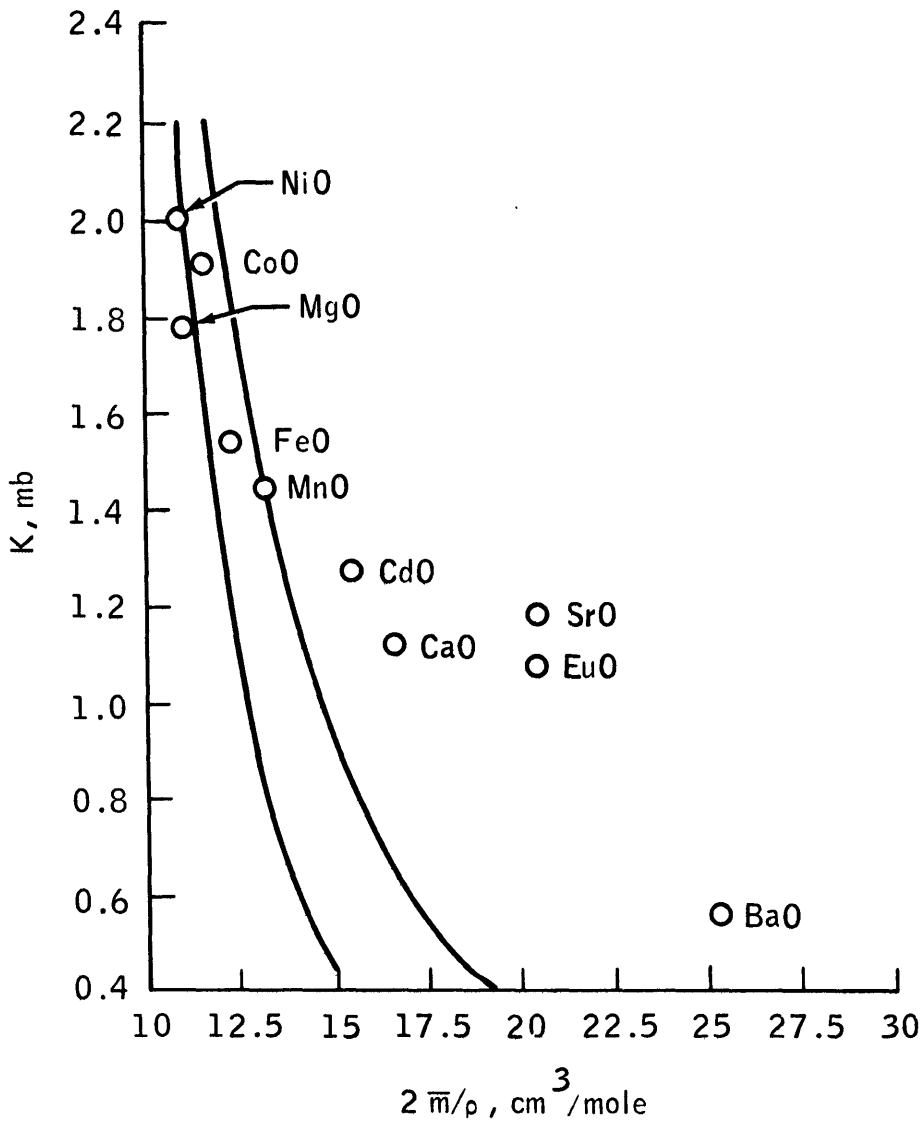

Figure IV-4.- Test of relationship $\ln K = A \ln(2\bar{m}/\rho) + C$ with data on oxides with the NaCl structure. Data from table IV-3.

V. A MODIFIED QUASI-HARMONIC EQUATION OF STATE AND GRUNEISEN'S RATIO

As concluded in chapter IV, the elastic properties of the various oxides and silicates are not correlated adequately by any of the universal equations of state. A stipulation of each of the universal equations is that the values of the elastic parameters are fixed by the mean atomic weight and density. For a particular oxide or silicate, temperature and pressure affect the elastic parameters only when a change in density occurs. Thus, the elastic parameters would not change if an increase in pressure were balanced by an increase in temperature so that the density remained unchanged. An equivalent statement of $q = q(\bar{m},\rho)$, where q is an elastic parameter, is

V-1) $$\left[\frac{\partial q(\bar{m})}{\partial \rho}\right]_T = \left[\frac{\partial q(\bar{m})}{\partial \rho}\right]_P .$$

Data on 10 oxides and silicates are listed in table V-1. A test of equation V-1, using the data from table V-1, was conducted. The test data are presented in table V-2. Except for K_s, the requirement that $q = q(\bar{m},\rho)$ fails, particularly, $v_p \neq v_p(\bar{m},\rho)$, which is a challenge to the validity of Birch's law. In chapter IV, Birch's law was the only universal law illustrated to be even marginally successful. A general conclusion, based on the arguments presented in chapter IV and on the failure of equation V-1, is that the universal equations of state are inadequate for reliable extrapolation to temperatures and pressures found in the mantle of the earth. The reliability of an extrapolation to mantle conditions is improved greatly if a theoretically sound equation of state tailored to a specific petrological model is used. The quasi-harmonic theory of lattice

dynamics is presently the only suitable theory. A development of the quasi-harmonic equation of state and an evaluation of the volume dependence of its key parameter, Gruneisen's ratio, is presented in this chapter.

Background

Two problems are inherent in the formulation of an equation of state. A theoretical expression is needed for the dynamic atomic interactions, and values are required for the interatomic forces. Roughly, the temperature dependence of the equation of state is derived from the dynamic solution, and the pressure dependence is derived from the interatomic forces. Although the interatomic potentials of the general form

$$u = -\frac{a}{r^n} + \frac{b}{r^m} \quad (m > n)$$

may be justifiable for ionic crystals, the interatomic forces must be obtained empirically for most materials.

Born and Huang (1954), Maradudin, et al. (1963), and others have reviewed the harmonic theory of lattice dynamics. Leibfried and Ludwig (1961) have reviewed the quasi-harmonic theory and the general anharmonic effects. Those parts of the quasi-harmonic theory pertinent to the geophysical use of the equation of state are discussed in this study. The notation used here conforms generally to that used by Maradudin, et al.

Consider a lattice of N cells, each cell l having volume v and containing r atoms. The atoms oscillate about mean positions determined by temperature and pressure. This theory differs from the harmonic theory in which these positions are equilibrium atom sites at zero P and T.

If ϕ is the potential energy of the crystal, a Taylor expansion of ϕ, based on mean position, is

V-2) $$\phi = \phi_o(V) + \left(\frac{1}{2}\right) \sum_{\substack{lsi \\ l's'j}} \phi,_{ij}\begin{pmatrix} ll' \\ ss' \end{pmatrix} u_i\begin{pmatrix} l \\ s \end{pmatrix} u_j\begin{pmatrix} l' \\ s' \end{pmatrix} + \ldots$$

where V is the total volume, $V = Nv$, $\phi_o(V)$ is the rest potential at volume V, $u_i\begin{pmatrix} l \\ s \end{pmatrix}$ is the displacement from equilibrium in the ith direction of the sth atom in the lth cell, and

$$\phi,_{ij}\begin{pmatrix} ll' \\ ss' \end{pmatrix} \equiv \left[\frac{\partial^2 \phi}{\partial u_i\begin{pmatrix} l \\ s \end{pmatrix} \partial u_j\begin{pmatrix} l' \\ s' \end{pmatrix}}\right].$$

Note that equilibrium requires the first-order term in equation V-2 to be zero. If the displacements are such that the third and higher terms are negligible (not the same as assuming that the displacements are small), V-2 becomes a simple quadratic equation. The kinetic energy for the crystal is

V-3) $$K = \frac{1}{2} \sum_{lsi} m_s \dot{u}_i^{\,2}\begin{pmatrix} l \\ s \end{pmatrix}$$

where $\dot{u}_i\begin{pmatrix} l \\ s \end{pmatrix}$ is the time derivative of $u_i\begin{pmatrix} l \\ s \end{pmatrix}$. A solution for the equation of motion

V-4) $$m_s \ddot{u}_i\begin{pmatrix} l \\ s \end{pmatrix} + \sum_{l's'j} \phi,_{ij}\begin{pmatrix} ll' \\ ss' \end{pmatrix} u_j\begin{pmatrix} l' \\ s' \end{pmatrix} = 0$$

is

V-5) $$u_i\begin{pmatrix} l \\ s \end{pmatrix} = m_s^{-1/2}\, u_i(s)\, e^{i[\omega t - \bar{k}\cdot\bar{x}(l)]}$$

where the amplitude $u_i(s)$ is independent of l and V, $\bar{x}(l)$ is the position vector of the lth cell, ω is the angular frequency, and $\bar{k}$ is the wave vector. The characteristic equation of equation V-4 is

V-6) $$\sum_{s'j}\left[D_{ij}\begin{pmatrix} \bar{k} \\ ss' \end{pmatrix} - \omega^2\delta_{ij}\delta_{ss'}\right]U_j(s') = 0$$

where

$$D_{ij}\begin{pmatrix} \bar{k} \\ ss' \end{pmatrix} = \left(m_s m_{s'}\right)^{-1/2}\sum_{l'}\phi_{,ij}\begin{pmatrix} ll' \\ ss' \end{pmatrix}e^{i\bar{k}\cdot[\bar{x}(l')-\bar{x}(l)]}.$$

The elements of the dynamical matrix are $D_{ij}\begin{pmatrix} \bar{k} \\ ss' \end{pmatrix}$. This matrix reflects the symmetry of the crystal.

Equation V-6 has nontrivial solutions only if

V-7) $$\left|D_{ij}\begin{pmatrix} \bar{k} \\ ss' \end{pmatrix} - \omega^2\delta_{ij}\delta_{ss'}\right| = 0$$

for any allowed choice of $\bar{k}$. Because $s = 1, \ldots,$ and $i = 1, 2, 3,$ equation V-7 is the 3r-degree equation in ω^2. Thus,

$$\omega = \omega_p(\bar{k}) \quad (p = 1,2,\ldots,3r).$$

Given boundary conditions for the oscillations, e.g., the displacement at the boundary is always zero, k may have only N discrete values. Therefore, $3rN$ solutions to equation V-6 exist. This situation might

have been anticipated from the three degrees of freedom of each of the rN atoms in the crystal.

The solutions (eq. V-5) are wavelike. The crystal dynamics can be considered as a problem of $3rN$ independent linear oscillators. The Helmholtz free energy for a set of oscillators is written as the sum of the equilibrium configurational energy, the zero point vibrational energy, and a term related to the thermal vibrational energy. Thus,

V-8) $$A = \phi(V) + \sum_{\omega} \frac{\bar{h}\omega}{2} + kT \sum_{\omega} \ln\left(1 - e^{-\bar{h}\omega/kT}\right).$$

Because ω is strictly a function of the equilibrium configuration or volume V, a new function $\psi(V)$ will be substituted for $\phi(V) + \sum_{\omega} \frac{\bar{h}\omega}{2}$.

The pressure is

V-9) $$P = -\left(\frac{\partial A}{\partial V}\right)_T = -\psi,_V + \left(\frac{1}{V}\right) \sum_{\omega} \left(\frac{\bar{h}\omega}{e^{\bar{h}\omega/kT} - 1}\right) \gamma_{\omega}$$

where

V-10) $$\gamma_{\omega} \equiv -\left(\frac{\partial \ln\omega}{\partial \ln V}\right).$$

The Gruneisen parameter γ_{ω} for the eigenfrequency ω is strictly a function of V. The quantity

$$\left(\frac{\bar{h}\omega}{e^{\bar{h}\omega/kT} - 1}\right) \equiv E_{\omega}$$

is the thermal vibrational energy of an oscillator having the eigenfrequency ω. Equation V-9 becomes the quasi-harmonic equation of state

V-11) $$P = -\psi,_V + \frac{1}{V}\sum_{\omega}\gamma_{\omega}E_{\omega}.$$

The only assumption to this point is that the third and higher order potential-energy terms are negligible to the formulation of the vibrational energy.

The Gruneisen assumption is that γ_{ω} can be replaced by an average value $\bar{\gamma}$ so that

V-12) $$P = -\psi,_V + \frac{\bar{\gamma}E_{vib}}{V}$$

where $E_{vib} = \sum_{\omega} E_{\omega}$. Equation V-12 is the Mie-Gruneisen equation of state. Because

V-13) $$\bar{\gamma} = \frac{\sum_{\omega}\gamma_{\omega}E_{\omega}}{E_{vib}},$$

$\bar{\gamma}$ is no longer strictly a function of volume but may also vary with the temperature. Because each E_{ω} had its own temperature dependence, a variation of temperature at constant volume may change $\bar{\gamma}$ even though each γ_{ω} is fixed.

New Support for a Modified Quasi-Harmonic Equation of State

An alternative to the 3rN distinct terms in $\bar{\gamma}$ is to assume that the γ_{ω} terms within each mode are identical. In terms of the mode n,

equation V-13 is

$$\text{V-14)} \qquad \bar{\gamma} = \frac{\sum_n \gamma_n E_n}{E_{vib}}$$

where E_n is the energy in mode n. Only three independent elastic modes exist for the cubic crystals. The temperature dependence of $\bar{\gamma}$ becomes manageable. In the following discussion, it is shown that the Gruneisen's ratios within a mode are independent of ω for covalently bonded crystals.

To illustrate a sufficient condition for $\gamma_n \neq \gamma_n(\bar{k})$, consider a crystal which has symmetry other than triclinic or monoclinic. The orientation of the eigenvectors for such a crystal is not dependent on $|\bar{k}|$. For this case, a transformation matrix A_{ni} exists (not dependent on $|\bar{k}|$), so that entries in the orthogonalized dynamical matrix are

$$\text{V-15)} \qquad D^n\begin{pmatrix}\bar{k}\\ ss'\end{pmatrix} = \sum_{ij} A_{ni}A_{jn}D_{ij}\begin{pmatrix}\bar{k}\\ ss'\end{pmatrix} \qquad (n = 1,2,3).$$

If the order of summation is reversed, then

$$\text{V-16)} \quad D^n\begin{pmatrix}\bar{k}\\ ss'\end{pmatrix} = \left(m_s m_{s'}\right)^{-1/2} \sum_{l'} e^{i\bar{k}\cdot[\bar{x}(l')-\bar{x}(l)]} \left\{\sum_{ij} A_{ni}A_{jn}\Phi_{,ij}\begin{pmatrix}ll'\\ ss'\end{pmatrix}\right\} .$$

The quantity in braces is strictly a function of the indices n, l, l', s, and s'. By denoting the quantity in brackets as $g^n\begin{pmatrix}ll'\\ ss'\end{pmatrix}$, equation V-16 can be written as

$$\text{V-17)} \qquad D^n\begin{pmatrix}\bar{k}\\ ss'\end{pmatrix} = \left(m_s m_{s'}\right)^{-1/2} \sum_{l'} g^n\begin{pmatrix}ll'\\ ss'\end{pmatrix} e^{i\bar{k}\cdot[\bar{x}(l')-\bar{x}(l)]} .$$

Consider a lattice centered on the atom $s_o(\bar{x}(l) = 0)$ with the nearest neighbors of type s_l. If the nearest neighbor forces are identical and dominate the dynamical interactions, then

$$\text{V-18)} \qquad D^n\begin{pmatrix}\bar{k} \\ s_o\end{pmatrix} = \left(m_{s_o} m_{s_l}\right)^{-1/2} g^n\left(|\bar{\Delta}|\right) \sum_{l'} e^{i\bar{k}\cdot\bar{\Delta}(l')}$$

where $\bar{\Delta}(l')$ quantities are the vectors to the nearest neighbor forces.

Because the boundary conditions require that $\bar{k} \cdot \bar{x}(l')$ be independent of volume, the volume derivatives of the solutions to the characteristic equation are

$$\text{V-19)} \qquad \frac{d}{dV}\left(\omega^2_n\right) = m_n\left[\frac{dg^n(|\Delta|)}{dV}\right] \sum_{l'} e^{i\bar{k}_n\cdot\bar{\Delta}(l')}$$

where n has $3r$ values for each eigenvector or a total of $9r$ values. From the definition of Gruneisen's ratio (eq. V-10),

$$\text{V-20)} \qquad \gamma_n = -\frac{1}{2}\frac{d \ln g^n(|\Delta|)}{d \ln V}.$$

The assumption of dominant nearest neighbor forces yields mode gammas that are independent of frequency or, equivalently, independent of temperature. Because of the charge neutrality of atoms in covalently bonded crystals, the nearest neighbor forces dominate. In support, consider that the total energy of a covalent solid is very nearly the sum of the energies of the individual covalent bonds (Ziman, 1964). Much of the bonding in oxides and silicates is covalent, i.e., the mode gammas for much of the material in the mantle and crust of the earth are largely independent of

temperature. Thus, the geophysically appropriate quasi-harmonic equation of state is

V-21) $$P = -\psi_{,V} + \frac{1}{V}\sum_{n} \gamma_n E_n$$

where the summation is over the $9r$ modes.

To evaluate the mode gamma of an elastic branch n, consider the phase velocity ω_n/k_n. The boundary conditions are that the crystal dimensions be an integral multiple of $2\pi/k_n$. The reciprocal of the round-trip travel time of a wave between two boundaries is

V-22) $$F_n(\omega) = \frac{\omega_n}{2\pi s}$$

where s is an integer. The mode gamma, in terms of $F_n(\omega)$, is

V-23) $$\gamma_n = -\frac{\partial \ln F_n(\omega)}{\partial \ln V}.$$

For those materials where $\gamma_n \neq \gamma_n(\omega)$, ω in the ultrasonic range may be chosen. Then,

V-24) $$\gamma_n = -V\left[\frac{\partial\left(\frac{F_n}{F_n^{\,o}}\right)}{\partial V}\right]_T$$

or

V-25) $$\gamma_n = K_T\left[\frac{\partial\left(\frac{F_n}{F_n^{\,o}}\right)}{\partial P}\right]_T$$

A measurement of the change in ultrasonic wave travel time with pressure yields Gruneisen's ratio for that mode (a direct application of the parameter (F_n/F_n°) that was used in chapter III).

The wave velocities in the solution to the dynamical equation are observable, as indicated in equation V-25. The solution was based on completely decoupled oscillators. Because the elastic parameters in the dynamical equation are related more closely to the static rather than the dynamic elastic constants, the ultrasonic waves are not truly eigensolutions to the dynamical equation. If the ultrasonic waves were eigensolutions to the dynamical equation, the phase velocities would be dependent only on volume, i.e., $(\partial v_n/\partial \rho)_P = (\partial v_n/\partial \rho)_T$. The data in table V-2 indicate that this is not true. Because the γ_n values in the quasi-harmonic equation of state were obtained from the volume derivative at constant temperature of the Helmholtz energy, the $(\partial v_n/\partial \rho)_T$ values probably are more nearly related to the solutions for γ_n.

The omission of the optic modes at room temperature is not serious; however, at mantle temperature, much of the vibrational energy is in the higher frequency modes. An approximation of the effect of the optic modes may be obtained by ignoring the band gaps. Each optic branch becomes an extension of an acoustic branch. For dominant, nearest neighbor forces, the acoustic γ_n would be the same as that for the appropriate optic branch. The summation in the modified quasi-harmonic equation V-21 would be over nine values of n (three solutions to each of the three principal directions) rather than over $9r$ values of n.

A New Expression for the Volume Dependence of Gruneisen's Ratio

The quasi-harmonic equation of state is often used to reduce shock data (Duvall and Fowles, 1963; Rice, et al., 1958). Because the locus of possible P-V points (the Hugoniot) for a shocked material is assumed to be an isentrope, the data reduction involves an estimate of adiabatic heating in the shock front. If a reversible process is assumed, the thermodynamic identity

V-26) $$T\,ds = C_V\,dT + T\left(\frac{\partial P}{\partial T}\right)_V dV = 0$$

can be integrated to yield

V-27) $$T = T_i e^{-\int_{V_i}^{V} \frac{\bar{\gamma}}{V}\,dV} .$$

To reduce the Hugoniot to an isotherm, one must depend heavily on equation V-27 or on the volume dependence of $\bar{\gamma}$. The uncertainty caused by this dependence is discussed by Knopoff and Shapiro (1969). A common approach has been to accept either the Slater (SL) or the Dugdale-MacDonald (DM) expressions for $\bar{\gamma}$. Thus,

V-28) $$\gamma_{SL} = -\frac{1}{6} + \frac{1}{2}\left(\frac{\partial K}{\partial P}\right) + \delta_{SL}$$

V-29) $$\gamma_{DM} = -\frac{1}{2} + \frac{1}{2}\left(\frac{\partial K}{\partial P}\right) + \delta_{DM}$$

where the $\delta_{SL,DM}$ are factors that force the $\gamma_{SL,DM}$ to agree with the thermal Gruneisen's ratio. Knopoff and Shapiro observe that neither

expression is sound theoretically. As demonstrated in figure V-1, the correct volume dependence of γ_{SL} or γ_{DM} has considerable importance.

Anderson and Kanamori (1968) reduced the Hugoniots for several oxides and silicates, including those for spinel, alumina, magnesium oxide, and forsterite. They calculated the parameters in the Birch-Murnaghan equation (appendix A) for several densities along the Hugoniot. For the Birch-Murnaghan equation of state,

$$\text{V-30)} \qquad P = \frac{3}{2} K_o \left[\rho/\rho_o^{\,7/3} - \rho/\rho_o^{\,5/3}\right] \left\{1 - \xi \left[\left(\frac{\rho}{\rho_o}\right)^{2/3} - 1\right]\right\},$$

the SL and DM Gruneisen's ratios are

$$\text{V-31)} \qquad \gamma_{SL} = \frac{11}{6} - \frac{2}{3}\xi + \delta_{SL}$$

$$\gamma_{DM} = \frac{3}{2} - \frac{2}{3}\xi + \delta_{DM}$$

The initial volume dependence of these Gruneisen's ratios are

$$\text{V-32)} \qquad \left(\frac{\partial \ln \gamma}{\partial \ln V}\right)^{o}_{SL} = \frac{2}{3}\frac{K_o}{\gamma}\left(\frac{\partial \xi}{\partial P}\right)_o$$

$$\left(\frac{\partial \ln \gamma}{\partial \ln V}\right)^{o}_{DM} = \left(\frac{\partial \ln \gamma}{\partial \ln V}\right)^{o}_{Sl} - \frac{2}{3}\left(\frac{\gamma + \frac{1}{6}}{\gamma}\right).$$

Data from the Anderson and Kanamori paper are given in table V-3 to show $\left(\frac{\partial \ln \gamma}{\partial \ln V}\right)^{o}_{SL}$ for several materials. The term $\frac{2}{3}\left(\frac{\gamma + \frac{1}{6}}{\gamma}\right)$ is small compared to

$\left(\frac{\partial \ln \gamma}{\partial \ln V}\right)^{o}_{SL}$. As observed by Takeuchi and Kanamori (1966), little difference exists between the SL and DM formulations.

The following discussion is to determine whether $\left(\frac{\partial \ln \gamma}{\partial \ln V}\right)^{o}_{SL}$ is reasonable. The difference between the ultrasonic $(\partial K_s/\partial \rho)_T$ and $(\partial k_s/\partial \rho)_p$ (table V-2) allows $(\partial \ln \gamma/\partial \ln V)_o$ to be estimated. The volume derivative at constant entropy of the Mie-Gruneisen equation of state (eq. V-12) for $\bar{\gamma} = \bar{\gamma}(V)$ is

V-33) $$P - K_s = -\left(V\psi,_V\right),_V + \bar{\gamma},_V E_{vib} + \bar{\gamma}\left(\frac{\partial E_{vib}}{\partial V}\right)_s.$$

The internal energy U is $\psi + E_{vib}$. Because $dU = -pdV$ at constant entropy, equation V-33 can be written as

V-34) $$K_s = \left(P + \psi,_V\right)\left(1 + \bar{\gamma}\right) + V\psi,_{VV} - \bar{\gamma},_V E_{vib}.$$

From the temperature derivative at constant volume,

V-35) $$\bar{\gamma},_V = \frac{1}{C_V}\left[\left(1 + \gamma\right)\left(\frac{\partial P}{\partial T}\right)_V - \left(\frac{\partial K_s}{\partial T}\right)_V\right].$$

Because $(\partial P/\partial T)_V = K_T\alpha$, $(\partial K_s/\partial T)_V = \rho\alpha(\partial K_s/\partial \rho)_T - \rho\alpha(\partial K_s/\partial \rho)_P$; and $\bar{\gamma} = K_T\alpha/\rho C_V$, then

V-36) $$\frac{\partial \ln \gamma}{\partial \ln V} = (1 + \gamma) + \frac{\rho}{K_T}\left[\left(\frac{\partial K_s}{\partial \rho}\right)_P - \left(\frac{\partial K_s}{\partial \rho}\right)_T\right].$$

The value of $(\partial \ln \gamma/\partial \ln V)_o$ for 10 compounds are listed in table V-4. Note that the values in table V-4 are an order of magnitude smaller than the values in table V-3. The assumed volume dependence of

the Gruneisen ratio used to reduce the shock-wave data is much too large. The isothermal equation, based on a constant Gruneisen's ratio, is probably closer to being correct than are the equations based on an SL or DM formula. The temperatures in a shock front are higher than were previously thought, and the isothermal P-V curves are not as steep. Because neither the SL nor the DM Formulations of Gruneisen's ratio is sound, the ultrasonic data should be used to obtain $(\partial\gamma/\partial V)_o$, and the linear approximation to γ, i.e., $\gamma = \gamma_o + (\partial\gamma/\partial V)_o \Delta V$ should be used for the reduction of the Hugoniot. This procedure is not practical for high-pressure polymorphs. In such cases, $(\partial \ln \gamma/\partial \ln V)_o = (1 + \gamma)$ might be a good alternative. For most of the compounds listed in table V-2, the second term in equation V-36 is small compared to $(1 + \gamma)$.

The $(\partial \ln \gamma/\partial \ln V)_o$ values are plotted against the specific volume in figure V-2. The trend is that the $(\partial \ln \gamma/\gamma \ln V)_o$ value is less for the more dense materials, which is consistent with O. Anderson's (1968) contention that Gruneisen's ratios for higher density polymorphs are smaller. If $(\partial \ln \gamma/\partial \ln V)_o = (1 + \gamma)$ and γ is smaller for the high density polymorph, then $(\partial \ln \gamma/\partial \ln V)_o$ is also smaller.

TABLE V-1.- DATA USED IN CHAPTER IV. EXCEPT FOR SPINEL CdO AND FORSTERITE, DATA WERE TAKEN FROM O. ANDERSON ET AL. (1968). SPINEL AND CdO DATA ARE FROM CHAPTER III. FORSTERITE DATA ARE FROM KUMAZAWA AND ANDERSON (1969).

	S.C. spinel	Polycrystal CdO	Polycrystal Al_2O_3	S.C. MgO	S.C. α-SiO_2	S.C. Garnet**	Polycrystal Mg_2SiO_4	Polycrystal ZnO	Polycrystal CaO	Polycrystal BeO
ρ	3.6245	7.8433	3.972	3.5833	2.6485	4.1602	3.224	5.621	3.345	3.008
$\bar{\gamma}$	.69	1.49	1.32	1.55	.69	1.22	1.17	.81	1.19	1.27
K_T	2016	1141	2505	1599	374	1757	1275	1389	1049	2186
α_v	22.3×10^{-6}*	32×10^{-6}	16.3×10^{-6}	31.2×10^{-6}	35.4×10^{-6}	21.6×10^{-6}	24.7×10^{-6}	15.0×10^{-6}	28.1×10^{-6}	17.7×10^{-6}
$\left(\frac{\partial v_P}{\partial P}\right)_T$	.00530	.00714	.00518	.00829	.0137	.00784	.0107	.00364	.0104	.00648
$\left(\frac{\partial v_P}{\partial T}\right)_P$	-.000441	-.000425	-.00037	-.00049	-.00027	-.00039	-.00048	-.00019	-.00051	-.00028
$\left(\frac{\partial v_s}{\partial P}\right)_T$	.00043	.00210	.00221	.00396	-.00338	.00217	.00358	-.00319	.0029	.00033
$\left(\frac{\partial v_s}{\partial T}\right)_P$	-.00020	-.00028	-.00031	-.00040	.000009	-.00022	-.00034	-.000039	-.00037	-.00020
$\left(\frac{\partial K_s}{\partial P}\right)_T$	4.58	5.31	3.98	4.49	6.4	5.43	5.37	4.78	5.23	5.52
$\left(\frac{\partial K_s}{\partial T}\right)_P$	-.257	-.215	-.16	-.16	-.10	-.20	-.15	-.13	-.14	-.12
$\left(\frac{\partial G}{\partial P}\right)_T$	.753	1.23	1.76	2.54	.45	1.40	1.80	-.69	1.64	.88
$\left(\frac{\partial G}{\partial T}\right)_P$	-.106	-.125	-.18	-.21	-.007	-.11	-.13	-.02	-.14	-.12

*Thermal expansion of spinel is from Skinner (1966). The value in the O. Anderson paper is 16.2×10^{-6}.
**The composition of the garnet is of an almandite-pyrope type.

TABLE V-2.- A COMPARISON OF THE DENSITY DERIVATIVES OF THE ELASTIC PARAMETERS AT CONSTANT TEMPERATURE WITH THOSE AT CONSTANT PRESSURE.

	$\rho\left(\frac{\partial v_P}{\partial \rho}\right)_T$	$\rho\left(\frac{\partial v_P}{\partial \rho}\right)_P$	$\rho\left(\frac{\partial v_s}{\partial \rho}\right)_T$	$\rho\left(\frac{\partial v_s}{\partial \rho}\right)_P$	$\rho\left(\frac{\partial K_s}{\partial \rho}\right)_T$	$\rho\left(\frac{\partial K_s}{\partial \rho}\right)_P$	$\rho\left(\frac{\partial G}{\partial \rho}\right)_T$	$\rho\left(\frac{\partial G}{\partial \rho}\right)_P$
Spinel	10.7	19.7	0.9	9.0	9.3×10^3	11.5×10^3	1.5×10^3	4.8×10^3
CdO	8.1	13.3	2.4	8.7	6.1×10^3	6.7×10^3	1.4×10^3	3.9×10^3
Al_2O_3	13.0	22.7	5.5	19.0	10.0×10^3	9.8×10^3	4.4×10^3	11.0×10^3
MgO	13.3	15.7	6.3	12.8	7.2×10^3	5.1×10^3	4.1×10^3	6.7×10^3
α-SiO_2	5.1	7.6	-1.3	-.3	2.4×10^3	2.8×10^3	$.17 \times 10^3$	$.20 \times 10^3$
Garnet	13.8	18.0	3.8	10.2	9.5×10^3	9.3×10^3	2.5×10^3	5.1×10^3
Mg_2SiO_4	13.6	19.5	4.6	13.8	6.8×10^3	6.1×10^3	2.3×10^3	5.3×10^3
ZnO	5.1	12.7	4.4	2.6	6.6×10^3	8.7×10^3	-1.0×10^3	1.3×10^3
CaO	10.9	18.2	3.0	13.2	5.5×10^3	5.0×10^3	1.7×10^3	5.0×10^3
BeO	14.2	15.8	.7	11.3	12.0×10^3	6.8×10^3	1.9×10^3	7.0×10^3

TABLE V-3.- $\left(\frac{\partial \ \ell n \ \gamma}{\partial \ \ell n \ V}\right)$ FOR SLATER's DEPENDENCE OF γ ON VOLUME.

	$\left(\frac{\partial \ \ell n \ \gamma}{\partial \ \ell n \ V}\right)^{o}_{SL}$
Spinel	+17
$A\ell_2O_3$	+42
MgO	+10
Mg_2SiO_4	+21

TABLE V-4.- THE VOLUME DERIVATIVE OF GRUNEISEN'S PARAMETER FOR SEVERAL MATERIALS.

	Sp. vol.*	$\left(\frac{\partial \ \ell n \ \gamma}{\partial \ \ln V}\right)_o$
Spinel	5.27	2.8
CdO	8.19	3.0
Al_2O_3	5.13	2.3
MgO	5.63	1.3
α-SiO_2	7.56	2.8
Garnet	5.72	2.1
Mg_2SiO_4	6.65	1.6
ZnO	7.24	3.3
CaO	8.38	1.7
BeO	4.16	.0

*Specific volume is mean atomic weight/density and has units cc/mole.

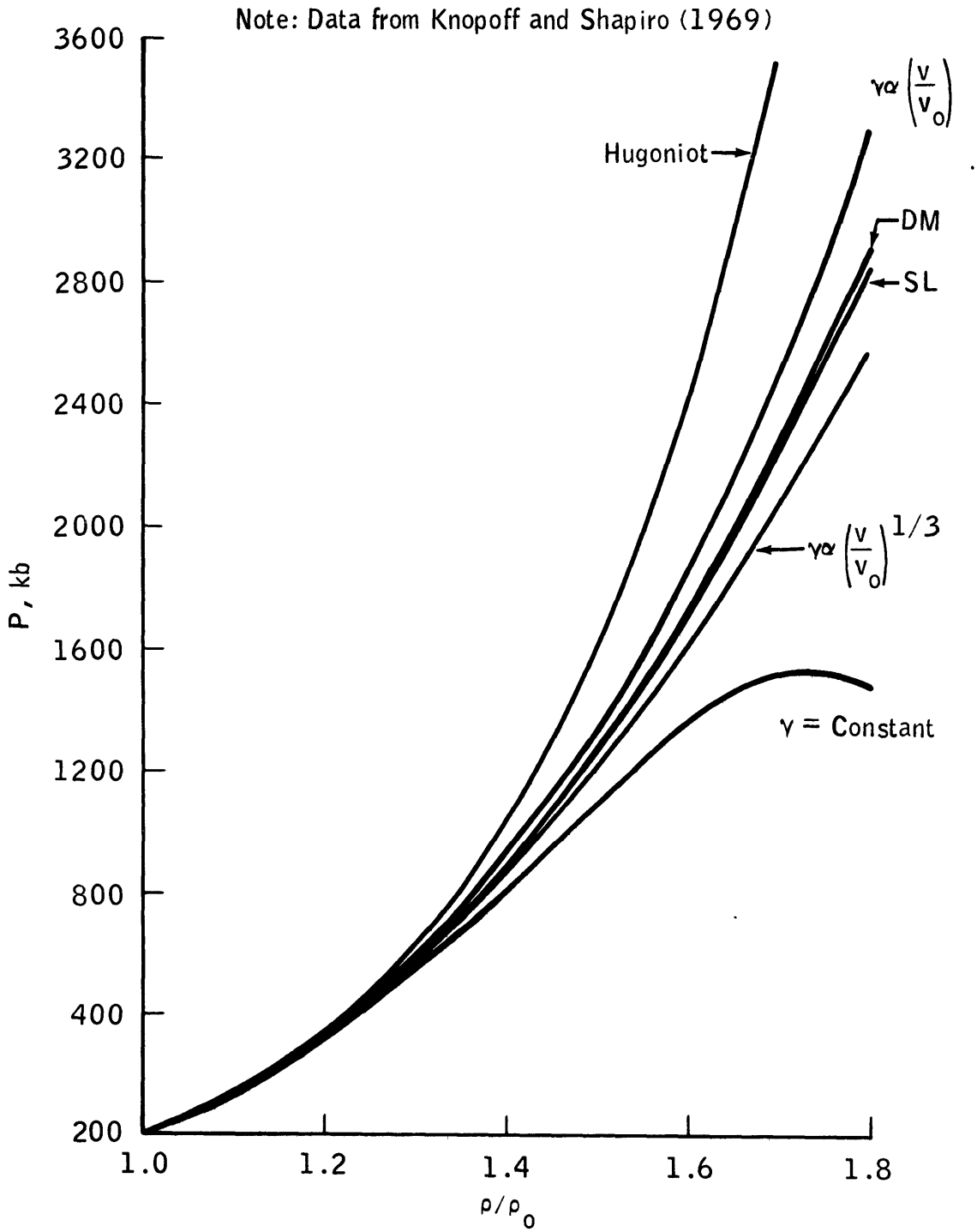

Figure V-1.- The effect of the choice of $\gamma(v)$ on the isotherm for silver.

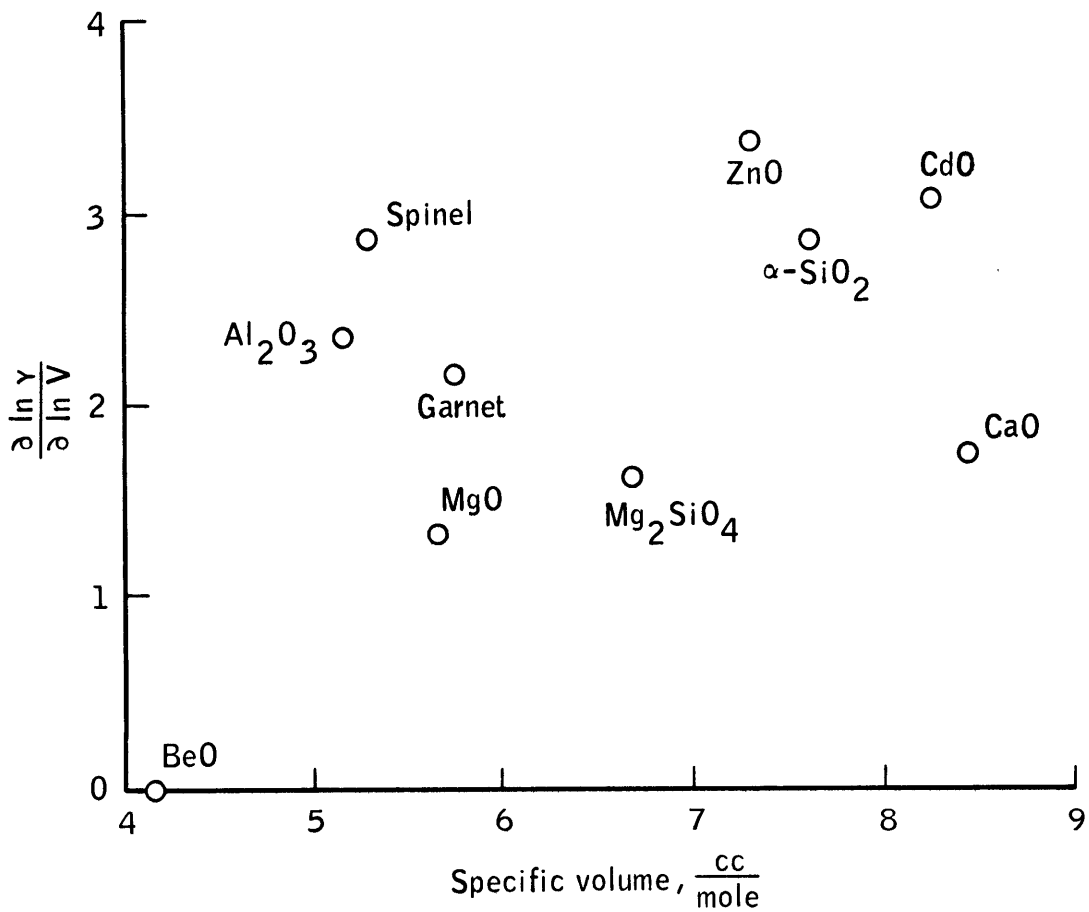

Figure V-2.- The dependence of the volume derivative of Gruneisen's parameter on specific volume.

VI. CONCLUSIONS

For an elastic parameter X, the effect of spherical pores on the parameter X is predicted adequately by Mackenzie's (1950) equations. However, the assumption of a linear dependence of X on pressure combined with the pressure derivatives of Mackenzie's equations is insufficient to predict reliably the effective $\partial X/\partial P$ as a function of porosity. When the data of a study must be very accurate, the porosity will have to be reduced to nearly zero, which is very difficult with modern hot-pressing techniques.

Comparison of the elastic properties of four spinels (Al_2O_3/MgO ratios of 1.1, 2.61, 3.0, and 3.5) shows an almost negligible dependence on stoichiometry. Because the mean atomic weights and the densities of the spinels are nearly the same, the result is consistent with the universal equations of state.

The O. Anderson-Nafe, Birch, and D. Anderson relationships are tested against the new data on spinel, magnetite, and cadmium oxide plus data from the literature on the elastic properties of other oxides and silicates. Numerous exceptions to each exist, and none of the relationships appear to have general validity for oxides and silicates. However, the Birch relationship may be useful for predicting the properties of some materials with restricted compositions. If the phase and compositional changes are barred, the O. Anderson-Nafe law and the ϕ law predict the strict dependence of an elastic property on density, i.e., $K_s = K_s(\rho)$.

If the nearest neighbor atomic forces dominate the interatomic lattice interactions, mode Gruneisen's ratios are independent of frequency. This dominance is realized in covalently bonded solids. For such

materials, measurement of ultrasonic mode gammas are particularly pertinent. The quasi-harmonic equation of state becomes

$$\text{VI-1)} \qquad P = -\psi,_V + \frac{1}{V}\sum_n \gamma_n E_n$$

where n is the elastic mode and γ_n is the ultrasonically determined mode gamma. Because most oxides and silicates are predominantly covalent, when possible, equation VI-1 should be used rather than the less accurate Mie-Gruneisen equation. Certainly, either equation VI-1 or the Mie-Gruneisen equation is preferable to any of the universal equations.

If the Gruneisen assumption that $\bar{\gamma}$ is independent of temperature is accepted, the volume derivative of Gruneisen's ratio is obtained readily, i.e.

$$\text{VI-2)} \qquad \left(\frac{\partial \ln \gamma}{\partial \ln V}\right)_o = (1 + \gamma) + \frac{\rho}{K_T}\left[\left(\frac{\partial K_s}{\partial \rho}\right)_P - \left(\frac{\partial K_s}{\partial \rho}\right)_T\right].$$

New data for spinel and cadmium oxide along with data for eight other oxides and silicates indicate that $(\partial \ln \gamma/\partial \ln V)_o$ is nearly $(1 + \gamma)$, which is an order of magnitude smaller that either the SL or DM approximation. Thus, equation VI-2 or, where ultrasonic data are unavailable, $(\partial \ln \gamma/\partial \ln V)_o = (1 + \gamma)$ should be used in the reduction of shock data. The isotherm derived from the Hugoniot is strongly dependent on the variation of Gruneisen's ratio with volume. To assume either the SL or the DM formula is not sufficient.

APPENDIX A

DERIVATION OF THE BIRCH-MURNAGHAN EQUATION OF STATE

The development of the Birch-Murnaghan equation can be found in Birch (1947, 1952). However, the derivation presented here has the advantage of modern nomenclature and brevity without sacrificing rigor.

If each point in an undeformed body is designated by a position vector whose components are a_i $(i = 1,2,3)$, and x_i are the coordinates of the point after deformation, then each point before deformation is uniquely related to some point after deformation by a function

A-1) $$a_i = a_i(x_1, x_2, x_3).$$

Consider an infinitesimal line segment da_i at a point a_i. The deformation transforms da_i to a line segment dx_i in the deformed body. By the functional relation of A-1,

A-2) $$da_i = a_{i,j}\, dx_j$$

where use is made of the usual summation convention and $a_{i,j}$ is $\frac{\partial a_i}{\partial x_j}$. The difference of the squares of this infinitesimal line before and after deformation is

A-3) $$\Delta(ds^2) = dx_i\, dx_i - da_j\, da_j$$

or, from A-2, in terms of the final coordinates,

A-4) $$\Delta(ds^2) = (\delta_{jk} - a_{i,j} a_{i,k}) dx_j\, dx_k,$$

where δ_{jk} is the Kronecker delta. The quantity ε_{jk}, defined as

A-5) $$\varepsilon_{jk} = (1/2)\left(\delta_{jk} - a_{i,j}a_{i,k}\right),$$

is called the Eulerian finite strain tensor. In terms of this strain tensor, equation A-4 becomes

A-6) $$\Delta\left(ds^2\right) = 2\varepsilon_{jk}\, dx_j\, dx_k.$$

We now want the constitutive relations. For a deformed body with surface S, volume V, and specific energy ϕ (either internal energy or Helmholtz energy), the change in total energy (adiabatically for internal energy or with a constant temperature for Helmholtz energy) due to an arbitrary, reversible, virtual displacement, $(\delta x)_i$, is

A-7) $$\int_V \rho\ \delta\phi\ dV = \int_S \sigma_{ij}(\delta x)_j n_i dS + \int_V F_j(\delta x)_j\ dV$$

where σ_{ij} are the stresses at the boundary, F_j are the body forces, and n_i is the unit normal to surface S with positive sense outward. Applying the divergence theorem and remembering the $\sigma_{ij,j} + F_i = 0$ for stress equilibrium, one may write A-7 as

A-8) $$\int_V \left(\rho\ \delta\phi - \sigma_{ij}\frac{\partial(\delta x)_j}{\partial x_i}\right) dV = 0$$

Since this is true for any region of V,

A-9) $$\rho\ \delta\phi - \sigma_{ij}\frac{\partial(\delta x)_j}{\partial x_i} = 0$$

It is generally assumed that the energy, ϕ, is some function of the deformation. If the Eulerian strain tensor is chosen as representative of that deformation, $\delta\phi$ can be expressed in terms of $\delta\varepsilon_{ij}$, i.e.,

A-10) $$\delta\phi = \frac{\partial\phi}{\partial\varepsilon_{mn}}\,\delta\varepsilon_{mn},$$

or, by definition A-5,

A-11) $$\delta\phi = -\frac{\partial\phi}{\partial\varepsilon_{mn}}\,a_{j,m}\delta a_{j,n}.$$

The operation of virtual displacement on A-2 yields

A-12) $$0 = a_{j,k}\,d\,(\delta x)_k + \delta a_{j,k}\,dx_k$$

since the operators d and δ are commutative. Division of A-12 by dx_n yields

A-13) $$0 = a_{j,k}\,\frac{\partial(\delta x)_k}{\partial x_n} + \delta a_{j,k}\delta_{k,n},$$

or,

A-14) $$\delta a_{j,n} = -\,a_{j,k}\,\frac{\partial(\delta x)_k}{\partial x_n}\,.$$

Therefore, by A-11,

A-15) $$\delta\phi = \frac{\partial\phi}{\partial\varepsilon_{mn}}\,a_{j,m}a_{m,k}\,\frac{\partial(\delta x)_k}{\partial x_n}\,,$$

and A-9 becomes

A-16 $$\left[\rho\left(\frac{\partial\phi}{\partial\varepsilon_{mn}}\right)a_{j,m}a_{j,k} - \sigma_{nk}\right]\frac{\partial(\delta x)_k}{\partial x_n} = 0.$$

Since $(\delta x)_k$ is arbitrary, its partial derivative with respect to x_n is also arbitrary. Thus, A-16 requires that

A-17) $$\sigma_{nk} = \rho\left(\frac{\partial\phi}{\partial\varepsilon_{mn}}\right)a_{j,m}a_{j,k} .$$

One should note that this is an entirely general definition of stress in terms of the deformed body.

. Expansion of ϕ around zero deformation yields

A-18) $$\phi = \phi_o + \left(\frac{1}{2}\right)\left(\frac{\partial^2\phi}{\partial\varepsilon_{mn}\varepsilon_{pl}}\right)_o \varepsilon_{mn}\varepsilon_{pl} + \ldots ,$$

where equilibrium required a zero linear term. Therefore, if the limiting approximation is made that third and higher order terms in ϕ can be ignored,

A-19) $$\sigma_{nk} = \rho\left(\frac{\partial^2\phi}{\partial\varepsilon_{mn}\partial\varepsilon_{pl}}\right)_o \varepsilon_{pl}a_{j,m}a_{j,k}$$

which can be written

A-20) $$\sigma_{nk} = \left(\frac{1}{2}\right)\left(\frac{\rho}{\rho_o}\right)C_{mnpl}\left(\delta_{pl}a_{j,m}a_{j,k} - a_{s,p}a_{s,l}a_{j,m}a_{j,k}\right),$$

where the constants C_{mnpl} are

A-21) $$C_{mnpl} = \rho_o \left(\frac{\partial^2 \phi}{\partial \varepsilon_{mn} \partial \varepsilon_{pl}} \right)_o$$

and are the elements of the elastic stiffness tensor.

If instead of considering a general deformation, one assumed an isotropic deformation in a cubic or isotropic materials, then the second order equation, A-20, becomes the one parameter Birch-Murnaghan equation. For instance, assume

A-22) $$a_i = \left(\frac{\rho}{\rho_o} \right)^{1/3} x_i$$

where ρ and ρ_o are the densities in the deformed and undeformed states, respectively. Note that the Eulerian strain becomes

A-23) $$\varepsilon_{jk} = (1/2) \left(1 - \left(\rho/\rho_o \right)^{2/3} \right) \delta_{jk}.$$

Equation A-20 is easily written in the Birch-Murnaghan form

A-24) $$P = 3/2\ K_o \left[\left(\frac{\rho}{\rho_o} \right)^{7/3} - \left(\frac{\rho}{\rho_o} \right)^{5/3} \right]$$

where P is hydrostatic pressure and

A-25) $$K_o = 1/3 \left(C_{1111} + 2C_{1122} \right).$$

Since the instantaneous bulk modulus K is

A-26 $$K \equiv \rho \frac{\partial P}{\partial \rho}$$

equation A-24 and this definition yields

A-27 $$K = 3/2\ K_o \left[(7/3)\left(\frac{\rho}{\rho_o}\right)^{7/3} - (5/3)\left(\frac{\rho}{\rho_o}\right)^{5/3} \right] .$$

APPENDIX B

ULTRASONIC WAVE REFLECTION AND REFRACTION AT A SEAL

Figure B-1 shows an ultrasonic wave u_i traveling in a material g and impinging on a seal (designated by an $_o$) at $x = 0$. The seal is generally less than a wavelength thick (Δ), although this analysis is not thickness dependent. The u_3 and u_4 are, respectively, the transmitted and reflected waves in the seal while u_5 is the transmitted wave in material m. u_2 is the total of the waves reflected by the seal. k and z are the wave vector, and mechanical impedance, respectively.

The propagating waves can be written

$$
\begin{aligned}
u_1 &= A_1 e^{i\left(\omega t - k_g x\right)} \\
u_2 &= A_2 e^{i\left(\omega t + k_g x\right)} \\
u_3 &= A_3 e^{i\left(\omega t - k_o x\right)} \\
u_4 &= A_4 e^{i\left(\omega t + k_o x\right)} \\
u_5 &= A_5 e^{i\left(\omega t - k_m x\right)},
\end{aligned}
\tag{B-1}
$$

where the A_j are complex.

Continuity at $x = {}_0$ and $x = \Delta$ requires

$$
\begin{aligned}
A_2 - A_3 \qquad - A_4 \qquad + 0 \qquad &= -A_1 \\
0 + A_3 e^{-ik_o\Delta} + A_4 e^{ik_o\Delta} - A_5 e^{-k_m\Delta} &= 0 .
\end{aligned}
\tag{B-2}
$$

Force balance yields

$$\text{B-3)}\quad \begin{aligned} z_g A_2 + z_o A_3 - z_o A_4 + 0 &= z_g A_1 \\ - z_o A_3 e^{-ik_o\Delta} + z_o A_4 e^{ik_o\Delta} + z_m A_5 e^{-ik_m\Delta} &= 0 \quad . \end{aligned}$$

The solutions for $\frac{A_2}{A_1}$ and $\frac{A_5}{A_1}$ are easily derived by dividing equations B-2 and B-3 by A_1 and solving the four linear independent equations. These equations are recast in matrix form as:

$$\text{B-4)}\quad \begin{bmatrix} 1 & -1 & -1 & 0 \\ 0 & e^{-ik_o\Delta} & e^{ik_o\Delta} & -e^{-ik_m\Delta} \\ z_g & z_o & -z_o & 0 \\ 0 & -z_o e^{-ik_o\Delta} & z_o e^{ik_o\Delta} & z_m e^{-ik_m\Delta} \end{bmatrix} \begin{bmatrix} A_2/A_1 \\ A_3/A_1 \\ A_4\ A_1 \\ A_5/A_1 \end{bmatrix} = \begin{bmatrix} -1 \\ 0 \\ z_g \\ 0 \end{bmatrix}.$$

By use of Cramer's rule,

$$\text{B-5)}\quad \frac{A_2}{A_1} = \frac{1}{D} \begin{vmatrix} -1 & -1 & -1 & 0 \\ 0 & e^{-ik_o\Delta} & e^{ik_o\Delta} & -e^{-ik_m\Delta} \\ z_g & z_o & -z_o & 0 \\ 0 & -z_o e^{-ik_o\Delta} & z_o e^{ik_o\Delta} & z_m e^{-ik_m\Delta} \end{vmatrix}$$

where D is the determinant of the coefficient matrix in B-4.

Similarly,

B-6) $$\frac{A_5}{A_1} = \frac{1}{D}\begin{vmatrix} 1 & -1 & -1 & -1 \\ 0 & e^{-ik_o\Delta} & e^{ik_o\Delta} & 0 \\ z_g & z_o & -z_o & z_g \\ 0 & -z_o\, e^{-ik_o\Delta} & z_o\, e^{ik_o\Delta} & 0 \end{vmatrix} .$$

D is easily shown to be

B-7) $$D = -2\left[\left(z_o z_g + z_o z_m\right)\cos k_o\Delta + i\left(z_g z_m + z_o^{\,2}\right)\sin k_o\Delta\right]\left(e^{-ik_m\Delta}\right) .$$

Similarly,

B-8) $$\left(\frac{A_2}{A_1}\right)D = -2\left[\left(z_o z_g - z_o z_m\right)\cos k_o\Delta + i\left(z_g z_m - z_o^{\,2}\right)\sin k_o\Delta\right]\left(e^{ik_m\Delta}\right)$$

and

B-9) $$\left(\frac{A_5}{A_1}\right)D = -4z_o z_g .$$

B-8 can be written

B-10) $$\frac{A_2}{A_1} = \frac{\left(z_o z_g - z_o z_m\right) + i\left(z_g z_m - z_o^{\,2}\right)\tan k_o\Delta}{\left(z_o z_g + z_o z_m\right) + i\left(z_g z_m + z_o^{\,2}\right)\tan k_o\Delta} .$$

In those instances where A_5/A_1 is used, the origin will be moved to $x = \Delta$. Therefore, u_5 should be multiplied by $e^{-ik_m\Delta}$.

B-9 becomes

$$\text{B-11)} \qquad \frac{A_5}{A_1} = \frac{2z_o z_g}{\left(z_o z_g + z_o z_m\right)\cos k_o\Delta + i\left(z_g z_m + z_o^2\right)\sin k_o\Delta} .$$

Note that neither A_2/A_1 nor A_5/A_1 is symmetric with respect to switching materials g and m.

To obtain the phase lag ϕ for each of the interactions, equations B-10 and B-11 will be cast in form $\left|A_2/A_1\right| e^{+i\phi}$ for B-10 and $\left|A_5/A_1\right| e^{-i\phi}$ for B-11. By multiplying both numerator and denominator by the conjugate of the denominator, one obtains for the phase angles

$$\text{B-12)} \qquad \phi\left(\frac{A_2}{A_1}\right) = \tan^{-1}\left[\frac{2\left(z_o z_g z_m^2 - z_o^3 z_g\right)\tan k_o\Delta}{\left(z_o^2 z_g^2 - z_o^2 z_m^2\right) + \left(z_g^2 z_m^2 - z_o^4\right)\tan^2 k_o\Delta}\right]$$

and

$$\text{B-13)} \qquad \phi\left(\frac{A_5}{A_1}\right) = \tan^{-1}\left[\frac{\left(z_g z_m + z_o^2\right)}{\left(z_o z_g + z_o z_m\right)}\tan k_o\Delta\right] .$$

A similar manipulation yields the absolute values

$$\text{B-14)} \qquad \left|\frac{A_2}{A_1}\right| = \left[\frac{\left(z_o z_g - z_o z_m\right)^2 + \left(z_g z_m - z_o^2\right)^2 \tan^2 k_o\Delta}{\left(z_o z_g + z_o z_m\right)^2 + \left(z_g z_m + z_o^2\right)^2 \tan^2 k_o\Delta}\right]^{1/2}$$

and

$$\text{B-15)} \qquad \left|\frac{A_5}{A_1}\right| = \frac{2z_o z_g}{\left[\left(z_o z_g + z_o z_m\right)^2\cos^2 k_o\Delta + \left(z_g z_m + z_o^2\right)^2\sin^2 k_o\Delta\right]^{1/2}} .$$

Note that while $\phi(A_2/A_1)$ is not symmetric with respect to switching materials g and m, $|A_2/A_1|$ is symmetric. Conversely, $\phi(A_5/A_1)$ is symmetric and $|A_5/A_1|$ is not symmetric. The symmetries are used in evaluating the total phase lag ϕ and the ratio of the reflected amplitudes off the two faces of the sample. (See section III.)

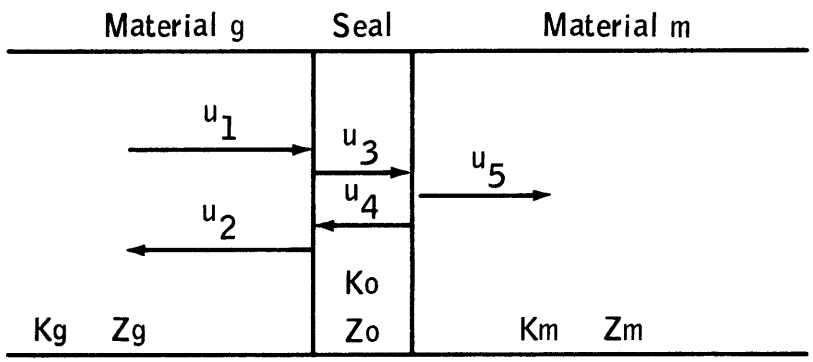

Figure B-1.- A schematic of the transmission u_5 and reflection u_2 of ultrasonic wave u_1 as it interacts with a seal. The K_i and Z_i are the wave vector and mechanical impedence, respectively.

APPENDIX C

WAVE PROPAGATION IN A CRYSTALLINE MEDIA, THE ELASTIC CONSTANTS, THE ISOTHERMAL CORRECTION AND THE ULTRASONIC ESTIMATE OF GRUNEISEN'S RATIO

The Christoffel relations are used to relate the ultrasonic velocities to single crystal elastic constants. A simple review is included here.

Given a crystalline material with density ρ, the time variation of the displacement vector u_i of a point in a volume $dx\ dy\ dz$ under a stress field σ_{ij} is

C-1) $$\rho \frac{\partial^2 u_i}{\partial t^2} dx\ dy\ dz = \frac{\partial \sigma_{ij}}{\partial x_j} dx\ dy\ dz.$$

Or, in terms of the usual constitutive relation,

C-2) $$\sigma_{ij} = C_{ijkl}\ \varepsilon_{kl},$$

where ε_{kl} is defined as $\frac{1}{2}\left(\frac{\partial u_k}{\partial x_l} + \frac{\partial u_l}{\partial x_k}\right)$, C-1 becomes

C-3) $$\rho \frac{\partial^2 u_i}{\partial t^2} = C_{ijkl} \frac{\partial^2 u_k}{\partial x_l \partial x_j}$$

since the elastic stiffness tensor C_{ijkl} is symmetric with respect to k and l. The material is assumed to be uniform though anistropic. A body wave travels through the medium in a direction parallel to $\bar{s}$

whose direction cosines are l_i and whose components are l_1x_1, l_2x_2, l_3x_3. The particle motion u_k, expressed in terms of $\bar{s}$ is

C-4) $$\frac{\partial u_k}{\partial x_l} = \left(\frac{\partial u_k}{\partial \bar{s}}\right)\left(\frac{\partial \bar{s}}{\partial x_l}\right)$$

and

C-5) $$\frac{\partial^2 u_k}{\partial x_l \partial x_j} = \left(\frac{\partial^2 u_k}{\partial \bar{s} \partial x_j}\right)\left(\frac{\partial \bar{s}}{\partial x_l}\right) + \left(\frac{\partial u_k}{\partial \bar{s}}\right)\left(\frac{\partial^2 \bar{s}}{\partial x_l \partial x_j}\right).$$

The last term in C-5 is zero since $\bar{s}$ is a linear function of the x_i. C-5 can be written

C-6) $$\frac{\partial^2 u_k}{\partial x_l \partial x_j} = \left(\frac{\partial^2 u_k}{\partial \bar{s}^2}\right)\left(\frac{\partial \bar{s}}{\partial x_j} \quad \frac{\partial \bar{s}}{\partial x_l}\right),$$

or

C-7) $$\frac{\partial^2 u_k}{\partial x_l \partial x_j} = \left(\frac{\partial^2 u_k}{\partial \bar{s}^2}\right)\left(l_j \quad l_l\right).$$

C-3 becomes

C-8) $$\rho\left(\frac{\partial^2 u_k}{\partial t^2}\right) = C_{ijkl} l_j l_l \left(\frac{\partial^2 u_k}{\partial \bar{s}^2}\right).$$

The elements λ_{ik} of a matrix defined by $\lambda_{ik} = C_{ijkl} l_j l_l$ are called the Christoffel constants.

If a wavelength character is attributed to the u_k, i.e.,

C-9) $$u_k = A_k e^{i(\omega t - \bar{k}\cdot\bar{s})}$$

where $\bar{k}$ is a wave vector along $\bar{s}$, then solving C-8 involves finding the eigenvalues of

C-10) $$\left(\lambda_{ik} - \rho v^2 \sigma_{ik}\right) u_k = 0$$

where the phase velocity v is defined as $v = (\omega/k)$. Equation C-10 is the Christoffel relation.

The measurements made in this study were on crystals with cubic symmetry and were such that $\bar{s}$ was either in the [100] or the [110] direction. For the [100] case, C-10 becomes

C-11) $$\begin{bmatrix} C_{11} - \rho v^2 & 0 & 0 \\ 0 & C_{44} - \rho v^2 & 0 \\ 0 & 0 & C_{44} - \rho v^2 \end{bmatrix} \begin{bmatrix} u_1 \\ u_2 \\ u_3 \end{bmatrix} = 0,$$

where the subscript notation 23 = 4, 31 = 5, 12 = 6 is used. Equation C-11 has three roots labeled

$$v_l = \frac{C_{11}}{\rho} \qquad \bar{u} \text{ along } [100]$$

$$v_s = \frac{C_{44}}{\rho} \qquad \bar{u} \text{ along } [010]$$

$$\dot{v}_s = \frac{C_{44}}{\rho} \qquad \bar{u} \text{ along } [001]$$

The subscripts l and s refer to longitudinal and shear waves, respectively. For the [110] case, C-10 becomes

$$\text{C-12)} \quad \begin{bmatrix} \frac{C_{11} + C_{44}}{2} - \rho v^2 & \frac{C_{12} + C_{44}}{2} & 0 \\ \frac{C_{12} + C_{44}}{2} & \frac{C_{11} + C_{44}}{2} - \rho v^2 & 0 \\ 0 & 0 & C_{44} - \rho v^2 \end{bmatrix} \begin{bmatrix} u_1 \\ u_2 \\ u_3 \end{bmatrix} = 0.$$

The three roots of equation C-12 are

$$v_l = \frac{C_{11} + C_{12} + 2C_{44}}{2\rho} \qquad \bar{u} \text{ along } [110]$$

$$v_s\,(1) = \frac{C_{44}}{\rho} \qquad \bar{u} \text{ along } [001]$$

$$v_s\,(2) = \frac{C_{11} - C_{12}}{2\rho} \qquad \bar{u} \text{ along } [1\bar{1}0]$$

These equations show that measurement of three velocities v_l, $v_s(1)$, and $v_s(2)$ in the [110] direction yield all three elastic constants of a crystal with cubic symmetry. Generally, measurements along a second direction, often the [100], are made to check consistency of results.

Stiffness constants C_{ijkl} measured ultrasonically apply to a dynamic situation. That is, adiabatic heat due to strain in the medium because of an elastic wave cannot flow distances on the order of the elastic wavelength. The passage of the wave is too rapid. Thus, in a lossless medium, ultrasonic velocity measurements determine the adiabatic or isentropic stiffness constants C_{ijkl}. A static measurement yields isothermal stiffness constants.

There are several situations where the distinction is important. Here, only the case of volume change under hydrostatic pressure is considered. The parameter expressing volume change with pressure P is the bulk modulus K and is defined as $K = -V(\frac{dP}{dV})$. The adiabatic bulk modulus is labeled K_s and the isothermal modulus is labeled K_T. K_s, in terms of the dynamic C_{ijkl}, is

C-13) $$K_s = \left(\frac{C_{11} + 2C_{12}}{3}\right).$$

A total differential of P is

C-14) $$dP = \left(\frac{\partial P}{\partial V}\right)_T dV + \left(\frac{\partial P}{\partial T}\right)_V dT$$

Thus, the partial derivative of P with respect to V at constant entropy S, is

C-15) $$V\left(\frac{\partial P}{\partial V}\right)_S = V\left(\frac{\partial P}{\partial V}\right)_T + V\left(\frac{\partial P}{\partial T}\right)_V \left(\frac{\partial T}{\partial V}\right)_S$$

where both sides have been multiplied by V. By definition of K,

C-16) $$K_s = K_T - V\left(\frac{\partial P}{\partial T}\right)_V \left(\frac{\partial T}{\partial V}\right)_S$$

Since

C-17) $$\left(\frac{\partial P}{\partial T}\right)_V = -\left(\frac{\partial V}{\partial T}\right)_P \left(\frac{\partial P}{\partial V}\right)_T,$$

and since the definition for volume thermal expansion is $\alpha = \frac{1}{V}\left(\frac{\partial V}{\partial T}\right)_P$, C-16 becomes

C-18 $$K_s = K_T - K_T \alpha V \left(\frac{\partial T}{\partial V}\right)_S .$$

Similarly,

C-19) $$\left(\frac{\partial T}{\partial V}\right)_S = \left(\frac{\partial S}{\partial V}\right)_T \left(\frac{\partial T}{\partial S}\right)_V$$

Through use of the Maxwell relation

C-20) $$\left(\frac{\partial S}{\partial V}\right)_T = \left(\frac{\partial P}{\partial T}\right)_V,$$

C-18 becomes

C-21) $$K_s = K_T + VK_T{}^2\alpha^2 \left(\frac{\partial T}{\partial S}\right)_V.$$

The differential of the internal energy U is

C-22) $$dU = Tds - PdV$$

so that

C-23) $$\left(\frac{\partial U}{\partial T}\right)_V = T\left(\frac{\partial S}{\partial T}\right)_V .$$

Since $\left(\frac{\partial U}{\partial T}\right)_V$ is the specific heat at constant volume C_V, equations C-23 and C-21 yield

C-24) $$K_s = K_T + V\left(\frac{K_T{}^2\alpha^2}{C_V}\right)_T,$$

or,

$$K_s = K_T\left[1 + T\alpha\left(\frac{VK_T\alpha}{C_V}\right)\right] .$$

Equation C-25 is used to calculate Ks/K_T; however, the equation is often expressed in terms of Gruneisen's parameter γ. From the text, it is easily shown that $\gamma = \frac{VK_T}{C_V}$, therefore,

C-26) $$K_s = K_T\,(1 + T\alpha\gamma)\ .$$

There are instances where the elastic compliances S_{ijkl} are more convenient to use than the elastic stiffnesses C_{ijkl}. If C is the stiffness matrix and S is the compliance matrix,

C-27) $$S = C^{-1}.$$

Details of the element by element calculation are in Nye (1960). The results for materials having cubic symmetry are

C-28) $$S_{11} = \frac{C_{11} + C_{12}}{(C_{11} - C_{12})(C_{11} + 2C_{12})}$$

$$S_{12} = \frac{-C_{12}}{(C_{11} - C_{12})(C_{11} + 2C_{12})}$$

$$S_{44} = \frac{1}{C_{44}}$$

To apply the harmonic theory to the single crystal oxides, the $v_{p,s}$ must be related to measured ultrasonic velocities and estimates obtained for the thermal energy. If $f_{p,s}$ is the fraction of the thermal energy in modes p or s, at sufficiently high temperatures (above the Debye temperature (Slater, 1939)), $f_p = f_s = 1/3$, i.e.,

C-29) $$\gamma = \frac{\gamma_p + 2\gamma_s}{3}\ .$$

Also, from the Debye theory of specific heat, the vibrational energy at sufficiently low temperatures is proportional to $(\omega_{max})^{-1/3}$. Since $|\bar{k}|_{max}$ is independent of mode,

(C-30) $$E_{p,s} \alpha \frac{1}{(v_{p,s})^3}$$

and

(C-31) $$E_{vib} \alpha \frac{1}{(v_p)^3} + \frac{1}{(v_s)^3} .$$

Therefore,

(C-32) $$\bar{\gamma} = \frac{\gamma_p + 2\gamma_s (\frac{v_p}{v_s})^3}{1 + 2(\frac{v_p}{v_s})^3}$$

Experimental temperatures usually lie between the extremes of these assumptions. However, equations (C-29) and (C-32) are effective bounds for $\bar{\gamma}$. There is a method based on the Debye theory where the $f_{p,s}$ could be calculated directly. The complication is usually not warranted.

The v_p and v_s may best be obtained from an integration of the solutions to the Christoffel relation. As we have seen, velocity solutions v for a wave traveling in a direction with cosines l_i must satisfy

(C-33) $$|C_{ijkl} l_j l_l - \rho v^2 \delta_{ik}| = 0.$$

which is a third order determinant in v^2. For an eigenvector l_i, the square roots of the three solutions are labeled $v_p(l_i)$, $v_{s(1)}(l_i)$, and $v_{s(2)}(l_i)$, where subscript p is attached to the highest velocity. If the average of a value v, over the three principal directions, is denoted by $\langle v \rangle$, then

(C-34)
$$v_p = \langle v_p(l_i) \rangle$$

$$v_s = \frac{1}{2} \langle v_{s(1)}(l_i) + v_{s(2)}(l_i) \rangle .$$

An additional assumption implicit in equation C-31 is that the concentration of allowed wave vectors is independent of direction. This is so for crystals having cubic symmetry.

Although the v_p and v_s in equation C-34 are the appropriate parameters for the modified quasi-harmonic model, it is probably adequate to consider only the isotropic elastic properties of an aggregate of the single crystals. Hill (1952) has shown that the so called Voigt elastic constants

(C-35)
$$K_v = (\tfrac{1}{3})(C_{1111} + 2C_{1122})$$

$$G_v = (\tfrac{1}{5})(C_{1111} - C_{1122} + 3C_{1212})$$

and the Reuss elastic constants

(C-36)
$$K_R = \frac{3}{(S_{1111} + 2S_{1122})}$$

$$G_R = \frac{5}{(4S_{1111} - 4S_{1122} + 3S_{1212})}$$

are upper and lower bounds, respectively, for the bulk and shear moduli of a polycrystal. This polycrystal has an isotropic distribution of single crystals with elastic stiffnesses C_{ijkl} and elastic compliances S_{ijkl}. Hill suggests that measured elastic constants fall near the averages of the Voigt and Reuss limits. Although there are closer but more complex bounds (Hashin and Shtrikman, 1962), the Hill averages will suffice. The result is

$$v_p = \left(\frac{K_H + \frac{4}{3} G_H}{\rho}\right)^{1/2} \tag{C-37}$$

$$v_s = \left(\frac{G_H}{\rho}\right)^{1/2}$$

Equation C-37 was used to estimate the $\gamma_{p,s}$ in chapter III.

APPENDIX D

CRYSTAL CUTTING AND POLISHING TECHNIQUES

Rough orientations of the magnetite and the spinel crystals were estimated from their morphologies. With the desired faces thus identified, the crystals were embedded in paraffin on a goniometer supplied as part of the Laue X-ray camera. A series of patterns were made with successive adjustments of the goniometer until the desired orientation was achieved to ±1/2 degree.

The goniometer was then mounted on the bed of a surface grinder. The faces were ground with a 400 grit wheel and finished with a 600 grit wheel. The crystals were cooled during grinding by a water-rust inhibitor mixture.

The samples were ground with some trepidation since in previous experience with fused quartz and polycrystalline alumina, uneven frictional heating had resulted in cracking of the surfaces. Undoubtedly, the greater care taken grinding the magnetite and spinel crystals was warranted.

After being ground, the samples were mounted in the end of a one-inch inside diameter stainless steel tube, that slid freely, but without wobble, in an aluminum frame. Figure D-1 is a cross section of the apparatus as it sits on a polishing wheel. So that the bottom of the aluminum frame would not be worn by the polishing wheel, three 1/2-inch-diameter alumina (Lucalox) legs were inset into the frame's base. Although automatic polishing systems were tried, this hand-held aluminum frame and piston worked best.

After mounting the sample in the piston, the crystal faces were polished on a piece of plate glass with 8μ alumina. Finally, 1μ alumina was used on a hard silk wheel. Although a slight tendency for the edges to round might have been reduced by a careful matching of the polishing powder

to the crystal, the method as outlined yielded surfaces on the spinel with less undulation than a wavelength of light to within a millimeter of the edges. In the case of magnetite, several flaws in the crystal made polishing the surface to less than a few wavelengths of light impossible. The lower estimates of accuracy of velocity given in the text for magnetite are, in part, a reflection of these surface flaws.

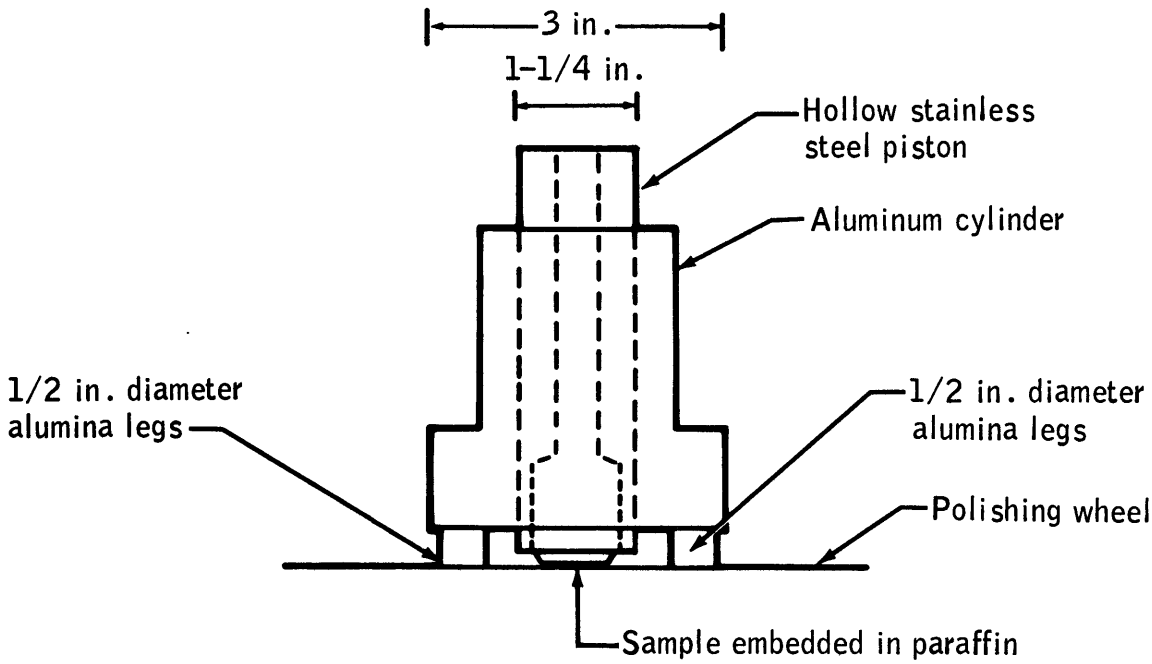

Figure D-1.- Frame for holding sample during polishing. The stainless steel piston floats freely in the cylinder. The polishing force can be varied by changing the length of the piston since the piston's weight is on the surface being polished.

APPENDIX E

THE PHASE COMPARISON TECHNIQUE AND ERROR ANALYSIS

There are several reviews of methods for measuring sound velocity, e.g., McSkimin (1964) and Simmons (1965). The phase comparison technique, developed by McSkimin (1953), lends itself to high precision measurements with relatively simple electronics. Figure E-1 is a schematic of the hardware and figure E-2 shows the wave trajectory in the buffer rod and sample. The buffer rod permits removal of the active element, the quartz transducer, from elastic interactions with and the environment of the sample. The equipment built for this study at moderate pressures was to be used in studies at high temperature as well. Above 500° C, a quartz crystal loses its piezoelectric character so that isolation of the transducer from the furnace is essential. The assembly shown in Figure E-2 was inside the pressure vessel.

The buffer and reflecting rods were made of fused quartz obtained from Syncor, Inc. Their cylindrical surfaces were threaded on a cylindrical grinder to reduce surface waves and to scatter side reflections. The end of the buffer rod were polished by the A. D. Jones Optical Co. of Burlington, Massachusetts, to less than a wavelength of sodium light and the ends made parallel to 15 seconds of arc. Aluminum was evaporated onto the blunt end of the rod to form an electrically conducting layer under the quartz transducer. (Previously, evaporated gold had been tried but was found to be less durable.) The 1/2-inch-diameter quartz transducer was epoxied to the aluminum film. Removal of the transducer simply lifted the film under the transducer. Redeposition of the film is a simple process. Only transducers polished to the fundamental frequency were used. X-cut transducers were used to generate compressional waves and AC-cut to generate shear waves.

In the phase comparison technique, a continuous (cw) burst (shown as a in figure E-2) is sent down the buffer rod so that reflections off the two sample faces interfere. Ultrasonic interferometry is a more descriptive term than phase comparison. The frequency f_1 of the cw is varied until either a maximum (constructive interference) or a minimum (destructive interference) is obtained for the overlap portion of the resulting envelope (wave c and pattern iv in figure E-2). The minimum or null was arbitrarily used. The condition for a null is that the travel time be

E-1) $$\left(n + \frac{1}{2}\right)\frac{1}{f_1} = \frac{2L}{v} + \left(\frac{\phi}{2\pi}\right)\frac{1}{f_1}$$

where n is an integer, L is the length of the sample, v is phase velocity in the sample, and ϕ is the phase lag of reflections or transmissions at seals caused by impedance mismatches and finite seal thicknesses.

n may be found by measuring velocity v_{approx} by the pulse travel time method (Birch, 1960) and finding the number of wavelengths at frequency f_1 in the distance

E-2) $$2L + \left(\frac{\phi}{2\pi} - \frac{1}{2}\right)\frac{v_{approx.}}{f_1} .$$

This method was used in the case of magnetite.

n may also be obtained by finding the next higher frequency f_2 that results in a null. The condition for this is

E-3) $$\left(n + 1 + \frac{1}{2}\right)\frac{1}{f_2} = \frac{2L}{v} + \left(\frac{\phi 2}{2\pi}\right)\frac{1}{f_2} .$$

For the first approximation the travel times are assumed to be independent of frequency. Thus,

E-4) $$\left(n + 1 + \frac{1}{2}\right)\frac{1}{f_2} = \left(n + \frac{1}{2}\right)\frac{1}{f_1}$$

or,

E-5) $$n = \frac{1}{2} + \frac{1}{\left(\frac{f_2}{f_1} - 1\right)}$$

The electronics system, similar to that used by McSkimin (1953), Verma (1960), and others is shown in figure E-3. The low drift (less than 0.005% over 10 minutes) 606A signal generator supplied a continuous RF sine wave variable over the desired 5- to 20-MHz range. Frequency was measured with a digital counter to seven significant figures. The signal was amplified and gated by an Arenberg PG-650C. A wide band amplifier was used between the source and the gated amplifier for isolation and to drive the gated amplifier to its design limit of about 100 volts peak-to-peak into 50 ohms for small duty cycles. The internal gate of the PG-650C was set for about 80 bursts per second. Pulse lengths were varied between 3 and 10 μsec. The electrical signal passed through a discriminator to the quartz transducer. This discriminator behaved electrically (fig. E-4(a)) to reduce the escape of low level ringing in the tank circuit of the gated amplifier and present a high impedance to the low level signals coming from the transducer. The network between B and C (fig. E-4(b)) limited the voltages seen at input of the preamplifier PA-620-SN. This preamplifier had an adjustable bandwidth which was set at 1.3 MHz. Maximum gain of the preamplifier and the amplifier, WA-600-E, was 120 dB. This gain was never needed. The usual setting

was at about 90 dB. The preamp was necessary more for its filter characteristics than for gain. The signal was rectified in the last stages of the WA-600-E and displayed on the Tektronix 585A oscilloscope.

EVALUATION OF PHASE ANGLE

The seals, s(1) and s(2), form a mechanical link between the buffer rod and sample. To avoid many of the seal problems normally incurred, the assembly was mechanically loaded. A force of 15 lb was applied between the quartz transducer and the fused quartz reflecting rod. With nothing between the buffer rod and sample, submicroscopic variations in surfaces were still sufficient to eliminate sound transmission. Gold foil only 0.00005 inch thick inserted between the buffer rod and sample as well as between the sample and reflecting rod permitted the 20 MHz compressional waves to pass. The malleability of gold allowed it to absorb irregularities in the surfaces. Copper also worked but could not be obtained sufficiently thin. Platinum made a poor seal.

For shear wave transmission more adhesion was needed between the buffer rod and sample. Because petroleum ether, the pressure medium, dissolves the resins or vacuum greases that have previously been used, a new type seal was developed. Clear Seal, a silicone rubber made by GE, worked quite well.

ϕ is written

E-6) $$\phi = \phi\begin{pmatrix} a \\ c \end{pmatrix} + \phi\begin{pmatrix} c \\ d \end{pmatrix} + \phi\begin{pmatrix} d \\ e \end{pmatrix} - \phi\begin{pmatrix} a \\ b \end{pmatrix}$$

where $\phi\begin{pmatrix} i \\ j \end{pmatrix}$ is the phase lag between the elastic waves i and j in figure E-2. Mathematical expressions in terms of the thickness of the seal and the mechanical impedances of the buffer rod, seal, and sample can be assigned each $\phi\begin{pmatrix} i \\ j \end{pmatrix}$ (appendix B). The thickness of the gold foil is

supplied by the manufacturer and the mechanical impedance of gold is about 62.5×10^5 g/sec-cm^2. Changes with pressure were ignored.

In the case of shear wave seals, neither the seal thickness nor the mechanical impedance of the Clear Seal were known. A special plug (fig. E-5) for the pressure vessel was fabricated and the amplitude of a wave reflected off the end of the plug was noted before and after coating it with a thick layer of Clear Seal. This amplitude was recorded as a function of pressure to 10 kilobars. If R is the ratio of reflected to transmitted wave amplitudes, then the mechanical impedance, z_o, of the Clear Seal is

E-7) $$z_o = z_p\left(\frac{1 - R}{1 + R}\right)$$

where z_p is the shear wave mechanical impedances of the steel plug. The results of these measurements are shown in figure E-6. For the pressure range of 1 to 10 kilobars, the shear wave mechanical impedance of the Clear Seal is approximately

E-8) $$z_o = [1.45 - 0.11P(kb)] \times 10^5 \text{g/sec-cm}^2.$$

In addition to mechanical impedance, the thickness of the Clear Seal bond is needed. Or, as shown in appendix B, the quantity $\tan k_o\Delta$ is needed rather than the thickness. k_o is the wave vector in the seal and Δ is the seal thickness. $(k_o\Delta)$ is obtained from the ratio of amplitudes

of reflected waves off seals s(1) and s(2) (fig. E-2). Using the equations in appendix B, one obtains

$$\text{E-9)} \qquad \sin^2 k_o\Delta = \left[\frac{4z_b z_s\left(\frac{A_b}{A_e}\right) - \left(z_b + z_s{}^2\right)}{\left(\frac{z_b z_s}{z_o} + z_o\right)^2 - \left(z_b + z_s\right)^2}\right]$$

where z_b, z_s, and z_o are the mechanical impedances of the buffer rod, sample, and seals, respectively, and $\left(\frac{A_b}{A_e}\right)$ is the ratio of amplitudes of reflected waves b and e. Values for seal thicknesses of the Clear Seal bond were around 0.00004 inch at 10 kilobars. Although z_o was corrected for pressure, $k_o\Delta$ was not. The value at 10 kilobars was used throughout. This resulted in a large uncertainty for shear wave studies of ±20% in $k_o\Delta$.

ERROR ANALYSIS

Equation E-1 recast as

E-10) $$v = \frac{2Lf}{\left(n + \frac{1}{2} - \frac{\phi}{2}\right)}$$

lends itself to error analysis. That is,

E-11) $$\frac{\delta v}{v} = \pm \frac{\delta L}{L} + \frac{\delta f}{f} + \frac{v\left(\frac{\phi}{2\pi}\right)}{2Lf}.$$

The precision micrometer allows a δL of $\pm 5 \times 10^{-5}$cm. For magnetite ($f = 5 \times 10^{6}$/sec), Δf could be found to ± 200 sec^{-1}. $\frac{\delta f}{f} = \frac{v}{2Lf}\left(\frac{h}{360}\right)$ where h is the uncertainty in degrees of picking a minimum. For $v_p(110)$ of magnetite $2L = 2.7$ cm, $v = 7.4 \times 10^{5}$cm/sec. This results in a $\frac{\delta f}{f}$ of $10^{-3}h$, or $h \simeq y$. The sensitivity of ± 200 sec^{-1} in f yields a precision of 4 parts in 10^{4}. Since the magnetite data was extrapolated to room pressure, this should be doubled to ± 8 parts in 10^{4}. An additional limit of accuracy lies in ϕ. From appendix B, the terms in equation E-6 are

$$\phi\begin{pmatrix}a\\c\end{pmatrix} = \phi\begin{pmatrix}d\\e\end{pmatrix} = \tan^{-1}\left[\frac{\left(z_b z_s + z_o^{\,2}\right)}{\left(z_o z_b + z_o z_s\right)} \tan k_o\Delta\right]$$

E-12) $$\phi\begin{pmatrix}c\\d\end{pmatrix} = \tan^{-1}\left[\frac{2\left(z_o z_s z_b^{\,2} - z_o^{\,3} z_s\right)\tan k_o\Delta}{\left(z_o^{\,2} z_s^{\,2} - z_o^{\,2} z_b^{\,2}\right) + z_s^{\,2} z_b^{\,2} - z_o^{\,4}\right)\tan^2 k_o\Delta}\right]$$

$$\phi\begin{pmatrix}a\\b\end{pmatrix} = \tan^{-1}\left[\frac{2\, z_o z_b z_s^{\,2} - z_o^{\,3} z_b \tan^2 k_o\Delta}{\left(z_o^{\,2} z_b^{\,2} - z_o^{\,2} z_s^{\,2}\right) + \left(z_b^{\,2} z_s^{\,2} - z_o^{\,4}\right)\tan^2 k_o\Delta}\right]$$

where, again, o, b, and s refer to the seal, buffer rod, and sample, respectively. Roughly, $z_s = z_b$ so that $\phi\begin{pmatrix}c\\d\end{pmatrix} = \phi\begin{pmatrix}a\\b\end{pmatrix}$. Therefore,

E-13) $$\phi \simeq 2\phi\begin{pmatrix}a\\c\end{pmatrix}.$$

Since $k_o\Delta$ is much less than 2π,

E-14) $$\phi \simeq 2\left(\frac{z_b z_s + z_o^2}{z_b z_o + z_o z_s}\right)k_o\Delta.$$

For $z_b \simeq z_s$,

E-15) $$\left(\frac{\phi}{2\pi}\right) \simeq \left(\frac{z_s}{z_o} + \frac{z_o}{z_s}\right)\frac{f}{v_o}\Delta$$

since $k_o = \frac{2\pi f}{v_o}$. Δ is about 10^{-4}cm and is known to better than ±20%, z_s and z_o are known to about 1%. Therefore,

E-16) $$\delta\left(\frac{\phi}{2\pi}\right) = 10^{-5}\left(\frac{z_s}{z_o} + \frac{z_o}{z_s}\right)\frac{f}{v_o}.$$

The total error, equation E-11, is

E-17) $$\frac{\delta v}{v} = \pm\left(\frac{5 \times 10^{-5}}{L} + 4 \times 10^{-4} + \frac{10^{-5}}{L}\left(\frac{v}{v_o}\right)\left(\frac{z_s}{z_o} + \frac{z_o}{z_s}\right)\right).$$

or,

E-18) $$\frac{\delta v}{v} \simeq \pm\left(4 \times 10^{-5} + 4 \times 10^{-4} + 6 \times 10^{-5}\right),$$

or about 5 parts in 10^4. Doubling this because of the extrapolation yields 1 part in 10^3 accuracy in velocity for the magnetite.

The error in the pressure derivative of velocity is

E-19) $$\frac{\delta\left(\frac{\partial v}{\partial P}\right)}{\left(\frac{\partial v}{\partial P}\right)} = \pm\left(2\left(\frac{\delta v}{v}\right) + 0.005\right).$$

0.005 reflects the uncertainty in pressure $\frac{\delta P}{P}$. The $2\left(\frac{\delta v}{v}\right)$ is 0.001 from equation E-18 so that $\frac{\delta\left(\frac{\partial v}{\partial P}\right)}{\left(\frac{\partial v}{\partial P}\right)}$ for magnetite was ±0.006.

The uncertainties in velocities for the single-crystal spinel and the polycrystalline cadmium oxide were ±0.03% (Chap. III). In their cases $\frac{\delta\left(\frac{\partial v}{\partial P}\right)}{\left(\frac{\partial v}{\partial P}\right)}$ was ±0.005. The temperatures were accurate to ±0.1° C yielding an inaccuracy in the temperature derivatives of 0.004. Often, the inaccuracies in the temperature derivatives were controlled by scatter in the data. The uncertainties listed in chapter III reflect both factors.

The data on magnetite was reduced on the Univac 1108 at NASA's Manned Spacecraft Center. The programs were written in FORTRAN V and are included in Appendix F.

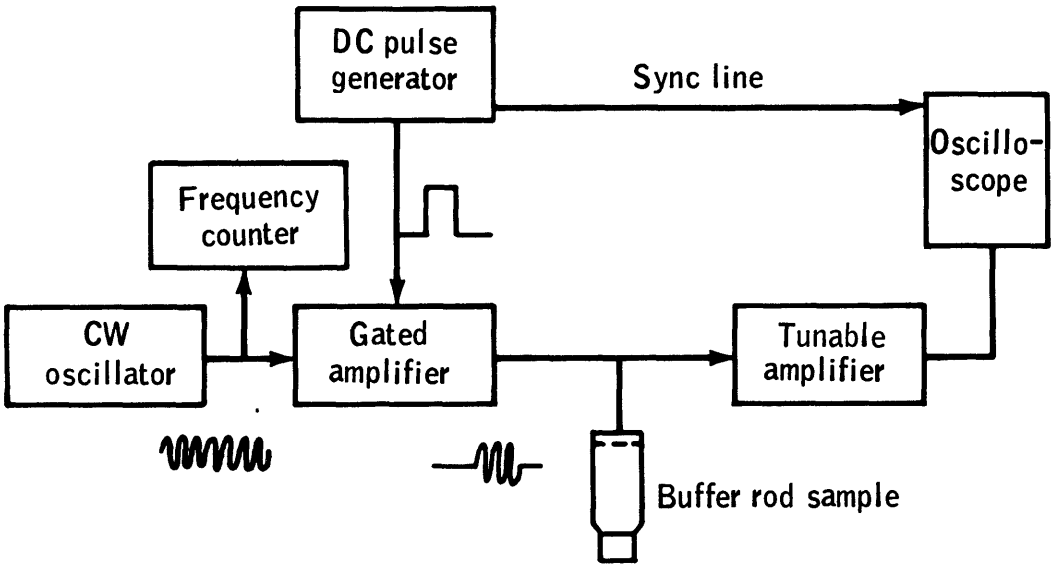

Figure E-1.- Circuit for the measurement of ultrasonic velocity. Adapted from McSkimin (1964).

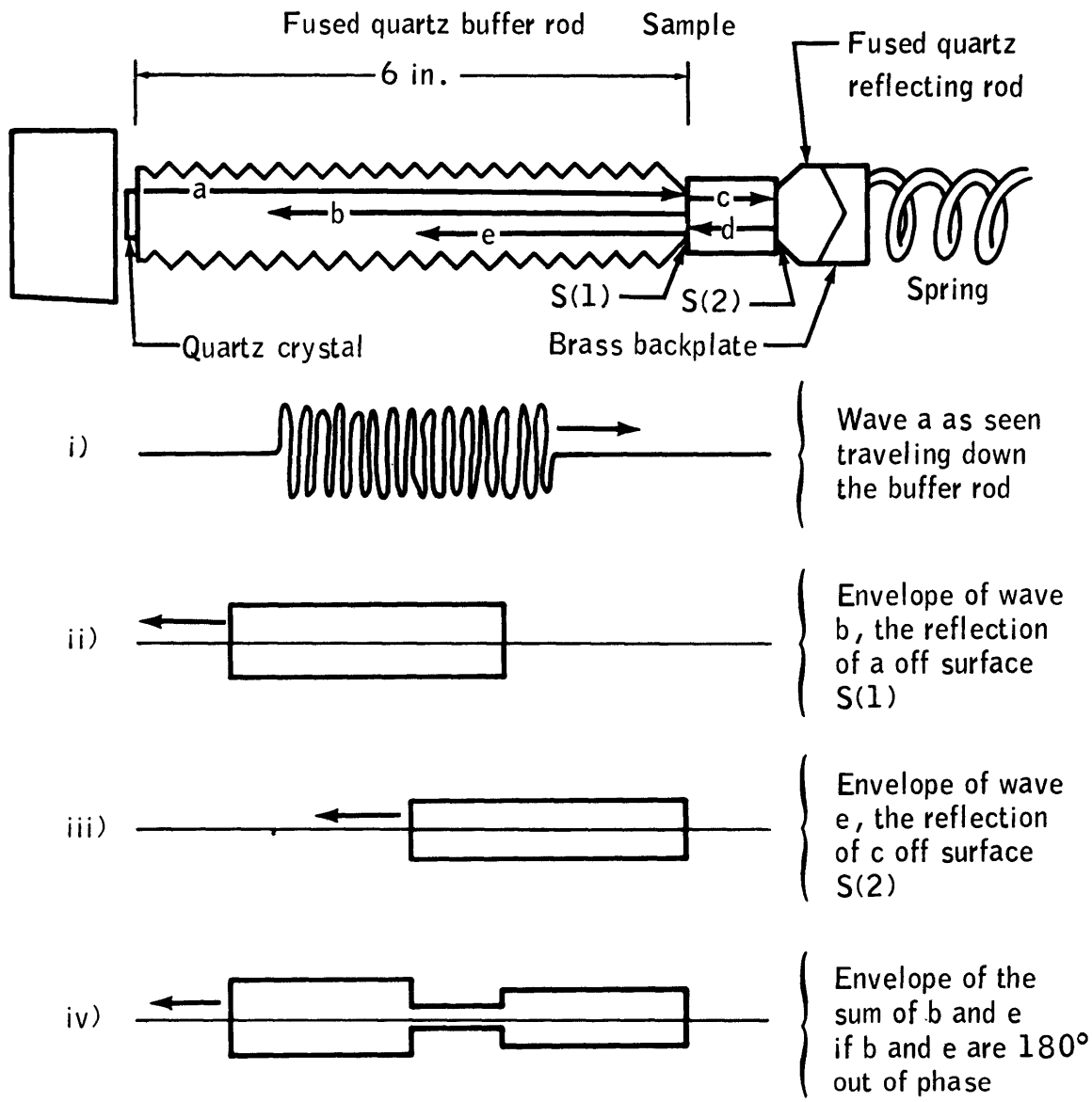

Figure E-2.- Diagram of the buffer rod and sample assembly and a schematic of the traveling elastic waves. Multiple reflections are ignored in the drawing for conceptual simplicity. Note that everything shown in the assembly is inside the pressure vessel.

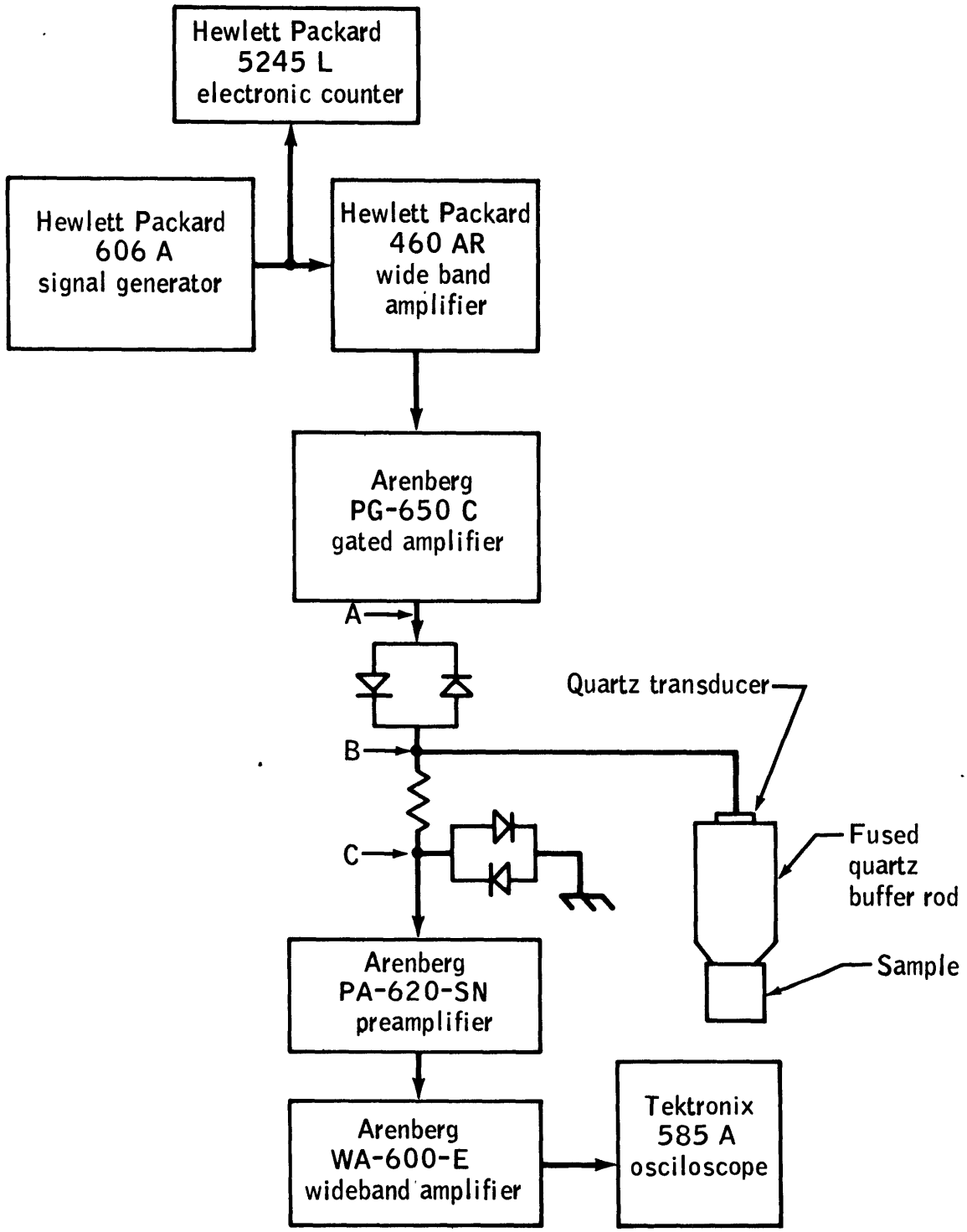

Figure E-3.- Block diagram of the electronics used.

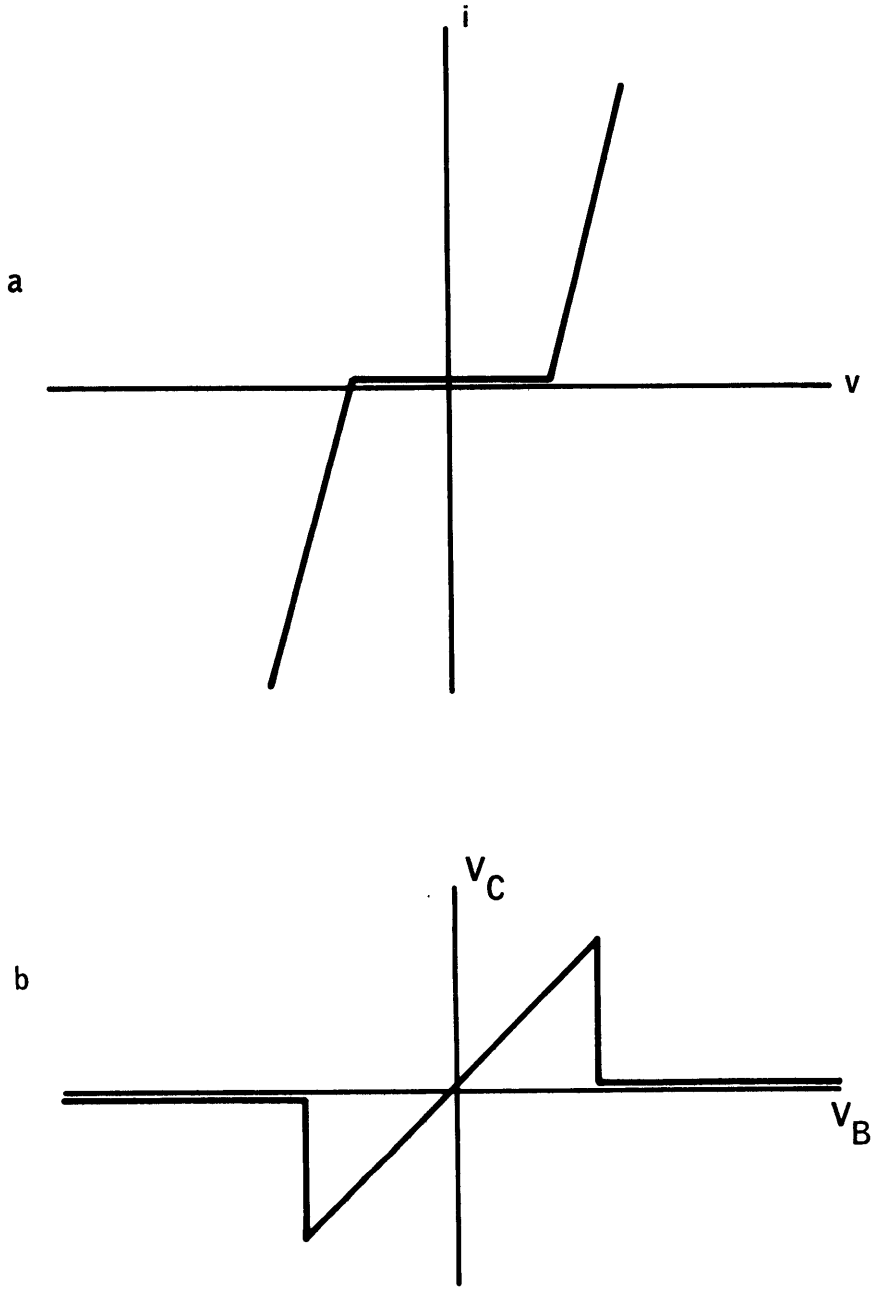

Figure E-4.- Idealizations of the two electrical networks in figure III-3; v and i are the voltage and current between points A and B; V_B and V_C are voltages with respect to ground at points B and C.

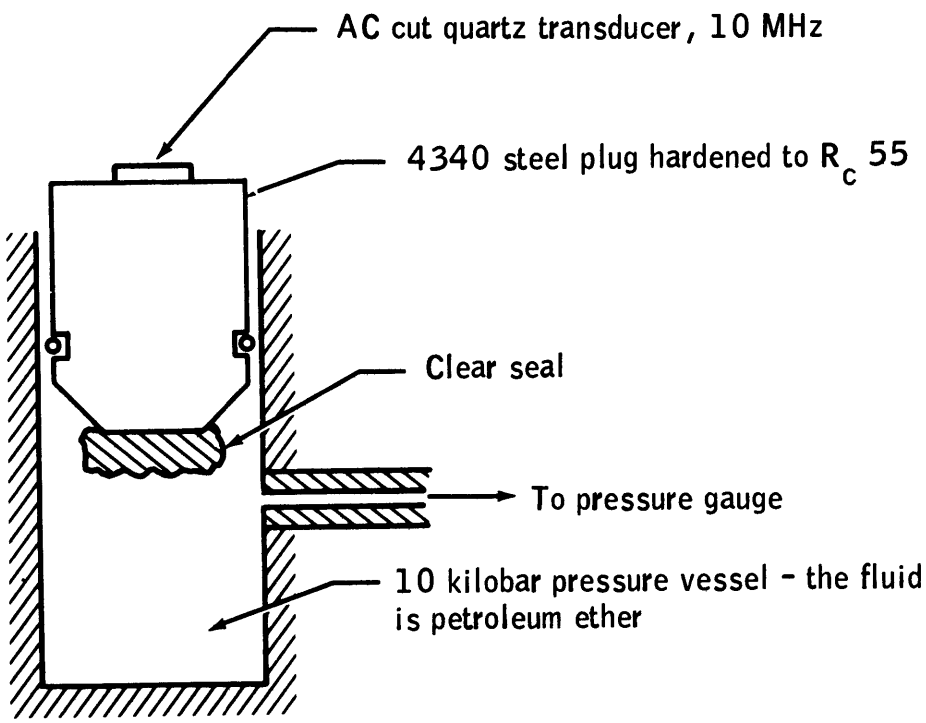

Figure E-5.- Schematic of equipment used to measure the mechanical impedance to shear waves of General Electric's Clear Seal.

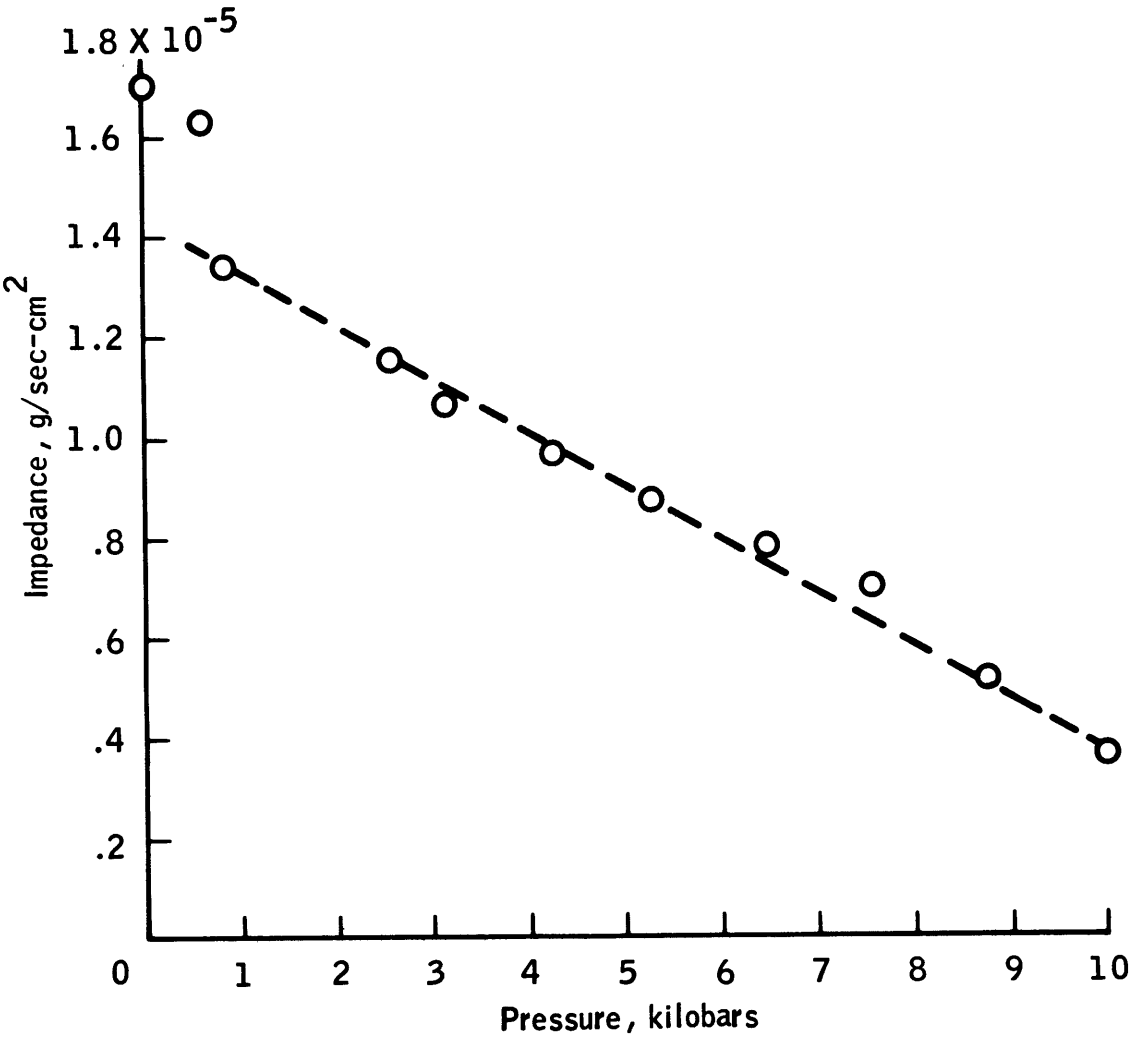

Figure E-6.- Mechanical impedance to shear waves of the silicone rubber, Clear Seal.

APPENDIX F

COMPUTER PROGRAMS

The following programs are written in Fortran V and are compatible with the Univac 1108 at NASA's Manned Spacecraft Center.

Main program — Computes velocity

```
    DO 4 N=1,25
   IMPLICIT INTEGER(L,M,N),REAL(A-K,O-Z)
    COMMON/X/DEL,ZEN,RHOS,ZO,ZB,L,FONE(25),FTWO(25),PHIP(25),PNUM(25)
  1 ,WNUM(25)/Y/A,B,C,AVDIF
    DIMENSION VZERO(25),VPHIP(25),P(25)
    READ(5,11) ZB,ZO,DEL,KAPPA,RHOS,ZEN
    WRITE(6,12) ZB,ZO,DEL,KAPPA,RHOS,ZEN
11  FORMAT(F5.2,1XF5.2,1XF6.5,1XF6.1,1XF6.3,1XF7.5)
12  FORMAT(45HITHIS PROGRAM IS BASED ON NULL INTERFEROMETRY,
  1 //4H ZB=,F5.2,2X4H ZO=,F5.2,2X5H DEL=,F6.5,2X7H KAPPA=,F6.1,
  22X6H RHOS=,F6.3,2X5H LEN=,F7.5,//73H   FONE(L)   FTWO(L)  PHIP   W
  3NUM     PNUM     P(L)      VZERO      VPHIP,1X/)
13  FORMAT (-6PF8.5,2XF8.5,2X,0PF4.3,6XF6.2,4XF6.1)
14  FORMAT (1H ,-6PF8.5,2XF8.5,2X,0PF5.3,2XF6.2,3XF6.1,3XF6.3,3X,
  1 -5PF8.5,3XF8.5)
15  FORMAT (7HOVPHIP=,-5PF8.5,3H +(,F9.6,9H) * P(KB),10X,7H AVDIF=,
  1 F3.5)
16  FORMAT (7HOVZERO=,-5PF8.5,3H +(,F9.6,9H) *P(KB),10X,7H AVDIF=,
  1 F8.5)
17  FORMAT (7HOVPHIP=,-5PF8.5,3H +(,F9.6,6H)*P +(,F8.6,6H)*P**2,
  1 10X,7H AVDIF=,F8.5)
18  FORMAT (7HOVZERO=,-5PF8.5,3H +(,F9.6,6H)*P +(,F8.6,6H)*P**2,
  1 10X,7H AVDIF=,F8.5)
    DO 1 L=1,25
    READ(5,13) FONE(L),FTWO(L),PHIP(L),WNUM(L),PHUM(L)
    IF (FONE(1).EQ.0.) GO TO 5
    VZERO(25)=0.
    VPHIP(25)=0.
    IF (FONE(L).EQ.0.) VPHIP(L)=0.
    IF (FONE(L).EQ.0.) VZERO(L)=0.
    IF (FONE(L).EQ.0.) GO TO 2
    WND=1./(FTWO(L)/FONE(L)-1.)
    IF (WNUM(L).NE.0.) GO TO 3
    FUFN=AINT(WND)
    REM=WND-RUFN
    IF (REM.OE..25.AND.REM.LT..75) WNUM(L)=RUFN+.5
```

```
      IF (REM.LT..25.OR.REM.GE..75) WNUM(L)=AINT(WND+.5)+.5
    3 IF (FTWO(L).EQ.0..AND.L.GT.1) WNUM(L)=WNUM(L-1)
      PHIP(L)=0
      IF (DEL.NE.0.) CALL PHIPIE(L)
      P(L)=(PNUM(L)-54.)/180.958
     ZENP=ZEN*(1.-P(L)/(c.*KAPPA))
      VPHIP(L)=2.*ZENP*FONE(L(/(WNUM(L)-PHIP(L))
      IF (PHIP(L).GE..5) VZERO(L)=2.*ZENP*FONE(L)/(WNUM(L)-.5
      IF (PHIP(L).LT..5) VZERO(L)=2*ZENP*FONE(L)/WNUM(L)
    1 WRITE(6,14) FONE(L),FTWO(L),PHIP(L),WNUM(L),PNUM(L),P(L),VZERO(L),
     1 VPHIP(L)
    2 CALL LSLIN(VPHIP,P)
      WRITE (6,15) A,B,AVDIF
     CALL LSLIN(VZERO,P)
      WRITE (6,16) A,B,AVDIF
     CALL LSBIN(VPHIP,P)
      WRITE (6,17) A,B,C,AVDIF
     CALL LSBIN(VZERO,P)
      WRITE (6,18) A,B,C,AVDIF
    4 CONTINUE
    5 CONTINUE
      END
```

Subroutine PHIPIE — Computes phase lag

```
     SUBROUTINE PHIPIE(L)
      COMMON/X/DEL,ZEN,RHOS,ZO,ZB,L,FONE(25),FTWO(25),PHIP(25),PNUM(25)
    1 ,WNUM(25)
      VO=3.3E5
      ZA=ZO
      IF (ZO.EQ.0.) VO=.13E5
      THETA=6.283*DEL*FONE(L)/VO
     IF (ZO.EQ.0) ZO=1.48-.0006*PNUM(L)
      V=2.*ZEN*FONE(L)/WNUM(L)
      ZA=V*RHOS/10**5
      A=((Z)**2+ZB*ZS)*TAN(THETA))/(ZO*ZS+ZO*ZB)
      B=2.*(ZB**2*ZO*ZS-ZS*ZO**3)*TAN(THETA)/(ZS**2*ZO**2-ZB**2*ZO**2
     1 +(ZS**2*ZB**@=ZO**4)*(TAN(THETA))**2)
      C=2.*(ZB*ZO*ZS**2-ZB*ZO**3)*TAN(THETA(/(ZB**2*ZO**2-ZS**2*ZO**2
     1 +(ZS**2*AB**2-ZO**4)*(TAN(THETA))**2
      PHIA=ATAN(A)
      PHIB=ATAN(B)
      PHIC=ATAN(C)
      D=(ZB**2-ZO**2)
      E=(ZS**2-ZO**2)
       IF(D.LT.0..AND.B.LE.0.) PHIB=3.1416+PHIB
       IF (D.LT.0..AND.B.GT.0.) PHIB=3.1416-PHIB
       IF (E.LT.0..AND.C.LE.0.) PHIC=3.1416+PHIC
       IF (E.LT.0..AND.C.GT.0.) PHIC=3.1416-PHIC
       PHIP(L)=(2.*PHIA+PHIB-PHIC)/6.283
```

```
 ZO=ZA
RETURN
END
```

Subroutine LSLIN — Computes least squares solution to $v = A + Bp$ where v is velocity, p is pressure, and A and B are adjustable parameters

```
      SUBROUTINE LSLIN(V,P)
      COMMON /Y/A,B,C,AVDIF
      DIMENSION V(25),P(25)
      IF (V(25).NE.0.) M=25
      IF (V(25).NE.).) GO TO 2
      DO 1 L=1,24
      IF (V(L+1).EQ.0.) M=L
    1 IF (V(L+1).EQ.0.) GO TO 2
    2 PSQ=0.
      PC=0.
      VP=0.
      VC=0.
      D=0
      DO 3 L=1,M
    3 PSQ=PSQ+P(L)**2
      DO 4 L=1,M
    4  PC=PC+P(L)
      DO 5 L=1,M
    5 VP=VP+V(L)*P(L)
      DO 6 L=1,M
    6 VC=VC+V(L)
      B=(VP-PC*VC/M)/(PSQ-PC**2/M
      A=(VC-B*PC)/M
      DO 7 L=1,M
    7 D=D+ABS(V(L)-A-B*P(L))
       AVDIF=D/M
      RETURN
      END
```

Subroutine LSBIN — Computes least squares solution to binomial,

$$v = A + Bp + Cp^2$$

```
      SUBROUTINE LSBIN(V,P)
      COMMON /Y/A,B,C,AVDIF
      DIMENSION V(25),P(25)
      IF (V(25).NE.0.) M=25
      IF (V(25).NE.0.) GO TO 2
```

```
      DO 1 L=1,24
      IF (V(L+1).EQ.0.) M=L
    1 IF (V(L+1).EQ.0.) GO TO 2
    2 PSQ=0.
      PC=0.
      VP=0.
      VC=0.
      PQU=0.
      PSQV=0.
      PFOR=0.
      DO 3 L=1,M
    3 PSQ=PSQ+P(L)**2
      DO 4 L=1,M
    4 PC+PC+P(L)
      DO 5 L=1,M
    5 VP+VP+V(L)*P(L)
      DO 6 L=1,M
    6 VC=VC+V(L)
      DO 7 L=1,M
    7 PQU=PQU+P(L)**3
      DO 8 L=1,M
    8 PSQV=PSQV+V(L)*P(L)**2
      DO 9 L=1,M
    9 PFOR=PFOR+P(L)**4
      BOT=2.*PSQ*PSU*PC+PSQ*PFOR*M-PQU**2*M-PFOR*PC**2-PSQ**3
      A=(PC*PQU*PSQV+PSQ*VP*PQU+PSQ*PFOR*VC-VC*PQU**2-PSQV*PSQ**2-PFOR
     1 *VP*PC)/BOT
      B=(VC*PQU*PSQ+PSQ*PC*PSQV+VP*PFOR*M-PSQV*PQU*M-VP*PSQ**2-PFOR*
     1 PC*VC)/BOT
      C=(PC*VP*PSQ+VC*PC*PQU+PSQV*M-PQU*VP*M-VC*PSQ**2-PSQY*PC**2)
     1 /BOT
      D=0.
      DO 10 L=1,M
   10 D=D+ABS(V(L)-A-B*P(L)-C*P(L)**2
       AVDIF=D/M
      RETURN
      END
```

Example of output from Program Main. These data were from an early study of the $v_p(100)$ of Spinel

THIS PROGRAM IS BASED ON NULL INTERFEROMETRY

ZB=13.48 ZO=61.76 DEL=.00013 KAPPA=2050.0 RHOS=3.582 LEN=1.34678

FONE(L)	FTWO(L)	PHIP	WNUM	PNUM	P(L)	VZERO	VPHIP
20.04707	20.38814	.000	59.50	1866.5	10.016	9.06051	9.06051
20.04736	20.38534	-.000	59.50	1867.0	10.019	9.06064	9.06064
20.04617	.00000	.000	59.50	1865.0	10.008	9.06012	9.06012
20.03521	.00000	.000	59.50	1681.0	8.991	9.05666	9.05666
20.02468	.00000	.000	59.50	1504.5	8.016	9.05334	9.05334
20.01564	.00000	.000	59.50	1319.0	6.991	9.05076	9.05076
20.00506	.00000	.000	59.50	1143.0	6.018	9.04741	9.04741
19.98882	.00000	.000	59.50	962.0	5.018	9.04154	9.04154

VPHIP= 9.02507 +(.003540) * P(KB) AVDIF= .00052

VZERO= 9.02507 +(.003540) * P(KB) AVDIF= .00052

VPHIP= 9.00781 +(.006090)*P +(-.000143)*P**2 AVDIF= .00645

VZERO= 9.00781 +(.006090)*P +(-.000143)*P**2 AVDIF= .00645

ZB = impedance of buffer rod
ZO = impedance of seal
DEAL = thickness of seal in cm.
KAPPA = bulk modulus of specimen, in kb.
RHOS = density of specimen
LEN = length of specimen
FONE, FTWO = adjacent frequencies for null
PHIP = phase lag ($\phi/2\pi$)
WNUM = (n+1/2) as in equation III-1
PNUM = associate with P
P(L) = conversion PNUM to P
VZERO = velocity if $\phi = 0$
VPHIP = velocity
The last two lines refer to a least squares fit to a binomial in P

APPENDIX G

ELASTICITY DATA OF THE POROUS GLASS SAMPLES

Included here are the data obtained on the porous glass samples. Pressure P is in bars, sample length L is in centimeters, and the reciprocal of travel time $F_{p,s}$ is in sec^{-1}. (The subscripts p or s refer to compressional or shear wave, respectively.)

Sample F, L = 1.3160

P	F_s	P	F_p
		0	222729
0	131778	211	222728
238	131833	513	222735
513	131856	729	222772
744	131893	1009	222857
1067	131891	1250	222809
		1505	222829
		1790	222846
		2018	222869

Sample 680, L = 2.4300

P	F_s	P	F_p
0	69965	0	N/A
244	69938	230	116757
544	69932	509	116723
748	69957	757	116721
1042	69938	1023	116720

Sample 680, L = 2.4300 - Continued

P	F_s	P	F_p
1239	69936	1248	116724
1538	69887	1508	116727
1774	69878	1769	116727
2014	69834	2004	116720
2287	69798		
2501	69754		

Sample 750, L = 2.3012

P	F_s	P	F_p
0	70502	0	121318
312	70473	239	121324
598	70448	478	121302
821	70431	728	121279
1001	70411	980	121275
1522	70302	1512	121241
2003	70190	2042	121189
2479	70072	2536	121162
		3025	121132

Sample 30, L = 1.5878

P	F_s	P	F_p
0	92748	0	154920
462	92568	259	154886
958	92396	513	154832

Sample 30, L = 1.5878 - Continued

P	F_s	P	F_p
1484	92267	734	154816
2012	91926	1003	154789
2517	91770	1248	154676
		1533	154605
		1788	154506
		2009	154398

Sample 29, L = 1.7496

P	F_s	P	F_p
0	80031	0	N/A
469	79852	227	138405
996	79679	500	138312
1535	79373	707	138256
2054	79149	1011	138116
2495	78992 (weak)	1239	138026
		1517	137922
		1754	137798

Sample 27, L = 2.2298

P	F_s	P	F_p
0	60966	0	N/A
247	60894	734	101834
525	60780	1026	101738
741	60708	1267	101604

Sample 27, L = 2.2298 - Continued

P	F_s	P	F_p
997	60605	1512	101495
1255	60498	1758	101415
1522	60398	1972	101344
		2248	101016

Sample 720, L = 2.7437

P	F_s
0	47740
361	47637
510	47607
744	47528
980	47428
1244	47334
1513	47227
1757	47133

REFERENCES CITED

Alers, G. A. and J. R. Neighbours, J. Phys. Chem. Solids 7, 58, 1958.

Alexandrov, K. S. and T. V. Ryzhova, Bull. Acad. Sci. USSR, Geophys. Ser., English Transl., 871, 1961.

Anderson, D. L., Recent evidence concerning the structure and composition of the earth's mantle, Physics and Chemistry of the Earth, Vol. 6, ed. L. H. Ahrens, F. Press, S. K. Runcorn, and H. C. Urey, Pergamon Press, New York, p. 1, 1965.

Anderson, D. L., A seismic equation of state, Geophys. J. Roy. Astron. Soc., 13, 9, 1967a.

Anderson, D. L., Phase changes in the upper mantle, Science, 157, 1165, 1967b.

Anderson, D. L. and H. Kanameri, Shock-wave equations of state for rocks and minerals, J. Geophys. Res., 73, 6477, 1968.

Anderson, O. L., A proposed law of corresponding states for oxide compounds, J. Geophys. Res., 71, 4963, 1966.

Anderson, O. L., Phys. Rev., 144, 553, 1966a.

Anderson, O. L., Some remarks on the volume dependence of the Gruneisen parameter, J. Geophys. Res., 73, 5187, 1968.

Anderson, O. L., Comments on the negative pressure dependence of the shear modulus found in some oxides, J. Geophys. Res., 73, 7707, 1968a.

Anderson, O. L. and R. C. Liebermann, Sound velocities in rocks and minerals, Vesiac State-of-the Art Report, Willow Run Laboratories, Institute of Science and Technology, Univ. of Michigan, Ann Arbor, 1966.

Anderson, O. L. and J. Nafe, The bulk modulus-volume relationship for oxide compounds and related geophysical problems, J. Geophys. Res. 70, 3951, 1965.

Anderson, O. L., E. Schreiber, R. C. Liebermann, and N. Soga, Some elastic constant data on minerals relevant to Geophysics, Rev. Geophys., 6, 491, 1968.

Binnie, W. P. and I. G. Geib, X-ray diffraction, Methods of Experimental Physics, 6A, ed. K. Lark-Horovitz and V. A. Johnson, Academic Press, New York, p. 203, 1959.

Birch, F., Bull. Geol. Soc. Am., 54, 263, 1943.

Birch, F., Finite elastic strain of cubic crystals, Phys. Rev., 71, 809, 1947.

Birch, F., Elasticity and constitution of the earth's interior, J. Geophys. Res., 57, 227, 1952.

Birch, F., The velocity of compressional waves in rocks to 10 kilobars, part 1, J. Geophys. Res., 65, 1083, 1960.

Birch, F., Composition of the earth's mantle, Geophys. J. Roy. Astron. Soc., 4, 295, 1961a.

Birch, F., Velocity of compressional waves in rocks to 10 kilobars, part 2, J. Geophys. Res., 66, 2199, 1961b.

Birch, F., Some geophysical applications of high-pressure research, Solids Under Pressure, ed. W. Paul and D. Warschauer, McGraw-Hill, New York, p. 137, 1963.

Birch, F., J. Geophys. Res., 69, 4377, 1964.

Bogardus, E. H., Third-order elastic constants of Ge, MgO, and fused SiO_2, J. Appl. Phys., 36, 2504, 1965.

Born, M. and K. Huang, Dynamical Theory of Crystal Lattices, Oxford Press, London, 1954.

Brace, W. F., J. Geophys. Res., 70, 391, 1965.

Bridgman, P. W., Collected Experimental Papers, 7 vols., Harvard University Press, Cambridge, 1964.

Brush, S. G., Theories of the equations of state of matter at high pressures and temperatures, Progress in High Temperature Physics and Chemistry, Vol. 1, ed. Carl A. Rouse, Pergamon Press, New York, p. 1, 1967.

Christensen, N. I., J. Geophys. Res., 71, 5921, 1966.

Chung, D. H., D. J. Silversmith, and B. B. Chick, A modified ultrasonic pulse-echo-overlap method for determining sound velocities and attenuation of solids, Rev. Sci. Instruments, 40, 718, 1969.

Chung, D. H. and G. Simmons, J. Appl. Phys., in press, 1968.

Chung, D. H., and G. Simmons, Pressure derivatives of the elastic properties of polycrystalline quartz and rutile, Earth and Planetary Sci. Letters, 1969.

Chung, D. H., G. R. Terwilliger, W. B. Crandall, and W. G. Lawrence, Elastic properties of magnesia and magnesium-aluminate spinel, Final report, Contract No. DA-31-124-ARO(D-23), Army Research Office, Durham, North Carolina, 1964.

Clark, S. P., Jr. and A. E. Ringwood, Density distribution and constitution of the mantle, Reviews of Geophys., 2, 35, 1964.

Coble, R. L. and W. D. Kingery, Effect of porosity on physical properties of sintered alumina, J. Am. Ceram. Soc., 39, 377, 1956.

Dana, E. S., A Textbook of Mineralogy with an Extended Treatise on Crystallography and Physical Mineralogy, 4th ed., Wiley and Sons, New York, 1949.

Daniels, W. B. and C. S. Smith, The pressure variation of the elastic constants of crystals, The Physics and Chemistry of High Pressure, Gordon and Breach, New York, p. 50, 1963.

Doraiswami, M. S., Elastic constants of magnetite, pyrite and chromite, Proc. Indian Acad. Sci., 25A, 413, 1947.

Doran, D. G. and R. K. Linde, Shock effects in solids, Solid State Physics: Advances in Research and Applications, Vol. 19, ed. F. Seitz and D. Turnbull, Academic Press, New York, p. 229, 1966.

Drickamer, H. G., R. W. Lynch, R. L. Clendenen, and E. A. Perez-Albuerne, X-ray diffraction studies of the lattice parameters of solids under very high pressure, Solid State Physics: Advances in Research and Applications, Vol. 19, ed. F. Seitz and D. Turnbull, Academic Press, New York, p. 135, 1966.

Duvall, G. E. and G. R. Fowles, Shock Waves, High Pressure Physics and Chemistry, II, ed. Bradley, Academic Press, Chap. 9, 1963.

England, A. W., Compressibility as a function of porosity for a glass containing spherical holes, M. S. Thesis, Massachusetts Institute of Technology, 1965.

England, A. W. and G. Simmons, Trans. Am. Geophys. Union 49, 321, abs., 1968.

Hashin, Z. and S. Shtrikman, On some variational principles in anisotropic and nonhomogeneous elasticity, J. Mech. and Phys. Solids, 10, 335, 1962.

Hearmon, R. F. S., An Introduction to Applied Anisotropic Elasticity, Oxford University Press, Oxford, p. 41, 1961.

Hill, R., The elastic behavior of a crystalline aggregate, Proc. Phy. Soc. (London), A65, 349, 1952.

Hughes, D. S. and J. H. Cross, Geophys. 16, 577, 1951.

Hughes, D. S. and H. J. Jones, Bull. Geol. Soc. Am., 61, 843, 1950.

Huntington, H. B., The Elastic Constants of Crystals, Academic Press, New York, 1958.

Knopoff, L., Equations of state of solids at moderately high pressures, High Pressure Physics and Chemistry, 1, ed. R. S. Bradley, Academic Press, New York, p. 227, 1963.

Knopoff, L. and J. N. Shapiro, Comments on the interrelationships between Gruneisen's parameter and shock and isothermal equations of state, J. Geophys. Res., 74, 1439, 1969.

Kumazawa, M. and O. L. Anderson, Elastic moduli, pressure derivatives, and temperature derivatives of single-crystal olivine and single-crystal forsterite, J. Geophys. Res., 74, 5961, 1969.

Liebermann, R. C. and E. Schreiber, Elastic constants of polycrystalline hematite, in press, 1968.

Leibfried, G. and W. Ludwig, Theory of anharmonic effects in crystals, Solid State Physics, 12, ed. F. Seitz and D. Turnbull, Academic Press, 1961.

Mackenzie, J. K. and R. Shuttleworth, A phenomenological theory of sintering, Proc. Phys. Soc. London, B, 62, 833, 1949.

Mackenzie, J. K., Elastic constants of a solid containing spherical holes, Proc. Phys. Soc. (London), 63B, 2, 1950.

Maradudin, A. A., E. W. Montroll, and G. H. Weiss, Theory of lattice dynamics in the harmonic approximation, Supl. 3 of Solid State Physics, ed. F. Seitz and D. Turnbull, Academic Press, 1963.

McQueen, R. G., S. P. Marsh, and J. N. Fritz, J. Geophys. Res., 72, 4999, 1967.

McSkimin, H. J., Measurement of elastic constants at low temperatures by means of ultrasonic waves - data for silicon and germanium single crystals, and for fused silica, J. Appl. Phys., 24, 988, 1953.

McSkimin, H. J., Ultrasonic methods for measuring the mechanical properties of liquids and solids, Physical Acoustics, IA, ed. Warren P. Mason, Academic Press, New York, p. 272, 1964.

McSkimin, H. J., P. Andreatch, Jr., and R. N. Thurston, J. Appl. Phys., 36, 1624, 1965.

McWhan, D. B., J. Appl. Phys., 38, 347, 1967.

McWhan, D. B., P. C. Soures, and G. Jura, Phys. Rev., 143, 143, 1966.

Newhouse, W. H. and J. J. Glass, Some physical properties of certain iron oxides, Econ. Geol., 31, 699, 1936.

Nye, J. F., Physical Properties of Crystals, Oxford Press, London, p. 147, 1960.

Papadakis, E. P., Ultrasonic phase velocity by the pulse-echo-overlap method incorporating diffraction phase corrections, J. Acoust. Soc. Am., 42, 1045, 1967.

Peselnick, L., R. Meister, and W. H. Wilson, Pressure derivatives of elastic moduli of fused quartz to 10 kb, J. Phys. Chem. Solids, 28, 635, 1967.

Pointon, A. J., and R. G. F. Taylor, Elastic constants of magnesia, calcia, and spinel at 16 GHz and 4.2° K, Nature, 219, 712, 1968.

Press, F., Earth models obtained by monte carlo inversion, in press, 1968.

Rice, M. H., R. G. McQueen, and J. M. Walsh, Compression of solids by strong shock waves, Solid State Physics, 6, ed. F. Seitz and D. Turnbull, Academic Press, 1958.

Robie, R. A., P. M. Bethke, M. S. Toulmin, and J. L. Edwards, X-ray crystallographic data, densities, and molar volumes of minerals, Handbook of Physical Constants, ed. S. P. Clark, Jr., Rev. ed. Geological Society of America, New York, p. 27, 1966.

Schmitt, H. H., Petrology and structure of the Eiksundsdal eclogite complex, Hareidland, Sunnmore, Norway, unpublished thesis, Harvard University, 1963.

Schreiber, E., Elastic Moduli of Single-Crystal Spinel at 24° C and 2 Kbar, J. Appl. Phys., 38, 2508, 1967.

Schreiber, E., unpublished data referred to by O. Anderson et al. (1968)

Schreiber, E. and O. L. Anderson, Pressure derivatives of the sound velocities of polycrystalline alumina, J. Am. Ceram. Soc., 49, 184, 1966.

Schreiber, E. and O. L. Anderson, Pressure derivatives of the sound velocities of polycrystalline forsterite, with 6% porosity, J. Geophys. Res., 72, 762, 1967.

Simmons, G., Velocity of compressional waves in various minerals at pressures to 10 kilobars, J. Geophys. Res., 69, 1117, 1964a.

Simmons, G., J. Geophys. Res., 69, 1123, 1964b.

Simmons, G., Ultrasonics in geology, Proc. I.E.E.E., 53, 1337, 1965a.

Simmons, G., Single crystal elastic constants and calculated aggregate properties, J. Graduate Research Center 34, Southern Methodist University Press, Dallas, 1965b.

Skinner, B. J., The thermal expansions of thoria, periclase, and diamond, Am. Mineral., 42, 39, 1957.

Slater, J. C., Introduction to Chemical Physics, McGraw-Hill, Inc., New York, 1939.

Smith, D. K., Techniques of high-temperature X-ray diffraction using metal ribbon furnaces, Norelco Reporter, Jan. - Mar., 1963.

Soga, N., Elastic properties of CaO under pressure and temperature, J. Geophys. Res., 73, 5385, 1968.

Soga, N., J. Geophys. Res., 72, 4227, 1967.

Takenchi, H. and H. Kanamori, Equations of state of matter from shock wave experiments, J. Geophys. Res., 71, 3985, 1966.

Thurston, R. N., H. J. McSkimin, and P. Andreatch, Jr., Third-order elastic coefficients of quartz, J. Appl. Phys., 37, 267, 1966.

Verma, R. K., Elasticity of some high-density crystals, J. Geophys. Res., 65, 3855, 1960.

Walsh, J. B., W. F. Brace, and A. W. England, Effect of porosity on compressibility of glass, J. Am. Ceram. Soc., 48, 605, 1965.

Weir, C. E., J. Res. NBS 56, 187, 1956.

Winchell, A. N., Elements of Optical Mineralogy: An Introduction to Microscopic Petrography, 4th ed., Pt. KK, Wiley and Sons, New York, 1956.

Wyckoff, R. W. G., Crystal Structures, Vol. 1, 2nd ed., Interscience Publishers, New York, 1963.

Ziman, J. M., Principles of the Theory of Solids, Cambridge University Press, p. 111, 1964.

BIOGRAPHICAL NOTE

Anthony Wayne England was born May 15, 1942, in Indianapolis, Indiana. He graduated from West Fargo High School, West Fargo, North Dakota, in May 1959 and the following September entered The Massachusetts Institute of Technology. He was accepted into the Five Year Honors Program in Geology and Geophysics and received the Bachelor of Science and Master of Science degrees simultaneously in February 1965.

His field experience includes a summer of geological mapping in Montana, a summer of exploration seismology in the Southwest United States with Texaco, a summer measuring heat flow in the South and Central United States, and a month assisting in the deployment of a magnetic array in Montana. He is presently involved with pilot and space systems training as a scientist astronaut with NASA.

He has published:

Walsh, J. B., W. F. Brace, and A. W. England, Effect of porosity on commpressibility of glass, J. Am. Ceram. Soc., 48, 605, 1965.

England, A. W., Gene Simmons, and D. Strangway, Lunar electrical conductivity, J. Geophys. Res., 1968.